2015-09-11

Mechanisms of Changes in Precipitation and Atmospheric Circulation from Anthropogenic Forcing

Jie He
University of Miami, jhe@rsmas.miami.edu

UNIVERSITY OF MIAMI

MECHANISMS OF CHANGES IN PRECIPITATION AND ATMOSPHERIC CIRCULATION FROM ANTHROPOGENIC FORCING

By
Jie He

A DISSERTATION

Submitted to the Faculty
of the University of Miami
in partial fulfillment of the requirements for
the degree of Doctor of Philosophy

Coral Gables, Florida

December 2015

UNIVERSITY OF MIAMI

A dissertation submitted in partial fulfillment of
the requirements for the degree of
Doctor of Philosophy

MECHANISMS OF CHANGES IN PRECIPITATION AND ATMOSPHERIC CIRCULATION FROM ANTHROPOGENIC FORCING

Jie He

Approved:

_____
Brian Soden, Ph.D.
Professor of Meteorology and
Physical Oceanography

_____
Amy Clement, Ph.D.
Professor of Meteorology and
Physical Oceanography

_____
Ben Kirtman, Ph.D.
Professor of Meteorology and
Physical Oceanography

_____
Clara Deser, Ph.D.
Senior Scientist
National Center for
Atmospheric Research
Boulder, Colorado

_____
Gabriel Vecchi, Ph.D.
Head of Climate Variations
and Predictability Group
Geophysical Fluid Dynamics Laboratory
Princeton, New Jersey

_____
Dean of the Graduate School

HE, JIE (Ph.D., Meteorology and Physical Oceanography)
Mechanisms of Changes in Precipitation and Atmospheric Circulation from Anthropogenic Forcing (December 2015)

Abstract of a dissertation at the University of Miami.

Dissertation supervised by Professor Brian Soden.
No. of pages in text. (118)

Simulating and understanding the anthropogenic changes in atmospheric circulation and precipitation is a great challenge in climate change studies. Current climate projections rely primarily on coupled atmosphere-ocean models (CGCMs). Due to limited computational resources, these CGCMs have to be run at resolutions that are too low to adequately resolve the climate system. In addition, the climatological biases in CGCMs could also undermine their skillfulness. An alternative model framework – the atmosphere-only models (AGCMs) has been long proposed owing to its superior computational efficiency and better sea surface temperature (SST) climatology. However, AGCMs are often criticized for its lack of coupling with an underlying ocean, and the fidelity of AGCMs for the simulation of anthropogenic climate change is yet to be demonstrated.

The first part of this dissertation seeks the optimal modeling framework for the projection of regional climate change by assessing the advantages and disadvantages of CGCMs and AGCMs. Results show that AGCMs are able to perfectly reproduce the anthropogenic climate change from the CGCMs despite the lack of two-way air-sea coupling. In addition, obtaining the pattern of SST change from the CGCMs is in general unnecessary for the simulation of anthropogenic climate change over land. Furthermore, results show that the inability of the CGCMs to simulate climate change largely results

from the inability to simulate the present-day climatology. The biases in climatology can be largely reduced in AGCMs with observed SST climatology. These results point to a greater utility of AGCMs for the projection of regional climate change.

The second part of this dissertation investigates the relative importance of direct radiative forcing and changes in SST for the anthropogenic changes in atmospheric circulation and precipitation. The global mean SST warming dominates many aspects of the atmospheric responses, including changes in moisture, the mean hydrological cycle and the extratropical precipitation. On the other hand, certain aspects of the atmospheric responses are driven by mechanisms other than the global mean SST warming. In the tropics, both the direct radiative forcing and the pattern of SST change contribute to weakening of the atmospheric circulation. In the subtropics, the precipitation declines are independent of the global mean SST warming but are dominated by fast responses to the direct radiative forcing and changes in SST pattern and land surface temperature.

Acknowledgments

I would like to thank my advisor Brian Soden for guiding me and making my dissertation writing fun. Dr. Soden has been very patient and encouraging throughout my Ph.D. studies. I have learned a lot from his wisdom and experience. He has also supported me financially for any conferences or workshops that would benefit me. I would also like to thank my wonderful committee members – Amy Clement, Ben Kirtman, Clara Deser and Gabriel Vecchi. They have never hesitated to share their knowledge with me whenever I need it. They have also helped me tremendously with my job application. I would like to especially thank Dr. Kirtman for the numerous discussions and arguments we have had, which often eventually made things much easier for me.

I would like to thank my dear classmates – Honghai, Johnna, Katinka, Ryan, Sharein and many more. We have gone through a wonderful journey together. I would also like to thank my sport and game buddies – Brent, Milan, Teddy and Peng. It has been a lot of fun to play and compete with these gentlemen. Many thanks also go to my dear friends outside RSMAS, especially Christine, Ana, Daniel and Emily, for supporting me and making my life exciting.

Last but not least, I would like to thank my Chinese family, including my parents, my cousins, my aunt Jennifer and my girlfriend Sheng. They have supported me unconditionally throughout my Ph.D. studies. I have been and will always be grateful for their love.

Table of Contents

List of Figures

List of Tables

Chapter 1: Introduction

1.1 Motivation

Precipitation and atmospheric circulation are among the most important elements of climate, affecting almost every aspect of society ranging from agriculture to daily human activities. As the greenhouse gas concentrations continue to rise, the characteristics of precipitation and circulation are almost certainly to change (e.g., Seager et al. 2007; Solomon 2007), posing serious socioeconomic challenges. To understand the climate responses to global warming, large collections of climate model projections have been analyzed (Meehl et al. 2007; Taylor et al. 2011). These climate models are the most advanced tools to provide knowledge about future climate. On the other hand, mycurrent climate models are far from perfect and the mechanisms of anthropogenic climate change are largely uncertain. This dissertation assesses some of the common model frameworks for climate change research and discusses potential improvements in the application of these frameworks. This dissertation also examines the mechanisms of anthropogenic climate change with an emphasis on the attribution of the robust responses in precipitation and atmospheric circulation, including the weakening of the tropical circulation, the subtropical drying and the extratropical moistening.

Our current projections of anthropogenic climate change rely primarily on the coupled ocean-atmosphere models (CGCMs). The incorporation of ocean coupling is essential for the simulation of a structured sea surface temperature (SST) change, which is important for tropical precipitation changes (Xie et al. 2010; Ma and Xie 2013). However, global CGCMs are typically run at resolutions that are too coarse to adequately

represent many processes that can influence regional changes in climate (e.g., mesoscale processes associated with sharp topographic variations and complex coastlines; Pielke and Wilby 2012; Hertwig et al. 2015; Zarzycki et al. 2015). Furthermore, current CGCMs often contain systematic biases in SST. In comparison, atmosphere-only models (AGCMs) can be run at much higher spatial resolutions and can incorporate the best estimate of climatological SSTs from observations. Therefore, AGCMs could potentially provide more realistic projections than CGCMs.

However, the fidelity of AGCM simulations for the study of anthropogenic climate change is not clear. AGCMs are often criticized for the absence of coupling with an underlying ocean. Studies have shown that the lack of two-way coupling causes an inconsistency in surface energy fluxes and limits an AGCM's ability to accurately simulate natural climate variability. For example, the lack of two-way coupling causes misrepresentation of the relationship between the Indian summer monsoon and El Niño-Southern Oscillation (e.g., Wang et al. 2005). But no studies have demonstrated the importance of two-way coupling on model projections of anthropogenic climate change. One of the goals here is to examine the important question of whether the lack of coupling limits AGCMs' usefulness for climate change studies.

In a typical global warming simulation, the AGCM is driven externally by two sources of forcing: the direct atmospheric radiative forcing and the warming of the ocean surface. Many recent studies have been trying to attribute the atmospheric responses directly to each type of forcing. For example, Deser and Phillips (2009) found that atmospheric radiative changes during 1950 - 2000 directly drive the strengthening of the mid-latitude westerly winds in the Southern Hemisphere. Such attribution studies are

important because they not only identify the physical drivers of climate change but also indicate the timescales of atmospheric responses as the direct radiative forcing occurs much faster than the warming of the ocean surface. For example, in the event of abrupt CO_2 emission, substantial changes in the atmospheric circulation occur immediately before changes in the global mean SST (e.g., Bony et al. 2013). This dissertation studies the individual impact of direct radiative forcing and sea surface warming with a focus on the tropical circulation weakening, subtropical precipitation decline and extratropical precipitation increase, all of which have emerged ubiquitously from current climate models.

Although the weakening of the tropical circulation is a robust projection, there is currently a lack of consensus on the physical drivers of the weakening. Ma et al. (2012) showed that the weakening of the Walker circulation is primarily driven by the sea surface warming. However, other studies have also shown a weakening of circulation under direct CO_2 forcing (e.g., Andrews et al. 2009; Bony et al. 2013; Thorpe and Andrews 2014). The weakening effect of the sea surface warming and the direct CO_2 forcing is expected as they both stabilize the atmosphere but their relative importance is unclear.

The subtropical drying and extratropical moistening are also robust projections of current climate models and were first identified as a simple thermodynamic response to the Clausius-Clapeyron increase of moisture in a warmer climate (Held and Soden 2006). Because the SST warming drives most of the moisture increase (e.g., Compo and Sardeshmukh 2009), it should also play an important role in the subtropical drying and extratropical moistening. However, more recent studies showed that the subtropical and

extratropical precipitation changes involve more than thermodynamic processes (e.g., Lorenz and DeWeaver 2007; Scheff and Frierson 2012a,b). The complexity of the mechanisms of subtropical and extratropical precipitation changes suggests that the mean SST warming may not be the sole driver.

1.2 Outline

This dissertation consists of five chapters. The first chapter examines the necessity of two-way coupling for the simulation of anthropogenic climate change. The goal is to provide an assessment of model frameworks that are not constrained by two-way coupling to have energetically consistent air-sea fluxes, such as AGCMs and flux-adjusted experiments. The second chapter studies the impact of the pattern of anthropogenic SST change, which has proven important for precipitation changes over tropical oceans. Here, the focus is on extratropics and land where climate change has the most direct socioeconomic impact. The third chapter examines the impact of SST biases on climate projections and builds on the results from the previous two chapters to provide a comparison between the performances from CGCMs and AGCMs. The last two chapters investigate the relative roles of direct atmospheric radiative forcing and sea surface warming on tropical circulation weakening and subtropical and extratropical precipitation change. The main approach for these two chapters is comparing AMIP-type and aqua planet simulations in which the forcing agents are specified separately.

Chapter 2: Does the Lack of Coupling in SST-forced Atmosphere-only Models Limit Their Usefulness for Climate Change Studies?

2.1 Background

Simulations of atmospheric general circulation models (AGCMs) have been widely used in studies of natural and anthropogenic climate change. For example, high-resolution time-slice AGCM simulations have been used in an effort to improve representation of regional precipitation change (e.g., Coppola and Giorgi 2005; May 2008; Kopparla et al. 2013). Likewise, AGCMs forced with prescribed sea surface temperature (SST) and radiative forcing changes (e.g., Deser and Phillips 2009; Ma et al. 2012; Bony et al. 2013) have been used to understand anthropogenic changes in the atmospheric circulation and analyze discrepancies between observed and simulated climate trends (e.g., Shin and Sardeshmukh 2011). However, AGCMs are often criticized for the absence of coupling with an underlying ocean. This coupling is necessary in order for the SST to respond to the atmospheric forcing. Studies have shown that the lack of two-way coupling causes an inconsistency in surface energy fluxes and limits an AGCM's ability to accurately simulate natural climate variability (e.g., Barsugli and Battisti 1998; Wu et al. 2006; Wang et al. 2005). However, no studies have demonstrated the importance of two-way coupling on model projections of anthropogenic climate change.

Model simulations of natural climate variability have shown that the lack of two-way coupling is most problematic in regions where atmospheric forcing strongly regulates the ocean mixed layer. These regions include the mid-latitudes (e.g., Cayan 1992; Deser and Timlin 1997; Barsugli and Battisti 1998) and certain parts of the tropics,

for example the Indian Ocean (e.g., Wu and Kirtman 2004; Krishna Kumar et al. 2005; Wang et al. 2005). In the mid-latitudes, the lack of two-way coupling results in a substantial reduction in atmospheric variability and large spurious surface energy fluxes (Barsugli and Battisti 1998; Bretherton and Battisti 2000; Chen et al. 2013). In the Indian Ocean, the lack of two-way coupling causes misrepresentation of the relationship between the summer monsoon and El Niño-Southern Oscillation (e.g., Wu and Kirtman 2004; Krishna Kumar et al. 2005; Wang et al. 2005).

While the importance of coupling with an underlying ocean has been clearly demonstrated for natural climate variability, its importance for anthropogenic climate change remains unclear. Obviously, a full interaction between ocean and atmosphere is necessary for predicting the pattern and amplitude of SST change in response to external forcing (e.g., Xie et al. 2010; Zheng et al. 2013). This chapter seek to assess the accuracy of AGCM simulations that are forced with anthropogenically-driven changes in SST, yet are not constrained by two-way coupling to have energetically-consistent air-sea fluxes. This question is not simply an academic one, but has important practical implications as AGCM simulations with prescribed SST changes offer a potentially valuable tool for downscaling coupled simulations (e.g., Coppola and Giorgi 2005; May 2008; Kopparla et al. 2013), yet the fidelity of such simulations is not clear.

Previous studies have examined this topic, but none have provided a conclusive answer due to limitations in the experimental design. For example, Cash et al. (2005) found that the 500mb height response to $2xCO_2$ from the AGCM simulations had a similar pattern but much smaller magnitude than that from the coupled simulations. However, the SST used to force the AGCMs differed substantially from the SST in the

coupled simulations in certain regions. Therefore, differences in the 500mb height response could be due to differences in SST forcing instead of the lack of two-way coupling.

In this chapter, I compare AGCM and coupled model simulations with consistent boundary conditions and radiative forcing to examine the importance of two-way coupling on anthropogenic climate change. I find that coupled model simulations of anthropogenic climate change can be well reproduced by AGCMs and that errors due to coupling with an underlying ocean are primarily limited to internal variability.

2.2 Model and Methods

2.2.1 Model simulations

The primary model archive for this study is a set of simulations conducted with the Community Earth System Model (CESM, Hurrell et al. 2013). The fully coupled configuration of CESM consists of atmosphere - Community Atmosphere Model, version 4 (CAM4), ocean - Parallel Ocean Program (POP2), land - Community Land Model (CLM4), and sea ice - Community Ice Code (CICE4). The atmosphere and land models are run on a finite volume grid of approximately 1.9° latitude by 2.5° longitude resolution, whereas the ocean and sea ice models are run on a displaced pole grid of approximately 1° resolution.

As stated above, the main objective of this chapter is to study the impact of two-way coupling on climate change that is a result of external forcing instead of internal variability. To isolate the externally forced climate change, I compare coupled and AGCM simulations with different concentrations of CO_2. Four sets of simulations are

performed with CESM, labeled according to their coupling and forcing characteristics. The "CPL_PI" simulation is run with fully coupled CESM with CO_2 fixed at the pre-industrial level of 284.7 ppm. The "CPL_1pct" simulation is also run with fully coupled CESM with CO_2 initiated at 284.7 ppm and increasing at 1 percent per year. The "AMIP_PI" and "AMIP_1pct" simulations are the so-called "perfect AMIP" reproduction of the "CPL_PI" and "CPL_1pct" simulations, respectively. ("AMIP" stands for Atmospheric Model Intercomparison Project.) In the "AMIP_PI" and "AMIP_1pct" simulations, only the atmosphere and land models are active and are forced with the same atmospheric composition as the coupled simulations and the daily mean SST and sea ice concentration from the coupled simulations. It is important to note that obtaining the magnitude and pattern of SST change from the coupled simulations is essential for ensuring correct SST forcing for the AGCM simulations. My experiments aim to determine whether AGCMs are able to accurately reproduce the anthropogenic climate change that result from such SST change, despite the energetically inconsistent surface fluxes due to the lack of coupling with an underlying ocean. Assuming the diurnal cycle of the boundary conditions is not important for long-term climate response, the difference between the "perfect AMIP" and the coupled simulations is entirely due to the lack of coupling with an underlying ocean. I also conduct the "perfect AMIP" simulations with monthly mean SST and sea ice concentration; the change in the temporal resolution of the boundary conditions from daily to monthly means does not change the conclusions of this chapter.

2.2.2 Methods

I use a 10-year epoch difference to characterize the change in the climatic mean state. Climate change under no external forcing (or entirely due to internal variability, herein referred to as $1xCO_2$) is calculated as the epoch difference between year 11 to 20 and year 1 to 10 in the pre-industrial simulations. This approach is validated using different epochs [for example, (41-50) – (11-20)], which does not change myconclusions. Climate change at the time of $2xCO_2$ ($4xCO_2$) is calculated as the epoch difference between year 71 to 80 (year 141 to 150) and year 1 to 10 in the 1pctCO2 simulations. The use of epoch differences to calculate climate change is validated using linear climate trends, which does not change myconclusions (not shown). The analysis presented here focuses primarily on precipitation change, which is a highly variable quantity of significant socioeconomic importance. However, mymain conclusion does not depend on the choice of variable.

While AGCM simulations have been widely used to study the changes in the mean state, they are also valuable in analyzing anthropogenic changes in climate extremes (e.g., Kharin et al. 2005; Allan and Soden 2008). It is therefore important to also evaluate the impact of two-way coupling on simulations of anthropogenic changes in climate extremes. To examine this, I compute the 10-year mean of the 99th percentile daily mean value at each grid point as an index of climate extremes. This calculation of climate extremes has been commonly used in previous studies (e.g., Emori and Brown 2005) and is validated using the 100th percentile and the 95th percentile, which does not alter myconclusions.

2.3 Results

2.3.1 CESM simulations

I first examined the impact of two-way coupling on anthropogenic changes in the climatic mean state. Consider changes in the 10-year mean precipitation at the time of $2xCO_2$ from the 1pctCO2 simulations (Fig. 2.1, middle column). Both the "CPL_1pct" and "AMIP_1pct" simulations show increased precipitation over central Africa, the West Indian Ocean and the West Tropical Pacific Ocean and decreased precipitation over the East Indian Ocean, the East Subtropical Pacific Ocean and the West Atlantic Ocean. Overall, the precipitation change at $2xCO_2$ is well reproduced by the "AMIP_1pct" simulation. However, errors due to the lack of two-way coupling exist over certain regions, including the Southern Indian Ocean, the Australian continent, the North Pacific and the Southwest Pacific. In these regions, the magnitude of errors is approximately the same as that of precipitation change itself. The spatial correlation between the coupled and uncoupled precipitation change at $2xCO_2$ is 0.79 (Table 2.1).

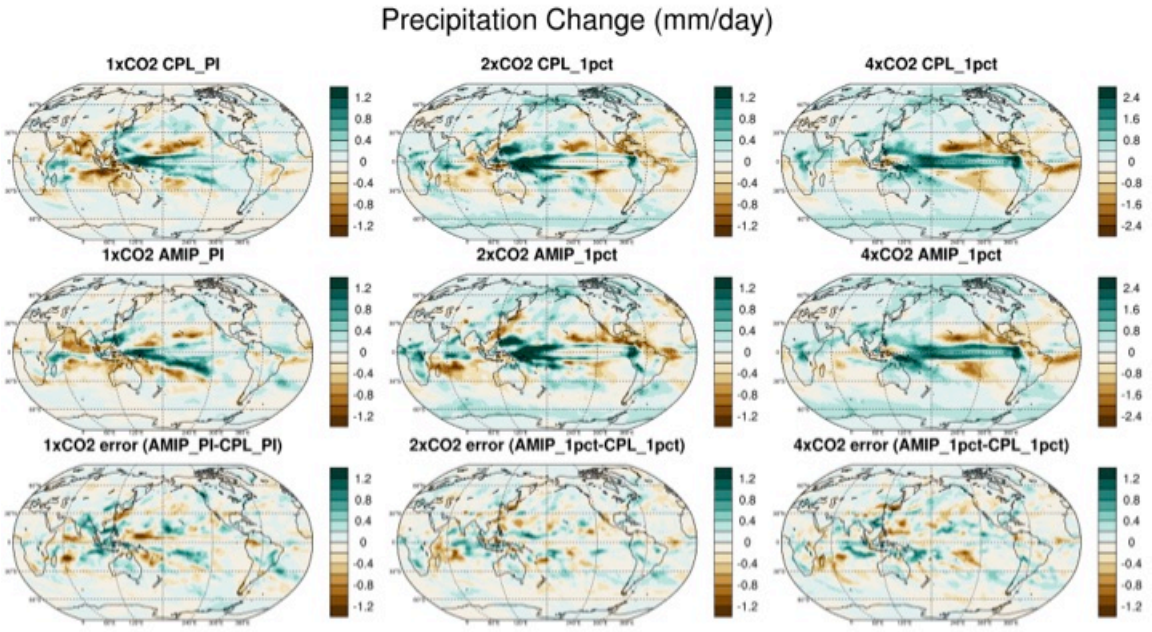

Figure 2.1 Precipitation change at (left) $1xCO_2$, (middle) $2xCO_2$ and (right) $4xCO_2$ from (top) coupled, (center) "perfect_AMIP" simulations and (bottom) error defined as the difference between the "perfect_AMIP" and coupled simulations.

	Precip	Latent Heat	Omega500	SLP
$1xCO_2$	0.60	0.37	0.45	0.22
$2xCO_2$	0.79	0.79	0.64	0.83
$4xCO_2$	0.93	0.95	0.85	0.87

Table 2.1 Spatial correlation of changes in precipitation, latent heat, vertical velocity at 500mb (Omega500) and SLP in the coupled and "perfect-AMIP" simulations at $1xCO_2$, $2xCO_2$ and $4xCO_2$.

Although $2xCO_2$ has been traditionally considered as a large enough forcing to isolate the externally forced signal from internal variability, this is not always the case. Deser et al. (2012) showed that the climate change at the time of $1.5xCO_2$ under the A1B scenario is dominated by internal variability. Likewise, changes in the 10-year mean precipitation at $2xCO_2$ from the "CPL_1pct" simulation (Fig. 2.1, top middle) have approximately the same magnitude and spatial coverage as that at $1xCO_2$ (Fig. 2.1, top left), which is entirely due to internal variability. Therefore, a large part of the precipitation change at $2xCO_2$ is a result of internal variability and a higher level of CO_2

increase is needed to elevate the externally forced signal above the internal variability. At the time of $4xCO_2$, the magnitude of precipitation change is approximately double that of internal precipitation variability (note the difference in scale between the top right panel and the top left panel in Fig. 2.1). Therefore, I can neglect internal variability and consider the precipitation change at $4xCO_2$ as mostly a response to CO_2 increase.

At the time of $4xCO_2$, changes in the 10-year mean precipitation are almost identical in the "CPL_1pct" and "AMIP_1pct" simulations. The spatial correlation between the coupled and uncoupled precipitation change rises to 0.93. The improvement of AGCM's performance with the increase of external forcing can also be seen in other variables (Table 1). This means that coupling with an underlying ocean becomes less crucial as the externally forced change increases relative to the internal variability. Furthermore, as the external forcing increases, the magnitude and the spatial coverage of errors due to the lack of two-way coupling remain approximately the same (compare the bottom 3 panels in Fig. 2.1). This indicates that the lack of coupling with an underlying ocean primarily affects the simulation of internal variability instead of the externally forced climate change.

To further show that errors due to the lack of two-way coupling in the "perfect AMIP" simulations are primarily related to internal variability, I calculate the moving RMS of epoch precipitation difference and errors using year 1 to 10 as the reference epoch (Fig. 2.2, top). For the pre-industrial simulations, the RMS of changes in the 10-year mean precipitation, which are entirely due to internal variability, stays approximately the same throughout the duration of the simulations. The errors in the epoch difference have approximately the same RMS as the epoch difference itself. For

the 1pctCO2 simulations, the RMS of each epoch difference increases as the CO_2 concentration rises, but the RMS of the errors stays the same as that from the pre-industrial simulations despite the increasing CO_2. This indicates that errors are insensitive to the presence or magnitude of the external forcing.

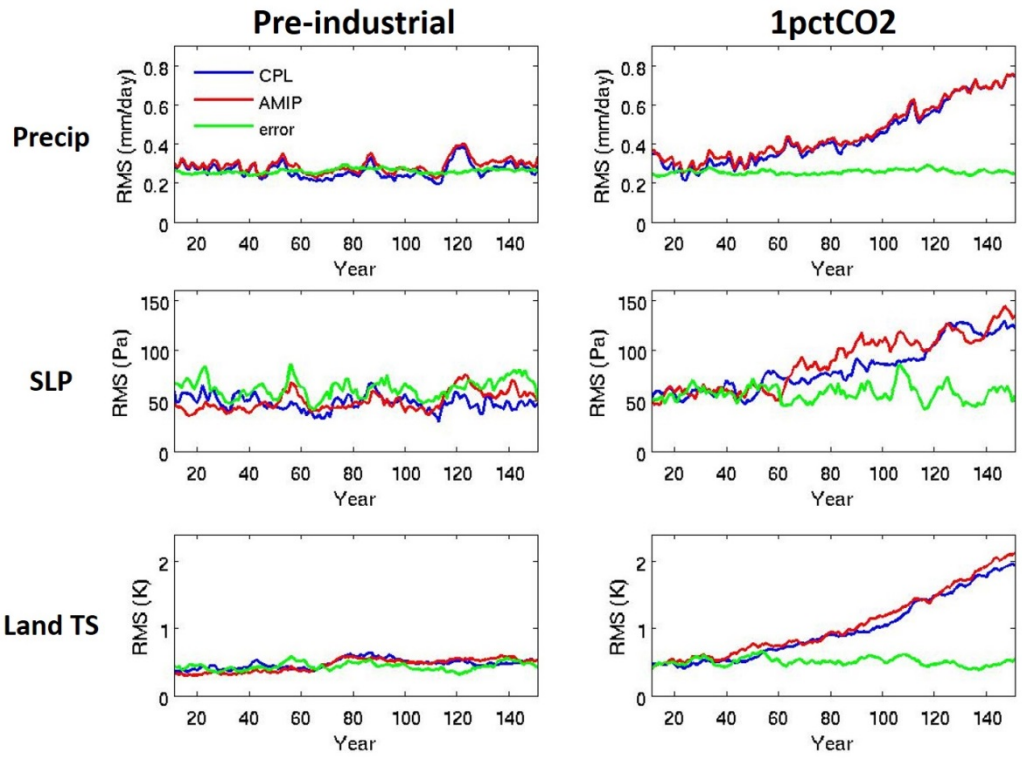

Figure 2.2 Moving RMS of changes in the 10-year mean (top) global precipitation, (middle) global SLP and (bottom) relative land surface temperature calculated as the difference between the moving epoch, which moves from year 11-20 to year 151-160 at time step of 1 year, and the reference epoch, which is fixed as year 1-10, from the (left) pre-industrial simulations and (right) 1pctCO2 simulations. The relative land surface temperature change is calculated by removing the global mean land surface temperature change from the total change. Numbers on the x-axis represent the first year of the moving epoch. Blue and red represent the moving RMS from the coupled and "perfect-AMIP" simulations, respectively. Green represents the moving RMS of errors, which is the difference between the climate change in the "perfect-AMIP" simulations and that in the coupled simulations.

The moving RMS for changes in the 10-year mean sea level pressure (SLP, Fig. 2.2, middle) and relative land surface temperature (Fig. 2.2, bottom) shows similar characteristics. Due to the fact that SLP is more susceptible to internal variability

compared to precipitation and surface temperature (Deser et al. 2012), the separation of SLP change from the errors happens more slowly in the 1pctCO2 simulation. Therefore, a high level of CO_2 forcing is needed in the AGCM simulations to overcome the errors.

To confirm that the errors are indeed related to internal variability, I show precipitation errors at $4xCO_2$ as a function of the averaging length of epochs that are used to calculate precipitation change (Fig. 2.3). As the averaging length increases, internal variability is reduced while the external forcing stays the same. As a result, errors due to lack of two-way coupling are reduced. The magnitude of precipitation errors for averaging length of 20 years is about half of that for averaging length of 5 years (Fig.3, bottom right). All the above evidences demonstrate that errors due to the lack of two-way coupling are related to internal variability, rather than externally-forced climate change.

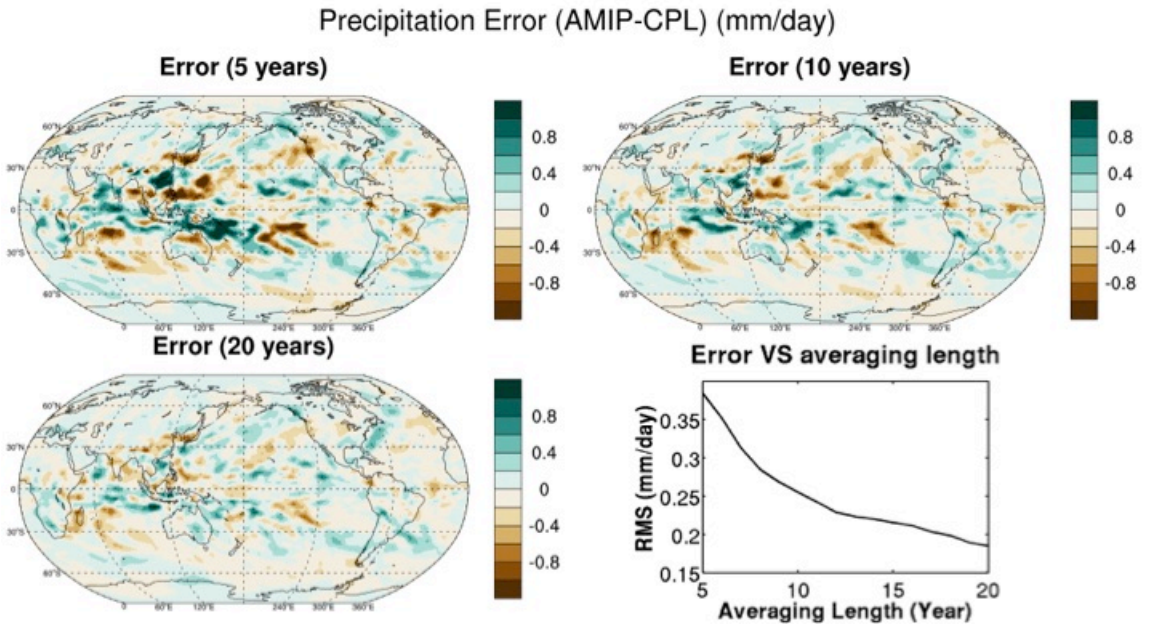

Figure 2.3 Precipitation errors at $4xCO_2$ as a function of the averaging length of epochs used to calculate precipitation change. The top left, top right and bottom left panels are maps of errors for averaging length of 5 years [(141-145) – (1-5)], 10 years [(141-150) – (1-10)] and 20 years [(141-160) – (1-20)], respectively. The three maps use the same color scale. The unit is mm/day. The bottom right panel is the RMS of error as a function of averaging length.

In addition to changes in the climatic mean state, I also examined the impact of two-way coupling on anthropogenic changes in climate extremes. Here, I present the results with changes in precipitation extremes, warm extremes and cold extremes, which are the most commonly studied variables of extreme climate changes. Figure 4 shows the moving RMS of changes in the global precipitation extremes, the land warm extremes and the land cold extremes. Compared to the mean precipitation (Fig. 2.2, top), precipitation extremes (Fig. 2.4, top) have larger amplitude in both the internal variability and the externally forced change (e.g., Emori and Brown 2005; Allan and Soden 2008). And as expected, precipitation extremes also have a larger amplitude in the errors due to the lack of two-way coupling, and a separation of signal and the errors requires a higher level of CO_2 forcing. Nevertheless, the RMS of errors is still the same in the pre-industrial and the 1pctCO2 simulations and stays flat during the increase of CO_2. This indicates that errors in the simulation of precipitation extremes are only related to the internal variability rather than the externally forced change.

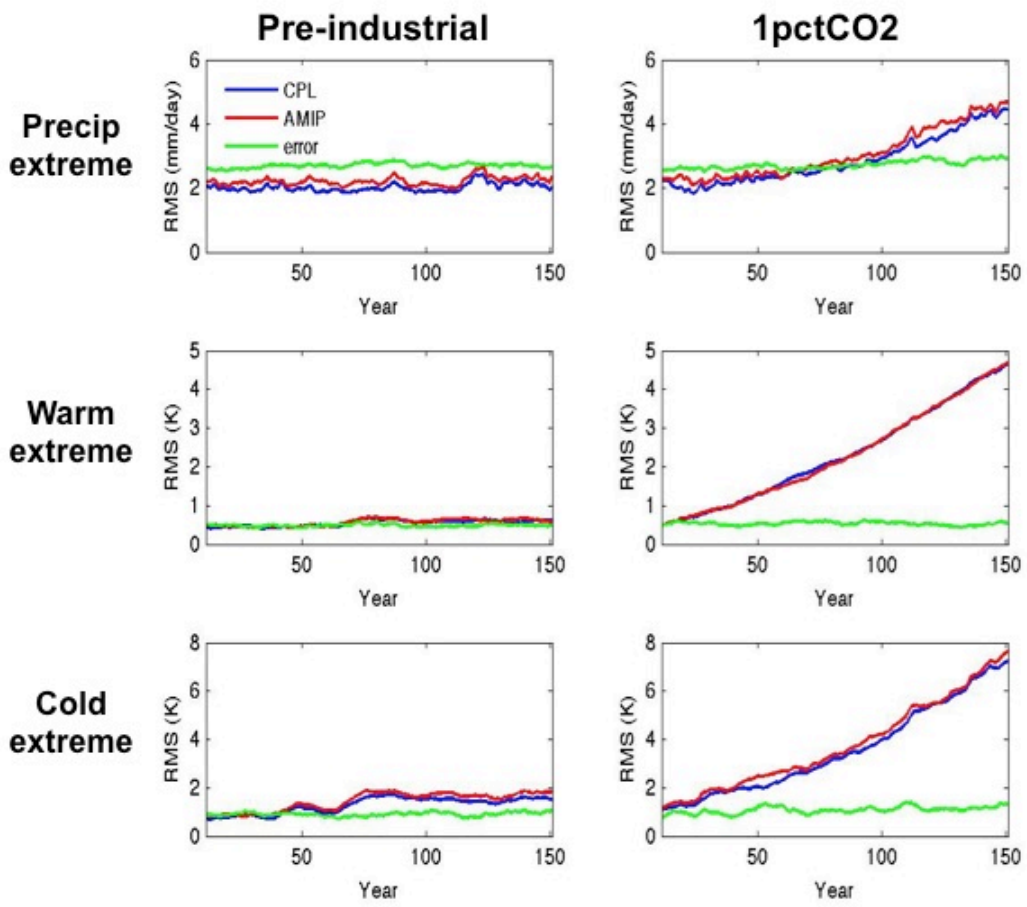

Figure 2.4 Same as Fig. 2.2 but for changes in global precipitation extremes (top), land warm extremes (middle) and land cold extremes (bottom).

Similar to the precipitation extremes, the moving RMS for the land warm extremes, (Fig. 2.4, middle) and land cold extremes (Fig. 2.4, bottom) also shows insensitivity of errors to the external forcing. These evidences indicate that AGCMs are able to reproduce the anthropogenic changes in climate extremes.

2.3.2 Stochastic linear model

The insignificance of coupling with an underlying ocean in the simulation of long-term climate change can be explained using a one-dimensional, stochastic, linear, coupled model. This model is a modified version of that in Barsugli and Battisti (1998,

their Eq. 2.1 and 2.2), which was used to study the effect of ocean coupling on natural climate variability. I kept the air-sea interaction terms and atmospheric stochastic forcing term from the original model and combined the original radiative damping term with an external forcing term to form a model suitable for studying both internally-generated and externally-forced climate change:

$$\frac{dTa}{dt} = \lambda_A (SST - Ta) + F_A + N_A \qquad (2.1)$$

$$\frac{dSST}{dt} = \lambda_O (Ta - SST) + F_O \qquad (2.2)$$

Eq. 1 and 2 are the simplified atmospheric model and ocean model, respectively. Subscript "A" refers to atmosphere, whereas subscript "O" refers to ocean. Ta and SST are the atmospheric temperature anomaly and the sea surface temperature anomaly, respectively, and λ is the linearized coefficient of combined sensible and latent heat flux. The value for λ_A is 23.9×10^{-7} s^{-1} and for λ_O is 12.7×10^{-8} s^{-1}. These coupling coefficients depend on the surface wind speed and stability and are here set to represent the mid-latitudes, following Barsugli and Battisti (1998). The radiative forcing term, F_A and F_O are set to -2.16 W/m^2 and 2.80 W/m^2, based on the radiative energy balance of the atmospheric column and at the ocean surface in the CPL_1pct simulation. N_A denotes the atmospheric Gaussian white noise forcing with a standard deviation of 1.0 K, following Barsugli and Battisti (1998). The time step for integration is set to 6 days. Although this idealized model may have various applications, its purpose here is to provide a simple framework for understanding the basic effects of two-way coupling on long-term climate change. While there is some sensitivity to the parameters, the qualitative analysis presented is valid for a wide range of parameters. For example, to also apply this

idealized model to the tropics, I reduce the coupling coefficients by 1/2 to account for the decrease of surface wind speed from mid-latitudes to the tropics (Wu et al. 2006). I will show results from both the mid-latitude and tropical versions of this model.

The coupled stochastic model was integrated for 600 months. The SST output was then used to force the uncoupled atmospheric model. The only difference between the coupled and uncoupled integrations is that the stochastic forcing is consistent with the SST forcing in the coupled integration but inconsistent with the SST forcing in the uncoupled integration. This results in different paths of the atmospheric temperature change (Fig. 2.5). Furthermore, this inconsistency between the ocean mixed layer and the atmosphere leads to spurious surface energy fluxes (Wu et al. 2006; Chen et al. 2013) and reduces the variance of the atmospheric temperature (Barsugli and Battisti 1998; Bretherton and Battisti 2000). Therefore, the internal variability of atmospheric temperature cannot be perfectly reproduced in the uncoupled simulation. However, the long-term change of atmospheric temperature is the same in the coupled and uncoupled integrations (Fig. 2.5, with a trend of 0.24 K/year). The insensitivity of long-term climate change to the existence of two-way coupling can be easily understood from this simple stochastic model. Because the long-term mean of the stochastic forcing term is zero, the long-term effect of stochastic forcing on the atmospheric temperature is also zero. Therefore, the long-term change in the atmospheric temperature is entirely determined by the atmospheric radiative forcing term and the SST forcing term, which are the same in the coupled and uncoupled integrations. The insignificance of the stochastic forcing term for long-term climate simulation is further shown in Fig. 2.5 (yellow line) by doubling the amplitude of the stochastic forcing term in the uncoupled atmospheric model.

Although the increase of stochastic forcing affects the variability of atmospheric temperature, the long-term trend of atmospheric temperature is unaffected.

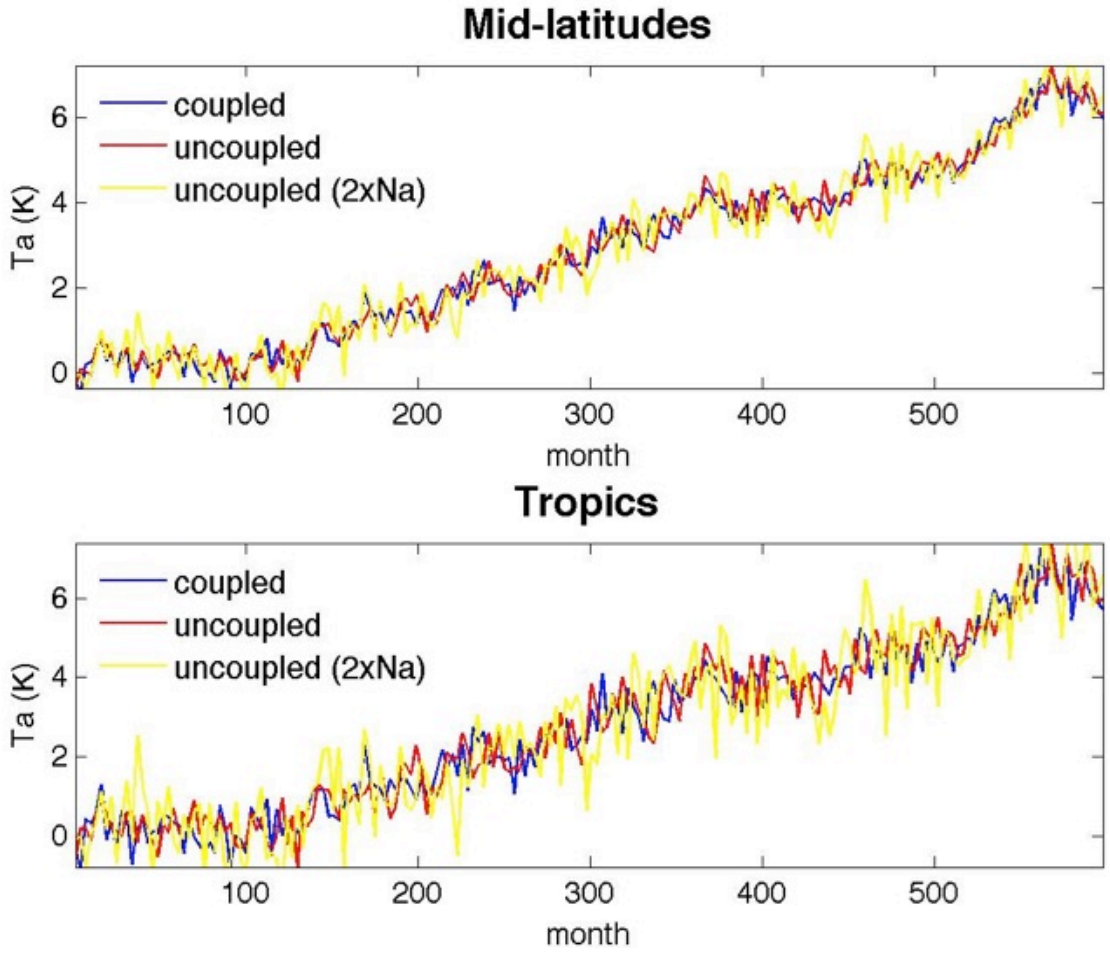

Figure 2.5 Time series of 3-month mean atmospheric temperature anomaly from the one-dimensional stochastic model for the (blue) coupled integration, (red) uncoupled integration and (yellow) uncoupled integration with double stochastic forcing. SST is the same in all three integrations. Top and bottom plots are from the mid-latitude and topical models, respectively.

2.4 Summary and Discussion

This chapter examined the role of two-way coupling in model simulations of anthropogenic changes in both the climatic mean state and climate extremes. Results from the coupled and uncoupled simulations of the CESM showed that errors due to the absence of coupling with an underlying ocean did not change in magnitude or spatial

coverage despite the increase of CO_2. The insensitivity of errors to the intensity of external forcing indicates that errors due to lack of two-way coupling are primarily related to the internal variability instead of externally forced change. A comparison between the coupled and AGCM simulations under pre-industrial conditions showed that the magnitude of errors due to lack of two-way coupling is comparable to the magnitude of decadal variability. However, errors become smaller as the signature of external forcing rises above internal variability and the AGCM successfully reproduced the precipitation change from the coupled simulation at the time of $4xCO_2$. These results justify the use of AGCMs for simulating anthropogenic changes in both the climatic mean state and climate extremes, but one should ensure that the magnitude of anthropogenic climate change is large enough to overcome the errors related to internal variability.

The insignificance of coupling with an underlying ocean in simulations of long-term climate change was explained using a stochastically-forced linear model. Decoupling causes inconsistency between the atmospheric stochastic forcing and the prescribed SST, which affects the simulation of internal climate variability. However, it does not affect the simulation of long-term climate change because the long-term mean contribution of stochastic forcing is zero. The analysis based on the linear model is consistent with the results from the comprehensive model and suggests that the results shown here from the CESM are applicable to all CGCMs. In addition, these results also suggest a greater application of flux-adjusted experiments, which have also been criticized for the lack of energetically consistent surface fluxes.

It is important to note that the insignificance of coupling with an underlying ocean does not imply insignificance of air-sea interaction. In a "perfect AMIP" simulation, the effect of air-sea interaction is partially incorporated in the pattern and magnitude of the prescribed SST changes, albeit in a "one-way" set up. My results show that AGCMs can accurately reproduce the anthropogenic climate change that is a result of such SST change, despite the lack of constraints for energetically consistent surface fluxes. This is in contrast to the behavior of AGCMs in seasonal forecast, in which a lack of two-way coupling could lead to errors even if a perfect SST anomaly is prescribed (e.g., Kumar et al. 2008).

Chapter 3: The Robustness of the Atmospheric Circulation and Precipitation Response to Future Anthropogenic Surface Warming

3.1 Background

Several recent studies have examined the spatial variations in long-term sea surface temperature (SST) change simulated by coupled climate models, especially in the tropics (e.g., Collins 2005; DiNezio et al. 2009; Xie et al. 2010). The response of tropical Pacific SST to global warming is often described as "El Nino-like" (e.g., Yu and Boer 2002; Collins 2005), although more recent studies argued that it could also be described as "equatorial warming" because the meridional SST gradient is more robust in climate models than the zonal SST gradient (Liu et al. 2005; DiNezio et al. 2009; Xie et al. 2010). Changes in the tropical Atlantic SST are also characterized by enhanced equatorial warming, whereas changes in the tropical Indian SST show a dipole pattern (Xie et al. 2010; Zheng et al. 2013), with enhanced warming over the West Indian Ocean.

The response of the tropical SST pattern to increasing CO_2 is important because of its potential impact on global climate through atmospheric teleconnections. Studies using both simplified and complex atmospheric general circulation models (AGCMs) suggested that localized changes in tropical SST alter the upper-level divergence and generate Rossby Waves, which modify extratropical circulation as they propagate poleward (Sardeshmukh and Hoskins 1988; Ting and Sardeshmukh 1993; Schneider et al. 2003). These studies have helped understand the response of extratropical circulation to El Nino. Under global warming, both the pattern and the spatial mean of tropical SST change. Yin and Battisti (2001) showed that changes in the tropical SST pattern are much more important than changes in the tropical mean SST for simulating the extratropical

circulation of the Last Glacial Maximum. However, Lu et al. (2008) showed that the response of the zonal mean circulation to global warming is somewhat opposite of that to El Nino forcing, despite an "El Nino-like" SST response in the tropical Pacific. This suggests that the impact of SST pattern change resulted from global warming should be different than that resulted from natural variability.

Previous studies have shown that large discrepancies exist between the historical tropical SST pattern changes of the past few decades in observations and model simulations, and suggested that these discrepancies may add large uncertainties to our understanding of future circulation change (Liu et al. 2005; Xie et al. 2010; Shin and Sardeshmukh 2011). For example, Shin and Sardeshmukh (2011, SS11 thereafter) showed that the warming pattern of tropical oceans is the key to simulating the circulation trend of the second half of the 20^{th} century over the landmasses around the North Atlantic Ocean (their Fig. 7). However, according to Deser et al. (2012), climate changes on multi-decadal time scales are dominated by internal variability. Therefore, the role of the tropical ocean warming pattern is expected to change as the signature of global warming becomes large enough to rise above the internal variability. The purpose of the present study is to understand the circulation response to the pattern of SST change as a result of increased CO_2 instead of internal variability. This study will achieve this by imposing a large warming signal (a 4K global mean SST increase), which is significantly larger than the amplitude of any known internal variability.

This chapter investigates the impact of the pattern of future SST change on atmospheric circulation by comparing AGCM simulations forced with a uniform SST increase and a structured SST increase using the pattern expected from future increases in

CO_2. As shown in the previous chapter, AGCMs are able to perfectly reproduce coupled simulations of anthropogenic climate change despite the lack of coupling with an underlying ocean, which lends credence to this approach.

3.2 Model Simulations

This chapter analyzes AGCM simulations that were performed as part of the Coupled Model Intercomparison Project, phase 5 (CMIP5). The AGCM simulations are 1) the control simulation (AMIP_ctrl), which was run from year 1979 to year 2008 forced with observed monthly mean SST and sea ice concentration, 2) the uniform SST increase simulation (AMIP_mean), which is the same as CTRL except adding a uniform +4K SST anomaly, 3) the structured SST increase simulation (AMIP_future), which is the same as CTRL except adding the SST anomalies as the composite of the SST responses taken from the "1pctCO2" coupled model CMIP3 experiments at the time of CO_2 quadrupling. The characteristics of the SST anomalies in the AMIP_future are described in Section 3.1.

Nine AGCMs are used: bcc-csm1-1, CanAM4, CNRM-CM5, HadGEM2-A, IPSL-CM5B-LR, MIROC5, MPI-ESM-LR, MPI-ESM-MR and MRI-CGCM3. All models were run with one realization. Details about the model simulations can be found at http://cmip-pcmdi.llnl.gov/cmip5/getting_started_CMIP5_experiment.html. Model data and description can be found at http://pcmdi3.llnl.gov/esgcet/home.htm.

Circulation changes due to uniform (structured) SST increase are defined as the climatological difference between the uniform (structured) AGCM and CTRL. The circulation changes are normalized by each model's global mean surface temperature

change and then averaged across models to yield a multi-model ensemble mean, in order to avoid dominance by models with large climate sensitivity. I present my results based on annual mean but my main conclusions do not depend on the season.

3.3 Results

The main result is that the atmospheric circulation is very insensitive to the pattern of future SST change, except over the deep tropical oceans. The effect of the pattern of SST change is most pronounced in tropical ocean precipitation change because the largest precipitation change occurs at the equator (Fig. 3.1, middle). This is consistent with previous studies (Xie et al. 2010; Ma et al. 2012; Ma and Xie 2013). As shown in Table 3.1, the precipitation – SST correlation is positive but small in the tropics and negative in the extratropics, indicating that changes in SST pattern could be important in certain tropical regions but insignificant at a global scale. Compared to oceanic precipitation, land precipitation (Fig. 3.1, right) and other atmospheric variables are even more insensitive to the pattern of future SST change. Table 3.1 shows the ensemble mean spatial correlation of AMIP_mean and AMIP_future response for land precipitation, sea level pressure (SLP) and 500-hPa vertical pressure velocity (ω500). The response of the atmospheric circulation to the uniform and structured SST increase is very similar in the tropics and almost identical in the extratropics, indicating the insensitivity of atmospheric circulation response to the pattern of SST change.

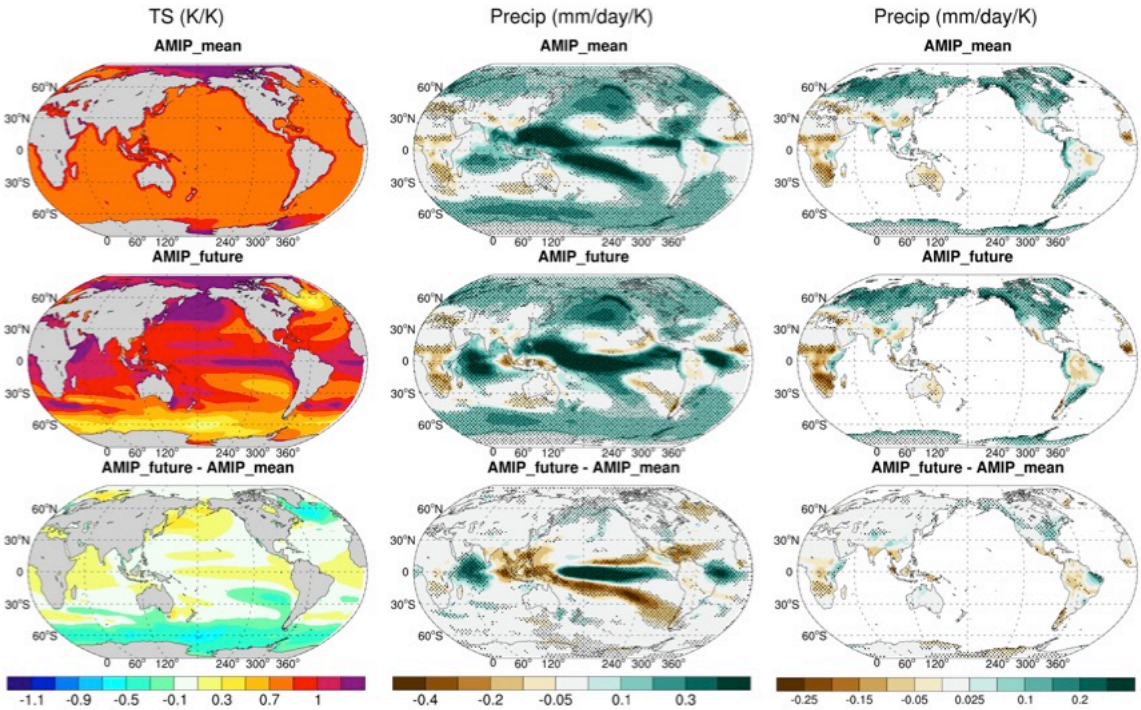

Figure 3.1 Ensemble mean changes in annual mean surface temperature (left) precipitation (middle) and land precipitation (right) for AMIP_mean (top), AMIP_future (center) and the difference between AMIP_mean and AMIP_future (bottom). All fields are normalized by the change in global mean surface temperature before ensemble averaging. Areas where at least 8 (out of 9) models agree on the sign of changes are stippled.

	Land Precip	SLP	ω500	Precip VS SST		Precip	ω500
	uniform VS structured	uniform VS structured	uniform VS structured	struct ured		uniform VS structured	uniform VS structured
Global	0.82	0.94	0.79	0.14	Pacific	0.48	0.62
Tropics	0.74	0.72	0.75	0.28	Atlantic	0.68	0.76
Extratropics	0.90	0.96	0.89	-0.04	Indian	0.58	0.74

Table 3.1 Multimodel mean of spatial correlation between the responses in AMIP_mean and AMIP_future response for global, tropics (30°S to 30°N), extratropics (poleward of 30°S and 30°N) and each tropical basin.

To compare with the work of SS11, which showed a large sensitivity of regional land precipitation to the observed pattern of SST change in the second half of the 20th century (their Fig. 7), I examine the global pattern of land precipitation changes in the uniform and structured simulations (Fig. 3.1, right). Note that the mean tropical SST increase in my simulations (4K) is about 9 times as large as that of SS11 (0.43K).

Contrary to SS11, the global pattern of precipitation over land is very insensitive to the pattern of SST change under increased CO_2. This suggests that either the response of the circulation becomes less sensitive to the pattern of SST change as the magnitude of the mean warming increases, or that pattern of warming used in SS11 – the observed warming from the second half of the 20th century – is more strongly influenced by internal variability rather than increasing CO_2. It further implies that the circulation responds differently to these two types of surface temperature changes, being more sensitive to the pattern of the response for internal variability compared to increased CO_2.

3.3.1 Tropics

The annual mean ω500 responses (δω500) to uniform and structured SST increase are dominated by their common features (Fig. 3.2, left). The forcing from both types of SST change reduces convection at the major climatological convective regions, namely south-central Africa, Indonesia and the Amazon rainforest. Also common in the two δω500 is the anomalous convection at the northern flank of convective regions and southeast Pacific. These common features, to the first order, are consistent with a weakening of the mean atmospheric circulation (e.g., Held and Soden 2006; Vecchi and Soden 2007). This weakening is a robust feature of all climate models and reflects the disparity between the rate at which water vapor and precipitation increase in a warming climate. Atmospheric moisture increases by about 7% per degree warming, whereas precipitation only increases at about 2% per degree warming, due to constraints imposed by the rate of atmospheric radiative cooling (Allen and Ingram 2002; Stephens and Ellis 2008). This means the upward mass flux, should weaken by about 5% per degree

warming. This argument does not rely on the pattern of SST change but simply the mean warming.

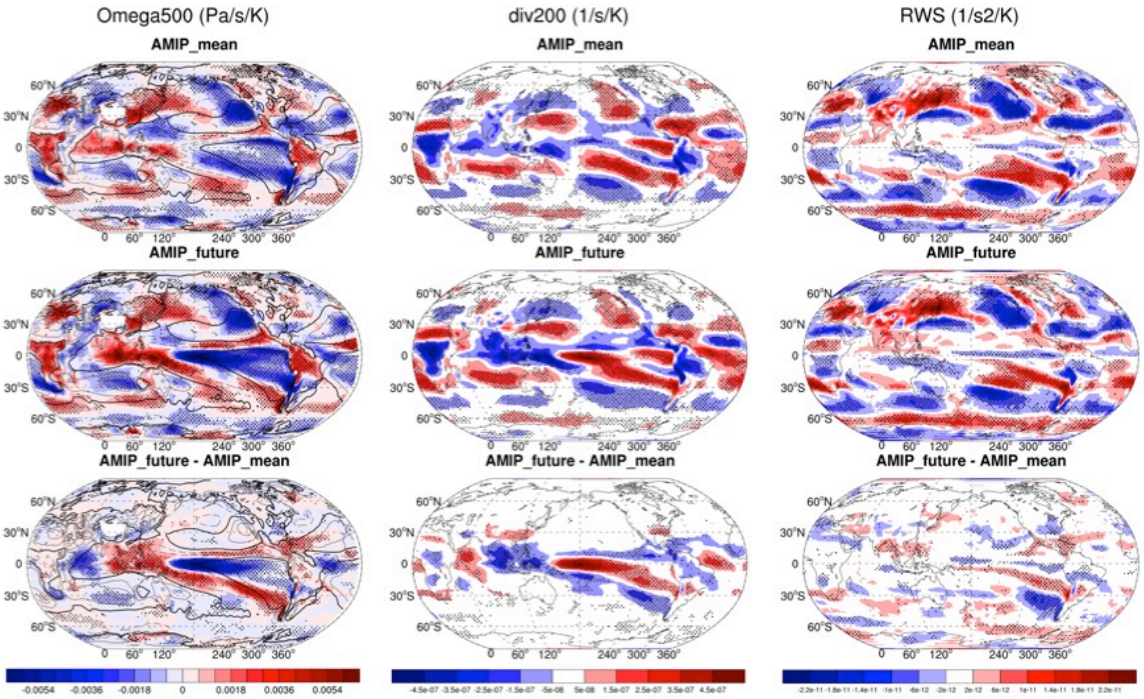

Figure 3.2 Same as Fig. 3.1, except for ω500 (left), 200mb divergence (middle) and RWS (right). The contours in the left column represent the climatological ω500; contour interval is 0.03 Pa/s. The zero contours are thickened. Dashed lines are for negative values.

As shown in Figure 3.2, δω500 (shading) in the tropics generally opposes the pattern of climatological ω500 (contour), consistent with a uniform weakening of the mean circulation. In the tropics this pattern of weakening has been attributed to the mean advection of the increased static stability (Ma et al. 2012). However, noticeable differences between the pattern of change and climatology do exist, especially outside of the tropics. The spatial correlation between climatological ω500 and δω500 is -0.43 and -0.48 for AMIP_mean and AMIP_future, respectively. Note that the spatial correlation between uniform and structured δω500 is 0.77. Therefore, part of the common features of tropical circulation change is likely caused by mechanisms other than the global energetic

constraints, such as changes in moisture and temperature advection and changes in convection height (Chou and Neelin 2004; Chou et al. 2009).

The differences in δω500 between AMIP_future and AMIP_mean are mostly confined at the equatorial oceans, including anomalous equatorial convection over the Pacific and Atlantic Ocean, anomalous subsidence over south Pacific and a dipole pattern over the Indian Ocean. These differences reflect the local changes in SST pattern (Fig.1, left), with warmer (colder) surface associated with anomalous convection (subsidence), consistent with Xie et al. (2010). The spatial correlation of δω500 between AMIP_mean and AMIP_future for each tropical basin (Table 3.1) shows that the impact of SST pattern change is the largest over the tropical Pacific Ocean and smallest over the tropical Atlantic Ocean. The δω500 correlation is 0.67 for the entire tropical ocean, which is larger than the precipitation correlation (0.55), a result expected from the cancellation between the slowing down of tropical circulation and the increase in moisture (Chadwick et al. 2013). The spatial correlation is higher for tropical land (0.87 for δω500 and 0.76 for precipitation change) than tropical ocean, indicating that the impact of SST pattern change does not extend much to land.

3.3.2 Extratropics

As shown in Table 3.1, changes in the annual mean extratropical circulation are almost identical between the AMIP_mean and AMIP_future simulations. Changes in extratropical SLP and stream function in both AGCM and coupled simulations feature a deepening of the Aleutian Low, a positive shift in the North Atlantic Oscillation and a positive shift in the Southern Annular Mode (Fig. H in supplementary material). These

common features of SLP changes have also been found in observations and other model simulations of climate trends of the past half-century (e.g., Schneider et al. 2003; Deser and Phillips 2009).

As shown in Fig. 3 (right), outside of the tropics the changes in circulation are not simply a weakening of the mean circulation, suggesting that other mechanisms are responsible for the similarity in the extratropical circulation change between the two AGCM simulations. Here, I hypothesize that the land and extratropical similarity may reflect the insensitivity of Rossby Wave generation to the pattern of SST changes in the tropics. Previous AGCM studies have shown that extratropical circulation is insensitive to local SST changes but are mostly influenced by tropical SST changes (e.g., Schneider et al. 2003; Schubert et al. 2004; Deser and Phillips 2009). The mechanism by which tropical SST variations influence extratropical circulation is through the poleward dispersion of Rossby Waves forced by tropical upper-level divergence (e.g., Sardeshmukh and Hoskins 1988; Ting and Sardeshmukh 1993; Schneider et al. 2003).

The similarity of land and extratropical circulation change is further explored by comparing the Rossby Wave generation in the AMIP_mean and AMIP_future simulations. Following Sardeshmukh and Hoskins (1988), the non-linear, frictionless Rossby Wave equation at upper troposphere can be written as

$$\frac{\partial \varsigma}{\partial t} + V_\psi \cdot \nabla \varsigma = -\varsigma \cdot D - V_\chi \cdot \nabla \varsigma \,. \qquad (3.1)$$

Here V_ψ and V_χ are the rotational wind and divergent wind, respectively. ς is the absolute vorticity. D is the divergence. The right hand side of Eq. 3.1 is generally considered as the Rossby Wave Source (RWS), which is often used to quantitatively

define the origin of Rossby Waves (e.g., Jin and Hoskins 1995; Kirtman et al. 2001). The change in RWS in response to global warming can be written as

$$RWS' = (-\varsigma \cdot D - V_\chi \cdot \nabla\varsigma)', \qquad (3.2)$$

which is dominated by $-\varsigma \cdot D'$. Therefore, changes in upper-level divergence are what essentially drive changes in RWS.

$$RWS' = -\varsigma \cdot D'. \qquad (3.3)$$

Changes in 200-hPa divergence field (Fig. 3.2, middle) generally follow δω500, with divergence (convergence) generated where δω500 is negative (positive). Overall, the 200-hPa divergence response is very similar in the AMIP_mean and AMIP_future simulations. Most differences between the AMIP_mean and AMIP_future simulations are near the equator.

According to Eq. 3.3, there must be large enough local absolute vorticity to cause RWS change. Near the equator, the planetary vorticity is close to zero and the relative vorticity is small because of weak wind shear. Therefore, very little RWS change is generated at the equator, despite large local divergence change (Fig. 3.2, right). The difference in the divergence change due to uniform and structured SST increase, which is mostly near the equator, is not efficiently transformed into a change in RWS. As a result, changes in RWS in the AMIP_mean and AMIP_future simulations are almost identical, with an ensemble mean global spatial correlation of 0.89. The insensitivity of the Rossby Wave generation to the pattern of SST change in the tropics is evident by comparing the pattern of RWS changes in the AMIP_mean and AMIP_future simulations (Fig. 3.2, right).

3.4 Summaries and Discussion

This chapter has shown that the atmospheric circulation is insensitive to SST pattern change by comparing AGCM simulations forced by uniform and structured SST increase. The structured SST increase is calculated from the response of an ensemble of coupled ocean-atmosphere models to increased CO_2. It features equatorial warming in the Pacific and Atlantic Ocean and a dipole pattern in the Indian Ocean as well as a polar amplification in the northern high latitudes. All nine AGCMs show that the response of atmospheric circulation to uniform and structured SST increase is very similar, with ensemble mean spatial correlation of about 0.75 in the tropics and 0.9 in the extratropics. This indicates a less significant impact of the SST pattern change compared to the global mean warming. In the tropics, the effect of SST pattern change is mostly confined in the deep tropical oceans, where enhanced warming increases convection. This "warmer-get-wetter" effect was shown in previous studies Xie et al. (2010) and is important in regard to changes in regional precipitation. Overall, the tropical circulation change is determined by a weakening of the mean circulation, with exceptions over deep tropical oceans. The mechanism by which tropical SST variations influence extratropical and land circulation is likely through the generation of Rossby Waves, which can be approximately quantified as the product of upper-level divergence change and absolute vorticity. The upper-level divergence change is very similar in the AMIP_mean and AMIP_future simulations. The difference in divergence change caused by changes in SST pattern is mostly at the equator where the absolute vorticity is small and therefore cannot be efficiently transformed into RWS.

Previous studies have suggested an important role of SST pattern change in determining regional climate change over land in the second half of the 20th century (e.g., Shin and Sardeshmukh 2011). The present study shows that such dependence is not present in model projections of future climate change due to increasing CO_2. Results from the CMIP5 data suggest that the atmospheric circulation is insensitive to the pattern of future SST change. This insensitivity supports the recent findings of Deser et al. (2012) that regional climate changes on multi-decadal time scales are dominated by internal variability rather than increasing CO_2. Based on the results in this paper, most of the future circulation change over land is a result of global mean warming instead of the pattern of SST change and we should have confidence in the pattern of future circulation change over land without full knowledge of the pattern of SST change.

Chapter 4: The Impact of SST Biases on Projections of Anthropogenic Climate Change: A Greater Role for Atmosphere-only Models?

4.1 Background

There is growing demand by the scientific community, policy makers and stakeholders for realistic projections of anthropogenic climate change. The main tools for such an endeavor are the coupled ocean-atmosphere models (CGCMs). However, global CGCMs are typically run at resolutions that are too coarse to adequately represent many processes that can influence regional changes in climate (e.g., mesoscale processes associated with sharp topographic variations and complex coastlines; Pielke and Wilby 2012; Hertwig et al. 2015; Zarzycki et al. 2015). In addition, by allowing the ocean to evolve freely, current CGCMs often contain systematic ocean biases (Fig. 4.1). Recent studies have shown that these biases undermine the CGCMs' skillfulness in seasonal climate predictions (Vecchi et al. 2014; Jia et al. 2015). Because many aspects of the changes in regional climate depend upon the unperturbed climatology (e.g., Held and Soden 2006; Scheff and Frierson 2012; Huang et al. 2013), climatological biases in CGCMs can lead to unrealistic projections of anthropogenic climate change. However, the full importance of having an unbiased climatology for the projection of anthropogenic climate change has been insufficiently addressed and possibly underappreciated.

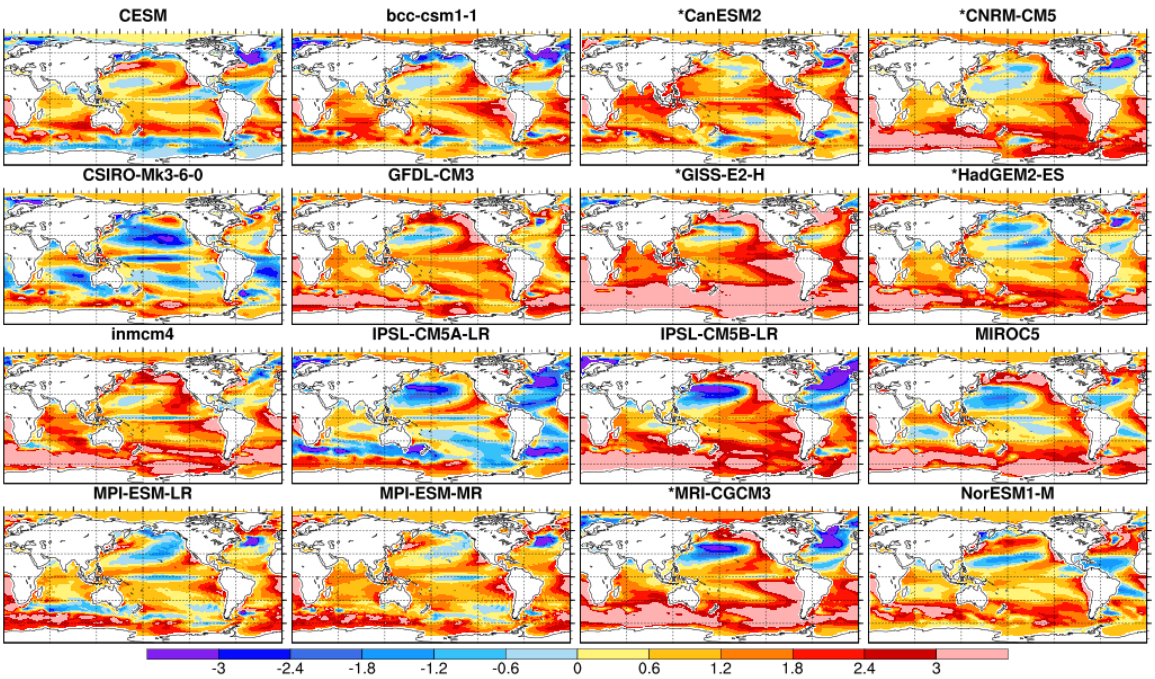

Figure 4.1 SST climatology biases in the CESM model and the 15 CGCMs from CMIP5. An asterisk indicates that the model's climatological SST is taken from the historical simulation (year 1982-2011). For the rest of the models, climatological SST is taken from the 1pctCO2 simulation during year 11-40 when the CO_2 level is similar to the observation during 1982 to 2011.

In comparison, atmosphere-only models (AGCMs) can be run at much higher spatial resolutions and can incorporate the best estimate of climatological SSTs from observations. Nevertheless, the current projections of anthropogenic climate change are primarily based on CGCM simulations under the assumption that the inclusion of full air-sea coupling to allow for a dynamic prediction of the SST change is crucial for the simulation of anthropogenic climate change. This study shows that having an unbiased climatological SST is more beneficial than a fully simulated pattern of SST change and implies that AGCMs are generally more skillful than CGCMs in the projection of anthropogenic climate change over land. This chapter focuses on global land regions, where the societal demand for accurate regional predictions is the greatest and where ocean coupling has the least impact on model simulations, as demonstrated in the previous chapter.

Note that there are other options for improving regional predictions and reducing climatological biases in SSTs, such as nested or stretched grid models (e.g., Zheng and Weisberg 2012; Talandier et al. 2014) and flux-adjusted coupled models (e.g., Magnusson et al. 2013; Vecchi et al. 2014). The goal is not to exclude any particular modeling framework, nor do I intend to diminish the importance or necessity of CGCMs. Rather this chapter examine the relative importance of having precise predictions of changes in the atmospheric boundary conditions (i.e., SSTs) versus having precise climatology of those boundary conditions. I believe that better qualifying and understanding this distinction will help to improve projections in all modeling frameworks and to optimize the selection of the most appropriate framework.

4.2 Data and Simulation

4.2.1 Individual impact of the forcing agents

I use an ensemble of 30-year AMIP simulations archived in CMIP5 to evaluate the relative impact of direct CO_2 forcing, global mean SST warming and the pattern of SST warming. These simulations are 1) AMIP_4xCO2 simulation, in which the atmospheric CO_2 concentration is quadrupled, 2) AMIP_4K simulation, in which a uniform 4K SST anomaly is prescribed and 3) AMIP_Future simulation, in which a structured SST warming is prescribed as the composite of the SST responses taken from the coupled model CMIP3 experiments at the time of CO_2 quadrupling. To ensure that the magnitude of forcing in the AMIP simulations match that in a coupled simulation, climate changes in the AMIP simulations are first scaled linearly to match the CO_2 and tropical SST forcing in the 1pctCO2 simulations. Specifically, the changes from the

quadrupled AMIP_4xCO2 simulation are multiplied by a factor of 3.3/4.0 to match the CO_2 increase in the 1pctCO2 simulation (where CO_2 increases by a factor of 3.3 between years 1 and 120); i.e., I assume that the climate responds linearly to increasing CO_2. I subtract AMIP_4K from AMIP_Future to get the response from the pattern of SST change. Finally, climate change is normalized by each model's global mean surface temperature change in the 1pctCO2 simulation. Nine models are used (as described in Section 3.2).

4.2.2 Model simulations with CESM

I conduct a suite of simulations with the Community Earth System Model (CESM, Hurrell et al. 2013) to assess the relative importance of climatological SST and the pattern of SST change. The fully coupled simulation is run with the 1pctCO2 scenario starting with the pre-industrial CO_2 concentration. The base climate is defined as year 11 to 40 when the CO_2 level is similar to the observation during 1982 to 2011, whereas the perturbed climate is defined as year 131 to 160. The "obsSST" simulation is run with the same CO_2 and SST anomaly as the fully coupled simulation but uses the merged Hadley-NOAA/OI SST (Hurrell et al. 2008) from year 1982 to 2011 as the climatological SST. The "modelSST" simulations are run with the same CO_2 and SST anomaly as the fully coupled simulation but use the historical SST (year 1982 to 2011) from five CMIP5 CGCMs: CanESM2, CNRM-CM5, GISS-E2-H, HadGEM2-ES and MRI-CGCM3. These five CGCMs are taken because they provide extended historical simulation to year 2011, whereas the other CGCMs generally stop at year 2005. The "uniform AGCM" simulation is run with a uniform SST warming calculated as the global mean SST change from the

fully coupled simulation. The “ensemblePattern” and “modelPattern” simulations are run with the SST anomaly from CMIP5 ensemble mean and the five individual CGCMs, respectively. The “uniform AGCM”, the “ensemblePattern” and the “modelPattern” simulations all use the climatological SST from the fully coupled simulation. All AGCM simulations are run for 34 years with the first 4 years discarded. All simulations are run with an approximate 2^{o} resolution for the atmospheric model.

4.2.3 Internal precipitation variability in the AMIP simulations from CMIP5

Due to the lack of multiple realizations for the AMIP simulations in CMIP5, it is not possible to quantify internal precipitation variability directly. Here I estimate the internal precipitation variability over land by using the pre-industrial control simulation and accounting for the contribution from ocean.

Internal variability from the pre-industrial control run is calculated as the difference between two non-overlapping 30-year segments. But this should not be the same as the internal variability in the AMIP simulations, which has no SST variability. To assess the contribution from the SST variability, I use the CESM large ensembles, which include a coupled 1100-year pre-industrial control simulation and an uncoupled 1100-year simulation forced with the climatological SST from the coupled simulation (Kay et al. 2014). As shown in Figure 4.2, land precipitation variability at multi-decadal (50 to 100 years) timescale is not heavily influenced by SST variability. Based on the ratio of precipitation variance at multi-decadal timescale between the coupled and uncoupled CESM simulation, I estimate that the RMS of internal precipitation variability

over land in the AMIP simulations is about 91.9% of that in the pre-industrial control simulation.

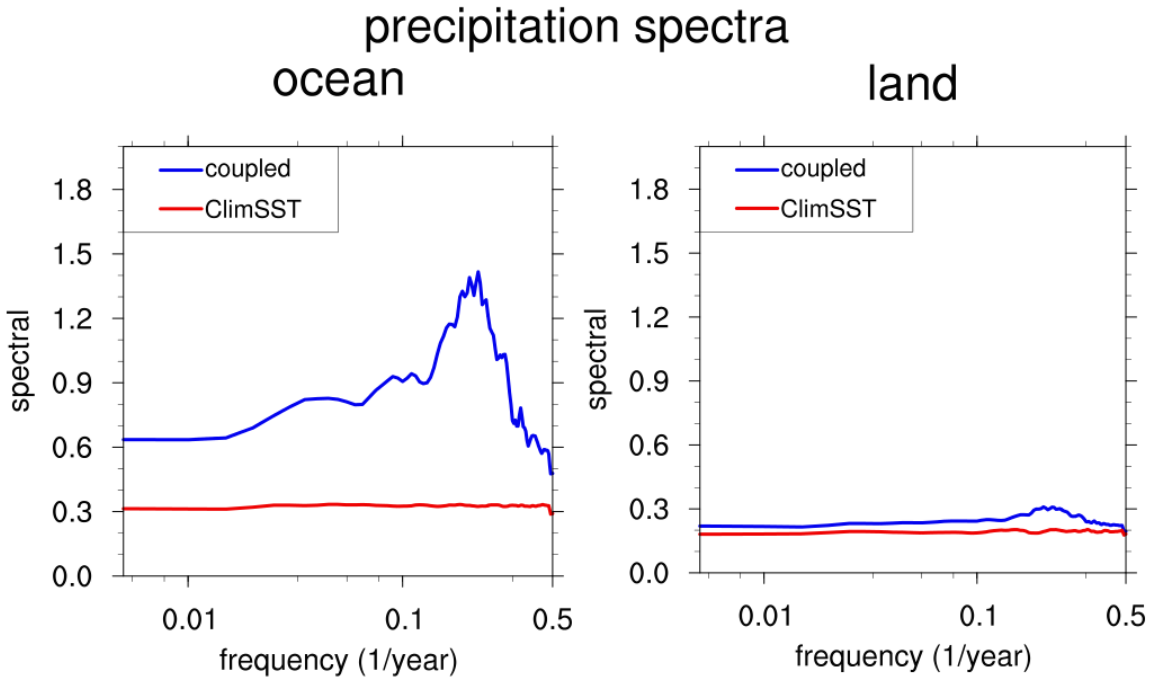

Figure 4.2 Precipitation power spectra averaged over ocean and land from the CESM large ensembles. Blue lines represent the coupled simulation, whereas red lines represent the uncoupled simulation forced with climatological SST. The power spectra are calculated as the average of 10 overlapping 200-year segments.

4.3 Results

In a typical global warming simulation, the atmosphere-land model is driven externally by two sources of forcing: the direct atmospheric radiative forcing, which is mainly due to the increasing CO_2, and the warming of the ocean surface, which can be separated into the global mean warming and the pattern of warming. While the CO_2 concentration and the global mean warming are relatively easy to determine, the pattern of SST change is much more uncertain (Ma and Xie 2013) and its simulation requires the incorporation of the ocean model.

I first assess the influence of the pattern of SST change on land climate change by comparing the relative impacts of direct CO_2 forcing, mean SST warming and pattern of SST change. Figure 4.3 shows the ensemble mean RMS of precipitation change driven by each forcing agent calculated from the CMIP5 models. Over ocean, the pattern of SST change is very important as it drives precipitation locally through the "warmer-get-wetter" mechanism (e.g., Xie et al. 2010; Ma and Xie 2013). Over land, however, the pattern of SST change is much less impactful compared to the direct CO_2 forcing and the mean SST warming. The magnitude of land precipitation change caused by the pattern of SST change (with internal variability subtracted) is less than 20% of that due to the mean SST warming. In addition to precipitation, the atmospheric circulation over land is also insensitive to the pattern of SST change, which can be explained by the insensitivity of Rossby wave generation to the anthropogenically-forced patterns of SST change (as demonstrated in the previous chapter).

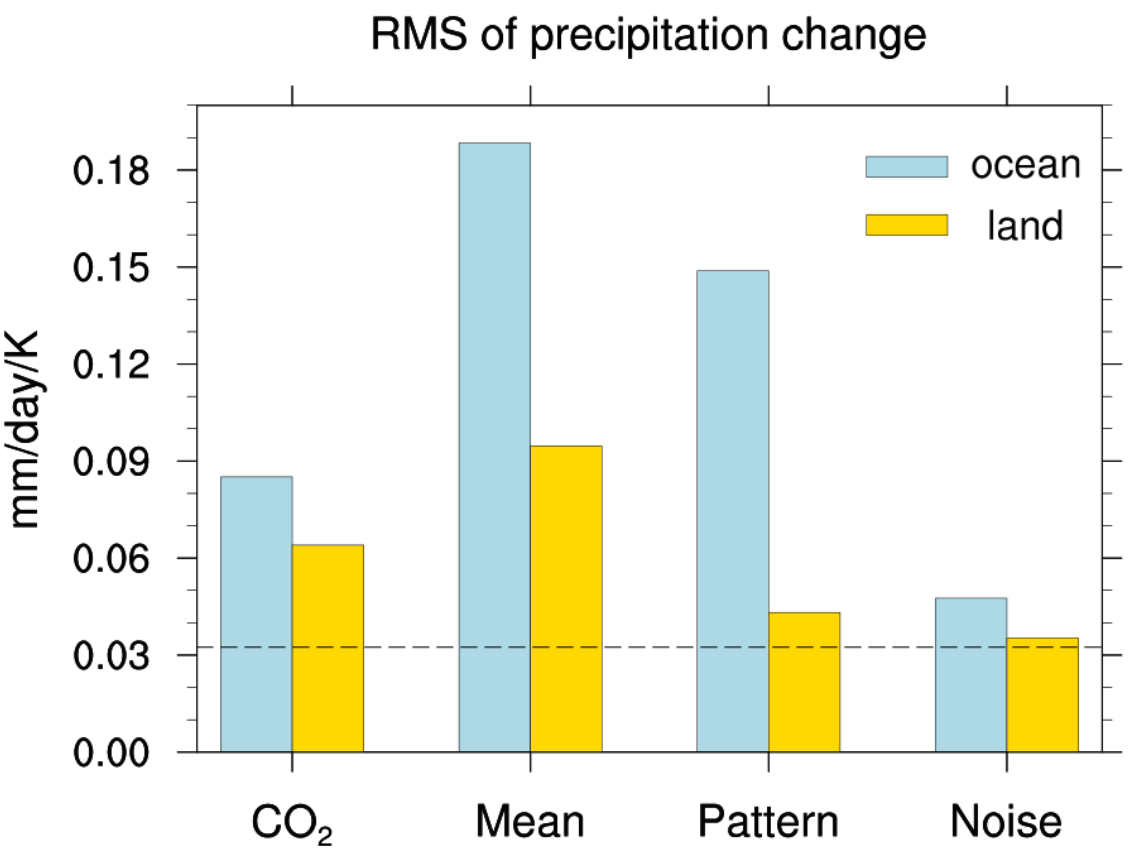

Figure 4.3 CMIP5 ensemble mean RMS of precipitation change associated with the direct CO_2 forcing, global mean SST warming and the pattern of SST change. Ensemble mean RMS of internal precipitation variability (noise) calculated from the pre-industrial control simulation is plotted for reference. Dashed line indicates the estimated RMS of internal precipitation variability over land for the AMIP simulations (Section 4.2.3). Blue represents changes over ocean, whereas yellow represents changes over land.

The insignificance of the pattern of SST change suggests the possibility of projecting land climate change with AGCMs, since the basic structure of this pattern is generally robust and has not evolved substantially over the past few generations of CGCMs (Fig. 4.4). Moreover, while the use of AGCMs for seasonal forecasts is often criticized due to the lack of energetically consistent surface fluxes, Chapter 2 showed that this does not pose an issue for the projection of anthropogenic climate change. Here, I build on this insight and use the CESM model to demonstrate that the anthropogenic

climate change can be well simulated by AGCMs that are only forced with a uniform SST warming and increasing CO_2 (uniform AGCMs).

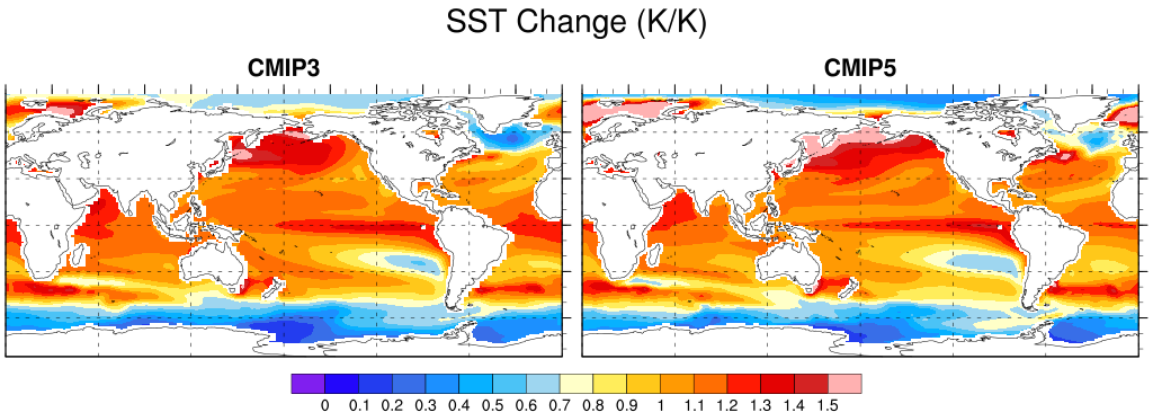

Figure 4.4 Ensemble mean changes in SST from CMIP3 and CMIP5 taken from the 1pctCO2 simulation. Changes are normalized by each model's global mean SST change before averaged across models.

As shown in Figure 4.5 (left), the change in precipitation over land is very similar in the fully coupled simulation and the uniform AGCM, with a spatial correlation of 0.82. Although discrepancy exists over certain regions (e.g., the Eastern China and the central East Africa, Kent et al. 2015), the magnitude and structure of precipitation is almost identical over most land regions. The similarity between the fully coupled simulation and the uniform AGCM is also evident in land surface temperature change and sea level pressure (SLP) change Figure 4.5 (middle and right). The fact that even the extreme case of a total removal of the pattern of SST change shows reasonable skillfulness further suggests that the simulation of a structured SST change should not be a priority for the projection of land climate change and that CGCMs may be less advantageous than the computationally more efficient AGCMs.

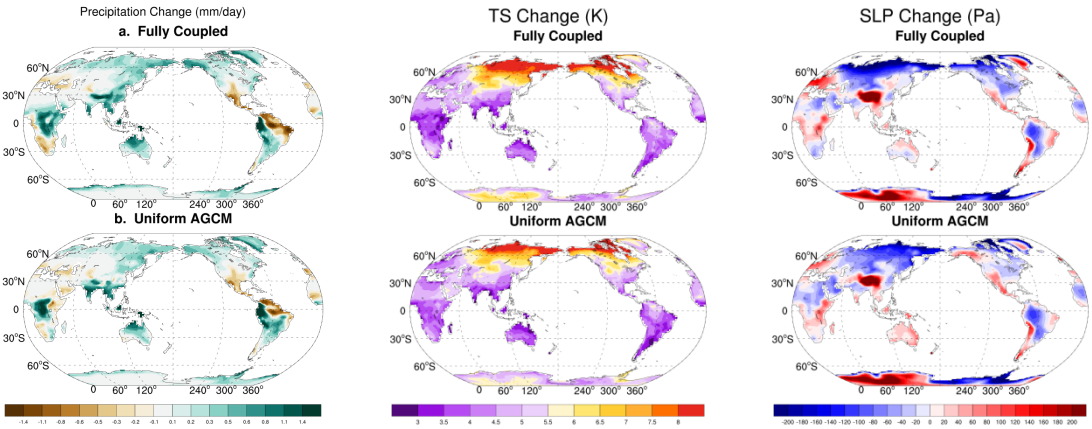

Figure 4.5 Changes in land precipitation (left), surface temperature (middle) and SLP (right) from the CESM simulations. (top) the fully coupled simulation and (center) the uniform AGCM simulation. The spatial correlation between the fully coupled and uniform AGCM simulations is 0.82, 0.96 and 0.91 for precipitation, surface temperature and SLP, respectively.

On the other hand, the projections from CGCMs may be deteriorated by the biases in the models' climatology. Previous studies have shown that many spatial structures of anthropogenic climate change are positioned relative to the structures of the climatology (e.g., Held and Soden 2006; Scheff and Frierson 2012; Huang et al. 2013). Here, I calculated the cross-model correlation of CGCMs' simulations of precipitation climatology and the corresponding projections of precipitation change (Fig. 4.6). Overall, models that have more similar precipitation climatology have more similar precipitation change. This further demonstrates the importance of having an accurate climatology for the prediction of climate change. Because the climatology of most atmospheric variables largely depends on the underlying SST, the correction of SST biases should substantially improve climate projections.

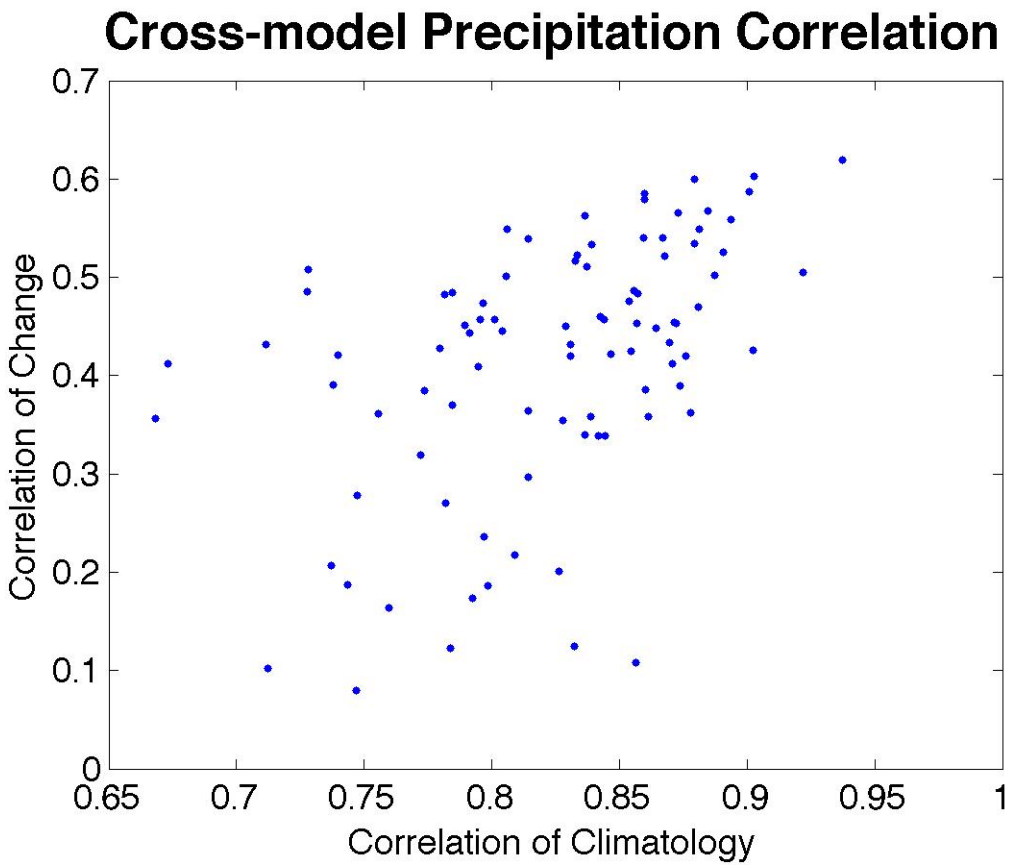

Figure 4.6 Scatter plot of cross-model spatial correlation of global precipitation climatology versus the corresponding spatial correlation of the change in precipitation. The positive correlation indicates that a higher degree of similarity in precipitation climatology generally leads to a higher degree of similarity in projected change in precipitation. 14 CGCMs from the CMIP5 1pctCO2 experiment are analyzed: bcc-csm1-1, CanESM2, CCSM4, CNRM-CM5, CSIRO-Mk3-6-0, GFDL-CM3, GISS-E2-H, HadGEM2-ES, inmcm4, IPSL-CM5B-LR, MIROC5, MPI-ESM-LR, MRI-CGCM3 and NorESM1-M.

To examine the relative importance of climatological SST compared to the pattern of SST change, I calculated the spatial correlation of some key variables between simulations in which either the climatological SST or the pattern of SST change is altered (Fig. 4.7). I first use the CESM model to compare the impact of model biases in the climatological SST and the impact of model biases in the pattern of SST change, which is defined as the deviation from the CMIP5 ensemble mean pattern of SST change. As illustrated in the scatter plot of Figure 4.7a, almost all variables show a correlation below

the diagonal line, which indicates that biases in the climatological SST has greater impact on the projected changes in the variables than differences in the pattern of SST change.

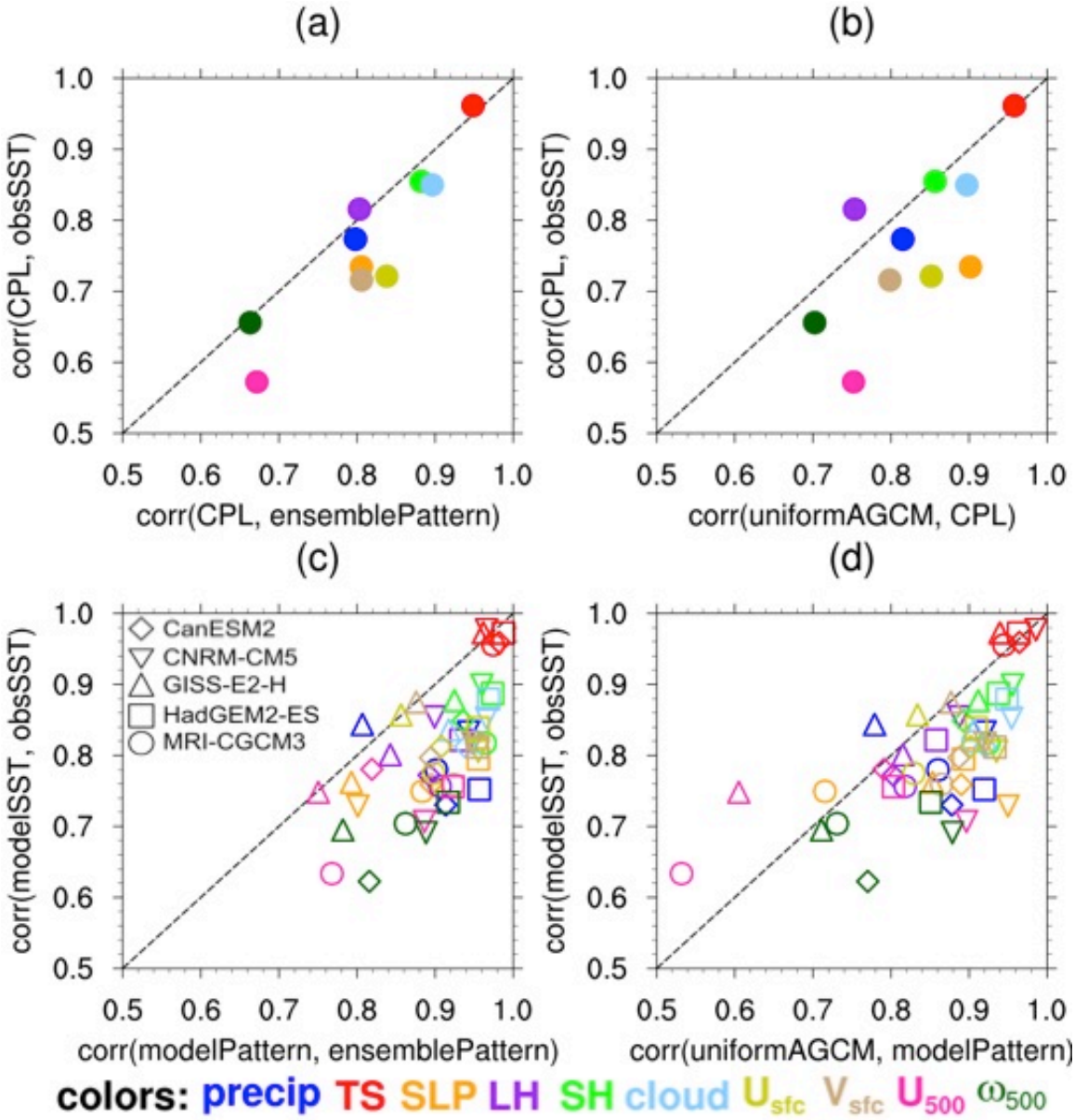

Figure 4.7 Scatter plots of spatial correlation between simulations with different climatology versus simulations with different pattern of SST change. The spatial correlation is calculated for land only. Colors indicate variables, which are precipitation, surface temperature, sea level pressure, surface latent heat, surface sensible heat, total cloud cover, surface U, surface V, 500mb U and 500mb vertical pressure velocity. The markers in (c) and (d) annotate the CGCMs from which the climatological SSTs and the patterns of SST change are taken.

Note that the CESM model has medium biases in climatological SST and relatively large biases in the pattern of SST change compared to the other CMIP5 models (Table 4.1). This suggests that incorporating the observed climatological SST should be more beneficial than improving the simulation of the pattern of SST change for projecting anthropogenic climate change over land. Figure 4.7b offers a complementary perspective to Figure 4.7a and shows that even the extreme case of a total removal of the pattern of SST has less impact than biases in the climatological SST.

	Global		Tropical (30°S-30°N)	
	Clim SST	δSST	Clim SST	δSST
CESM	0.991	0.57	0.92	0.60
bcc-csm1-1	0.992	0.76	0.92	0.81
*CanESM2	0.994	0.86	0.95	0.82
*CNRM-CM5	0.991	0.57	0.91	0.68
CSIRO-Mk3-6-0	0.992	0.72	0.94	0.74
GFDL-CM3	0.995	0.84	0.94	0.90
*GISS-E2-H	0.986	0.68	0.87	0.71
*HadGEM2-ES	0.993	0.81	0.94	0.90
inmcm4	0.990	0.59	0.91	0.43
IPSL-CM5A-LR	0.989	0.87	0.91	0.78
IPSL-CM5B-LR	0.978	0.65	0.85	0.82
MIROC5	0.991	0.85	0.91	0.79
MPI-ESM-LR	0.993	0.88	0.93	0.84
MPI-ESM-MR	0.994	0.85	0.94	0.82
*MRI-CGCM3	0.985	0.79	0.87	0.81
NorESM1-M	0.993	0.81	0.90	0.56

Table 4.1 CGCMs used to calculate the ensemble mean pattern of SST change. Also shown here is the spatial correlation of 1) CGCMs' climatological SST V.S. the observed climatological SST and 2) CGCM's relative SST change V.S. the ensemble mean relative SST change. An asterisk indicates that the model's climatological SST is taken from the historical simulation (year 1982-2011).

In Fig. 4.7c and 4.7d, I apply similar investigations to multiple CGCMs by conducting AGCM simulations in which the climatological SSTs and the SST changes are taken from individual CGCMs. It is almost impossible to analyze all the existent CGCMs; here I took the five CGCMs from the CMIP5 archive that provided historical SSTs of the same time period as the observation (Section 4.2.2). As shown in Figure 4.7c,

the CGCMs are more susceptible to biases in the climatological SST than differences in the pattern of SST change. For certain CGCMs, biases in the climatological SST lead to a major misrepresentation of changes in precipitation, sea level pressure, 500mb vertical velocity and zonal wind (with a spatial correlation below or close to 0.7 against the obsSST simulation). Furthermore, Fig. 4.7d shows that even the uniform AGCM simulation provides more realistic projections than CGCMs that contain SST biases. These results indicate the importance of calibrating the SST climatology for the simulation of anthropogenic climate change over land, which has not been sufficiently recognized or addressed.

4.4 Summaries and Discussion

Due to the limited computational resource, projecting the anthropogenic climate change over land requires prioritizing different elements in our simulations. For projecting solely the anthropogenically-forced component of climate change, our results suggest that the benefit of the ocean model for simulating the structure of SST change and two-way air sea coupling is inessential. Rather, the use of CGCMs can actually degrade regional projections of climate change by introducing biases in the climatological SSTs.

Furthermore, neither the global mean (Knutti and Sedlacek 2013) nor the pattern of sea surface warming has evolved significantly from CMIP3 to CMIP5 (Fig. 4.2), despite the substantial effort and computational resources devoted to these tasks. Therefore, by exploiting the insensitivity of land climate to the pattern of SST change, improved projections of regional climate change can be made using AGCMs combined

with our current knowledge regarding the likely pattern (and range of amplitudes) of future SST change. Alternatively, if initialized predictions are required, the use of flux-adjustments to correct the SST climatology of the CGCM could lead to greater consistency in model projections of climate change by reducing biases in the unperturbed climatology.

The development of the coupled ocean-atmosphere model is undoubtedly important. However, because of their climatological biases in SSTs, CGCMs may not be the best tool for regional climate change projections. Therefore, for the pragmatic and highly important purpose of projecting anthropogenic climate change over land, it may be wise to allocate greater resources towards higher resolution atmospheric models, which have already proven valuable for seasonal climate forecasts (Vecchi et al. 2014; Jia et al. 2015).

Chapter 5: Anthropogenic Weakening of the Tropical Circulation: The Relative Roles of Direct CO_2 Forcing and Sea Surface Temperature Change

5.1 Background

The atmospheric circulation plays a critical role in climate, influencing the global distributions of precipitation and temperature. A general weakening of tropical circulation has emerged unambiguously in model simulations of anthropogenic climate change (e.g., Held and Soden 2006; Vecchi and Soden 2007; Chadwick et al. 2013; Kociuba and Power 2015) and has been detected in observations of the past half-century

(e.g., Vecchi et al. 2006; Collins et al. 2010; Tokinaga et al. 2012), although the latter is partly due to natural variability (e.g., Power and Smith 2007; Meng et al. 2012; Power and Kociuba 2011).

The anthropogenic weakening of the tropical circulation can be explained from both thermodynamic and dynamic points of view. Thermodynamically, the faster increase in atmospheric moisture than precipitation requires the general weakening of the circulation (Held and Soden 2006). Dynamically, the weakening of tropical circulation can be expected as a result of the balance between convective heating, radiative cooling and increasing stratification (Knutson and Manabe 1995) or the vertical advection of stratification change (Ma et al. 2012). It may also reflect an enhanced gross moist stability (Chou and Neelin 2004) or the "upped ante" mechanism (Neelin et al. 2003; Chou et al. 2009) on a regional scale.

Although these mechanisms have helped understand the anthropogenic weakening of tropical circulation, the direct physical driver of the weakening is still a subject of ongoing investigation. Because the circulation weakens as the climate warms, one may

intuitively consider the weakening to be mostly driven by surface warming. However, Bony et al. (2013) found that a substantial portion of the circulation change occurred immediately in the abrupt quadruple CO_2 simulations when the surface has barely warmed. This indicates that the change in circulation is largely driven by the direct CO_2 forcing. Other studies have also shown a weakening of circulation under direct CO_2 forcing (e.g., Andrews et al. 2009; Chadwick et al. 2013b; Thorpe and Andrews 2014).

However, Chadwick et al. (2014) argued that the fast changes in circulation shown by Bony et al. (2013) were mostly driven by the pattern of sea surface temperature (SST) change, whereas the direct CO_2 forcing only contributed slightly. This indicates that the spatial weakening of circulation might be associated with the pattern of SST change. The importance of the pattern of SST change as a driver of circulation weakening has also been demonstrated in observations (e.g, Tokinaga et al. 2012).

This study aims to determine the relative roles of the direct CO_2 forcing, the mean SST warming and the pattern of SST change in weakening the tropical circulation. Coupled climate models can be insightful for understanding the circulation change since they include both the direct effect of increasing CO_2 and the indirect effects through changes in SST. However, they are not ideal for the purpose of attribution. This study isolates the effect of different kinds of forcing by means of ensemble AGCM simulations, in which only one forcing agent is specified. This technique allows us to establish a direct causal relationship between the forcing agents and changes in the atmospheric circulation. Although AGCM simulations of natural climate variability have been long criticized for their lack of coupling with an underlying ocean, Chapter 2 showed that the lack of ocean coupling has no effect on simulations of anthropogenic climate change (i.e.,

AGCMs are able to perfectly reproduce the anthropogenic climate change from CGCMs despite the lack of energetically consistent surface fluxes), lending credence to my approach.

The use of AGCM simulations with a single forcing agent has been applied to compare the individual impacts of direct atmospheric radiative forcing and SST change on the climate trend of the past half-century (e.g., Bracco et al. 2004; Compo and Sardeshmukh 2009; Deser and Phillips 2009). Most of these studies found approximately equal importance of direct atmospheric radiative forcing and SST change, although their results were susceptible to internal variability (Deser et al. 2012). Similar techniques have also been applied to investigate certain aspects of anthropogenic changes in tropical circulation. For example, Chapter 3 showed that the response of vertical velocity at 500hPa to a uniform SST warming generally opposed its climatology, indicating a weakening effect of the mean surface warming. Using the uncoupled GFDL model, Ma et al. (2012) showed that the mean SST warming weakened the Walker circulation, whereas the direct CO_2 forcing strengthened it. This strengthening effect of CO_2 is contradictory to the commonly believed stabilizing effect of CO_2 (e.g., Bony et al. 2013; Thorpe and Andrews 2014), and could be associated with the land-sea warming contrast (e.g., Joshi et al. 2008; Bayr and Dommenget 2013; Chadwick et al. 2014). This chapter seeks to extend and reconcile previous studies by offering a thorough investigation of the individual impacts of the direct CO_2 forcing, mean SST warming and pattern of SST warming on the weakening of tropical circulation.

5.2 Data and methods

5.2.1 Model simulations

I analyze the monthly output of coupled and atmosphere-only simulations from the Coupled Model Intercomparison Project, phase 5 (CMIP5) archive. The coupled simulations are forced with the "1pctCO2" scenario and represent the total effect of direct CO_2 forcing and SST changes. I define the mean climate as the average of years 1 to 20 and the perturbed climate as the average of years 121 to 140.

The atmosphere-only simulations are the same as described in Section 4.2.1. Note that the land warms slightly in the AMIP_CO2 simulation as a result of the direct CO_2 forcing (Fig. 5.1c); likewise, the land warms slightly less in the AMIP_mean simulation than the 1pctCO2 simulation (Fig. 5.1d and 5.1a) due to the lack of direct CO_2 forcing (Compo and Sardeshmukh 2009). To eliminate the impact from differences in land warming, I also analyze an ensemble of aqua planet simulations forced with quadruple CO_2 (aqua_CO2) and 4K uniform warming (aqua_mean). The aqua planet simulations are run for 5 years with prescribed SST.

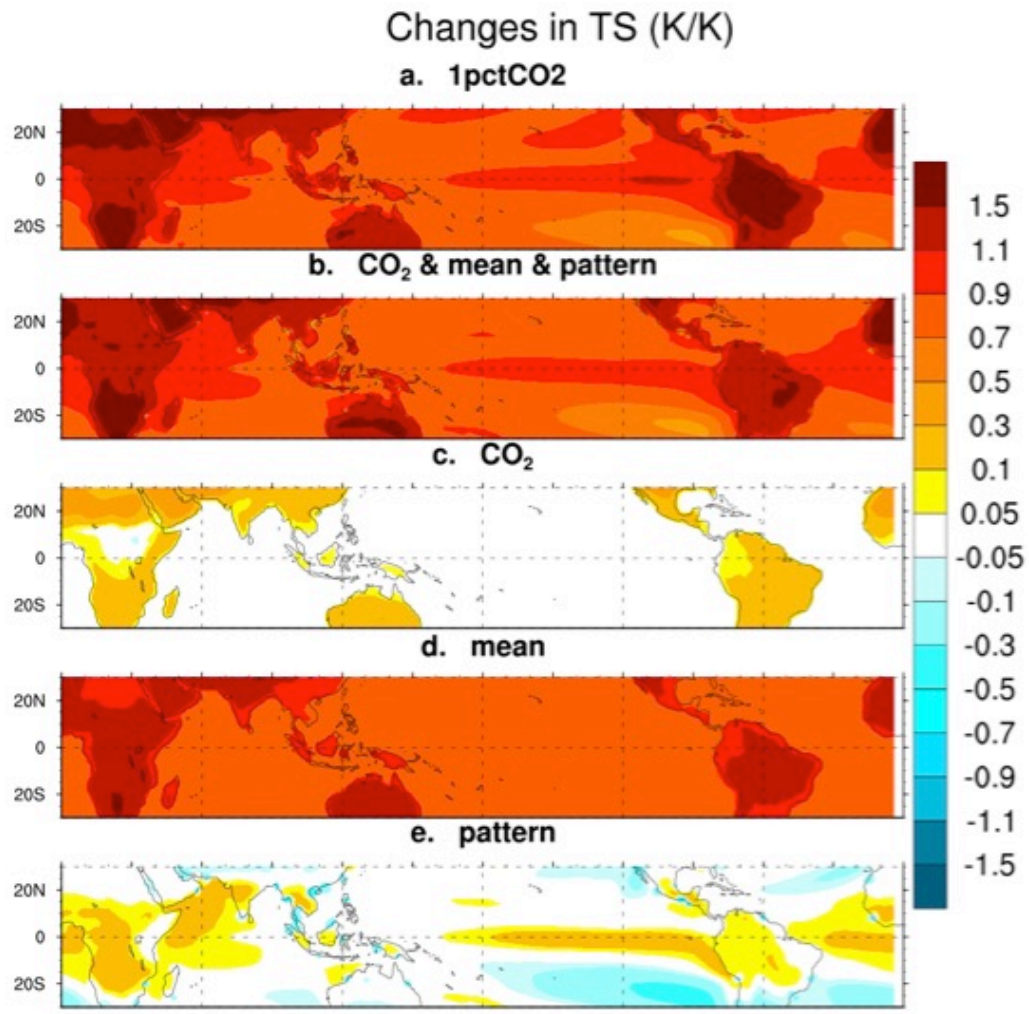

Figure 5.1 Ensemble mean changes in the tropical surface temperature from the 1pctCO2 (a), sum of AMIP_CO2, AMIP_mean and AMIP_pattern (b), AMIP_CO2 (c), AMIP_mean (d) and AMIP_pattern (e). Changes are normalized by each model's tropical mean surface temperature changes in the 1pctCO2 simulation before they are averaged across models to yield an ensemble mean. Note that the shading levels are not of equal intervals.

To equalize the magnitude of CO_2 and SST forcing in the coupled and AMIP simulations, climate changes in the AMIP simulations are first scaled linearly to match the CO_2 and tropical SST forcing in the 1pctCO2 simulations. Specifically, the changes from the quadrupled AMIP_CO2 simulation are multiplied by a factor of 3.3/4.0 to account for the smaller increase in CO_2 (which increases by only a factor of 3.3 between years 1 and 120) in the 1pctCO2 simulation; i.e., I assume that the climate responds linearly to increasing CO_2. Finally, climate change is normalized by each model's

tropical mean surface temperature change in the 1pctCO2 simulation and then averaged across models to yield a multi-model ensemble mean, in order to avoid dominance by models with large climate sensitivity.

5.2.2 Convective mass flux

I analyze the weakening of tropical circulation mainly through changes in the convective mass flux. Unfortunately, model simulated convective mass flux is not available for all the simulations. However, as convective rainfall dominates over large-scale rainfall in the tropics, one can constrain the convective mass flux through precipitation and boundary layer moisture (Held and Soden 2006):

$$M^* = P / q, \quad (5.1)$$

where P, q, M^* is precipitation, near surface specific humidity and the equivalent convective mass flux, respectively. Previous studies have shown that M^* is a valid approximation to the model simulated convective mass flux both in terms of tropical mean (Held and Soden 2006; Vecchi and Soden 2007) and spatial distribution (Chadwick et al. 2013a). Spatial changes in M^* are equivalent to spatial changes in the vertically integrated convective mass flux, with exceptions over steep orography in the Himalayas and Andes (Chadwick et al. 2013a).

5.3 Results

5.3.1 Tropical mean convective mass flux change

I begin my analysis of the tropical circulation weakening by examining changes in the tropical mean convective mass flux. Following Held and Soden (2006), I derive the proportional change in tropical mean convective mass flux as the difference between the proportional change in tropical mean precipitation and the proportional change in tropical mean near surface moisture:

$$\frac{\partial M^*}{M^*} = \frac{\partial P}{P} - \frac{\partial q}{q}. \qquad (5.2)$$

Figure 5.2 shows the proportional changes in tropical mean precipitation, moisture and convective mass flux from the 1pctCO2 simulation and AMIP simulations. In the 1pctCO2 simulation (Fig. 5.2a), the tropical mean moisture increases at 6.7%/K, close to the Clausius–Clapeyron relation, whereas the mean precipitation increases at 1.2%/K, as determined by the rate of atmospheric radiative cooling (e.g., Boer 1993; Soden 2000; Allen and Ingram 2002). The difference between the rate of moistening and rate of precipitation increase requires that the tropical mean convection weakens at 5.5%/K (Held and Soden 2006).

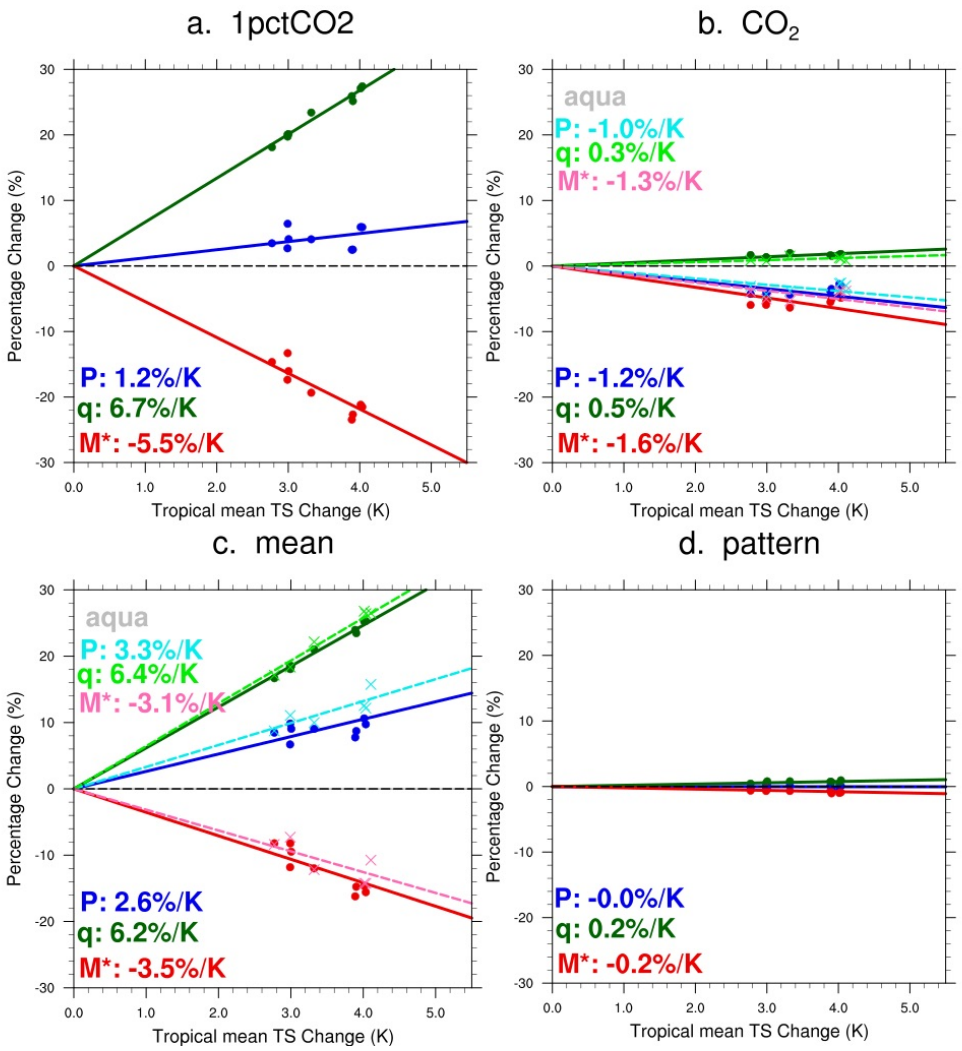

Figure 5.2 Tropical mean changes in precipitation (blue), moisture (green) and convective mass flux (red) from every model in the 1pctCO2 and AMIP simulations (dots) and the aqua planet simulations (crosses) plotted against each model's tropical mean surface temperature changes in the 1pctCO2 simulation. The tropics are defined as the region between 30^{o} S and 30^{o} N. The lines indicate the ensemble mean changes, with solid lines representing the 1pctCO2 and the AMIP simulations and dashed lines representing the aqua planet simulations. The text shows the ensemble mean changes after they are normalized by each model's tropical mean surface temperature changes in the 1pctCO2 simulation. Dark colors represent the 1pctCO2 and AMIP simulations and light colors represent the aqua planet simulations.

As shown in Figure 5.2, the sum of the hydrological changes in the AMIP_CO2, AMIP_mean and AMIP_pattern simulations is very close to those in the 1pctCO2 simulation, indicating the linearity of the hydrological changes. However, these changes are very unevenly distributed in the AMIP simulations. The pattern of SST change has virtually no effect on the topical mean hydrological cycle (Fig. 5.2d). The slight increase

in moisture is likely associated with the Equator – subtropical gradient in SST warming, which favors moistening in the lower latitudes (Xie et al. 2010). As a result, the tropical mean convection weakens slightly but only accounts for less than 4% of the total weakening.

In the AMIP_CO2 simulation (Fig. 5.2b), the near surface moisture increases at 0.5%/K as a result of the increase of the atmospheric temperature, whereas precipitation decreases at 1.2%/K due to the atmospheric radiative warming. This causes the mean convection to weaken at -1.6%/K, which accounts for about 30% of the total weakening. Because the land surface temperature is not fixed and warms slightly in the AMIP_CO2 simulation (Fig. 5.1c), the weakening of convection could be attributed to both the direct CO_2 forcing and land-sea warming contrast, which shifts convection from ocean to land (Chadwick et al. 2014 discussed latter in section 5.3.2). To eliminate the effect of land warming, I also analyze the direct CO_2 influence in the aqua_CO2 simulation. As shown in Fig. 5.2b, both the moistening and precipitation decrease is moderately reduced when the effect of land warming is removed, but the mean convection still weakens albeit at a smaller rate.

The mean SST warming is the dominant driver of changes in the tropical mean hydrological cycle (Fig. 5.2c). It accounts for almost the entire tropical mean moistening. It also increases the tropical mean precipitation at a higher rate than the fully coupled simulation due to the absence of atmospheric radiative warming associated with the direct CO_2 forcing. The tropical mean convection weakens at 3.5%/K under the mean SST warming, which accounts for about two thirds of the total weakening. The effect of mean SST warming on the weakening of the mean circulation is very similar in the

AMIP_mean and aqua_mean simulations, suggesting an insignificant impact of land-sea warming contrast on the tropical mean circulation weakening.

From a dynamic viewpoint, the relative roles of direct CO_2 forcing, mean SST warming and pattern of SST warming on the weakening of the tropical mean circulation can be explained through changes in the tropospheric static stability (Knutson and Manabe 1995; Ma et al. 2012). In climate change simulations, the warming reaches a maximum in the upper troposphere. This tropical-wide increase in tropospheric static stability is commonly expected from the moist adiabatic adjustment (Knutson and Manabe 1995), although it is more recently argued to be a vertical shift of the climatological temperature profile (O'Gorman and Singh 2013). Knutson and Manabe (1995) showed that the increased static stability allows for the weakening of convection while maintaining the balance between radiative cooling and convective heating. Ma et al. (2012) showed that the mean advection of the stratification change (MASC) acts as a weakening force on the overturning circulation and explains most of the total weakening of the Walker circulation and the Hadley cell, although the latter was partly counteracted by other factors. Based on these theories, one can evaluate the weakening effect of the forcing agents through the way they change the tropospheric static stability.

Figure 5.3 shows the change in tropospheric temperature in the 1pctCO2 simulation, the AMIP simulations and the aqua planet simulations. Most of the tropospheric warming and static stability increase results from the mean SST warming, which increases the latent heat release in the free troposphere. The direct CO_2 forcing causes weak atmospheric warming and a small increase in static stability in the lower troposphere. The sum of AMIP_CO2 and AMIP_mean reproduces well the total warming

in 1pctCO2. The warming effect of the pattern of SST change is even weaker, and is mostly in the high troposphere due to the anomalous convection associated with the enhanced equatorial warming (Xie et al. 2010). Overall, the individual impact of the forcing agents derived from changes in stratification is consistent with that from the thermodynamic theory by Held and Soden (2006).

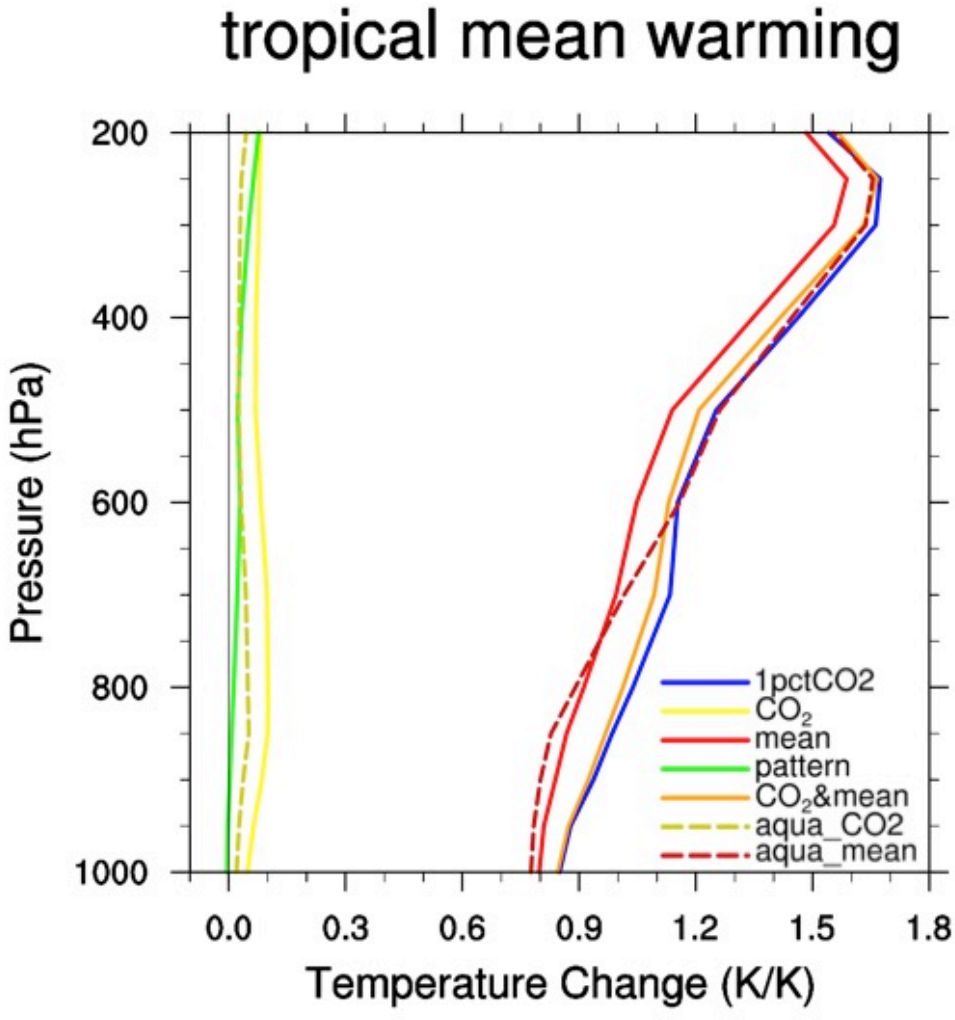

Figure 5.3 Ensemble mean vertical profile of the horizontal mean temperature change from the 1pctCO2, AMIP and aqua planet simulations. The orange line is the sum of AMIP_CO2 and AMIP_mean. The tropics are defined as the region between 30^{o} S and 30^{o} N. Changes are normalized by each model's tropical mean surface temperature changes in the 1pctCO2 simulation before they are averaged across models to yield an ensemble mean.

5.3.2 Spatial pattern of tropical circulation change

Figure 5.4 shows the spatial pattern of changes in convective mass flux from the 1pctCO2 and AMIP simulations. In the 1pctCO2 simulation (Fig. 5.4a), convection weakens almost everywhere in the tropics with the largest weakening in regions of climatological ascent, consistent with the MASC mechanism. On the other hand, convection strengthens over the equatorial Pacific, the northwest Indian Ocean and the Indian peninsular. The increased convection over the equatorial Pacific and the northwest Indian Ocean is also found in the AMIP_pattern simulation and is therefore associated with the enhanced SST warming (Xie et al. 2010). The increased convection over the Indian peninsular is reproduced in the AMIP_CO2 simulation, in which land-sea warming contrast plays a role. Therefore, it is likely caused by the enhanced land warming, which favors the development of monsoonal rainfall.

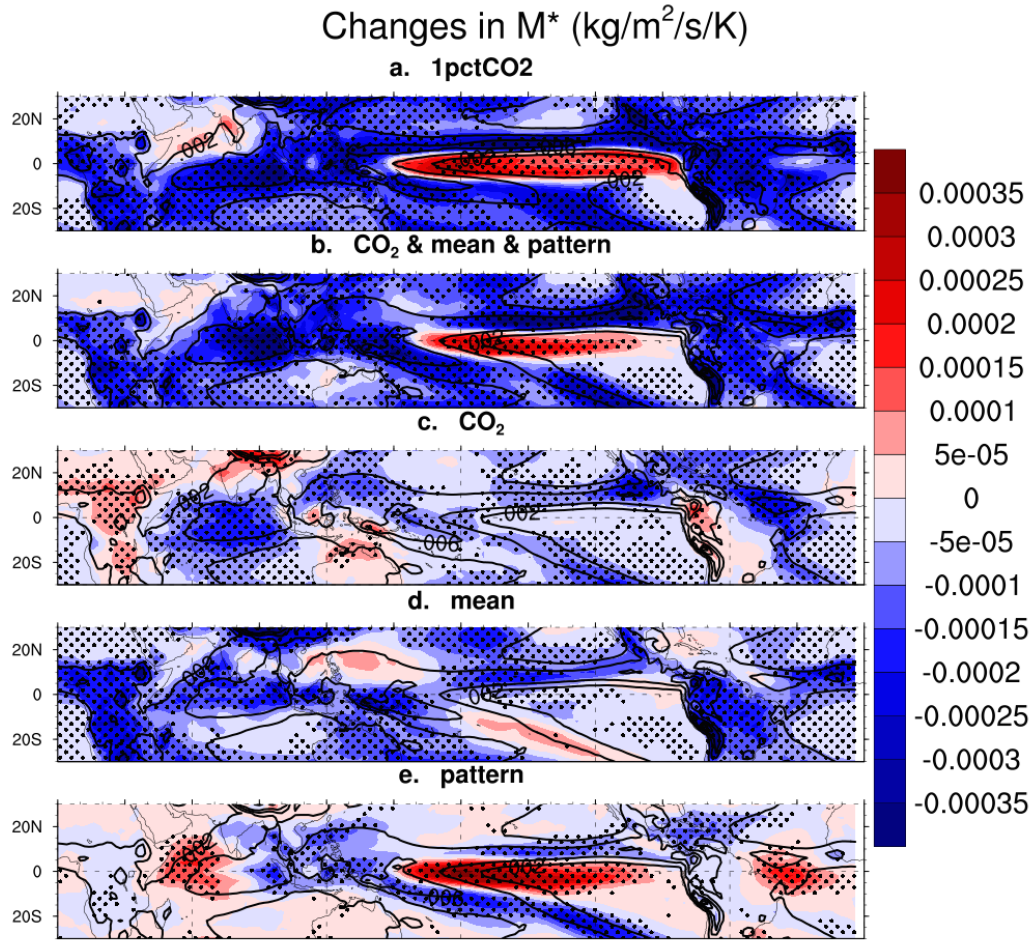

Figure 5.4 Ensemble mean changes in M* (shading) superimposed on the climatological M* (contour) from the 1pctCO2 (a) and the AMIP simulations (b through e). Changes are normalized by each model's tropical mean surface temperature changes in the 1pctCO2 simulation before they are averaged across models to yield an ensemble mean. Contour interval is $2*10^{-3}$kg/m^2/s. Areas where at least 8 (out of 9) models agree on the sign of change are stippled.

The spatial change in convective mass flux in the 1pctCO2 simulation is well reproduced by the sum of AMIP_CO2, AMIP_mean and AMIP_pattern, with a spatial correlation of 0.82 (Fig. 5.4b). Noticeable discrepancies exist over the southeast Pacific, the south equatorial Atlantic and the northwest Indian monsoon region. Due to the different climatological SST in the 1pctCO2 and AMIP simulations, the discrepancies in convection change are likely caused by differences in the climatological convective mass flux, as the pattern of weakening closely follows the pattern of large climatological

convection in both the 1pctCO2 and the sum of AMIP simulations (Ma et al. 2012; Chadwick et al. 2013a). These discrepancies may also be due to the differences in the pattern of SST change in AMIP_pattern and each coupled model.

In the AMIP_CO2 simulation (Fig. 5.4c), convection weakens over most of the tropical oceans. The weakening of convection is also produced in the aqua_CO2 simulation but with overall smaller magnitude (Fig. 5.5a). This indicates that the weakening in the AMIP_CO2 simulation is largely driven by the stabilization effect of increasing CO_2 but land-sea warming contrast may also play also an important role, which is consistent with the results from the solar experiment in Chadwick et al. (2014). In both the AMIP_CO2 and the aqua_CO2 simulations, the strongest weakening happens in regions of large climatological convection, suggesting that the MASC mechanism might also apply to circulation weakening in the CO_2 only simulations. The weakening effect of the direct CO_2 forcing certainly plays a role over land (Cao et al. 2012; Bony et al. 2013), but is overpowered by the strengthening effect of the land surface warming.

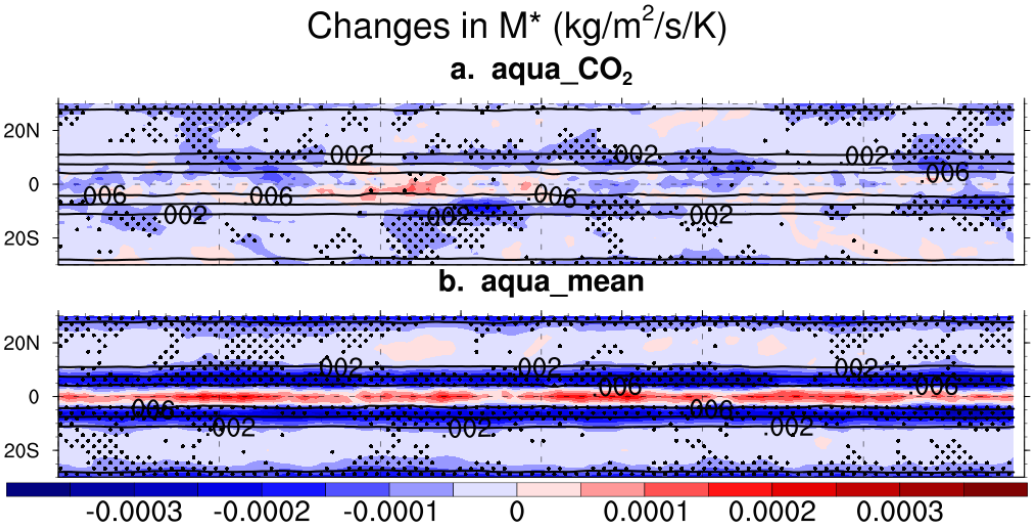

Figure 5.5 Ensemble mean changes in M* (shading) superimposed on the climatological M* (contour) from the aqua planet simulations. Changes are normalized by each model's tropical mean surface temperature changes in the 1pctCO2 simulation before they are averaged across

models to yield an ensemble mean. Contour interval is $2*10^{-3}$kg/m^2/s. Areas where at least 5 (out of 6) models agree on the sign of change are stippled.

The mean SST warming weakens convection almost everywhere in the tropics (Fig. 5.4d), with an overall larger magnitude than that from the direct CO_2 forcing. The strongest weakening is mainly found over the center of climatologically convective zones, consistent with previous studies (Ma et al. 2012; Chapter 3). Strong weakening also happens at certain edges of convective zones, including the northwest Indian Ocean, the northern Pacific Ocean and the equatorial Atlantic. This may likely reflect the "upped ante" mechanism, in which convection is suppressed through the advection of dry air from the less-moistened subsidence regions into the convective regions (Neelin et al. 2003; Chou et al. 2009). Despite the overall weakening, the mean SST warming also strengthens convection over the northwest Pacific and the east bound of the south Pacific ITCZ. This may be associated with the increase of moisture in the lower troposphere, which overpowers the increase of dry static stability to yield a reduced gross moist stability (Chou and Neelin 2004; Chou et al. 2009). However, the strengthening of convection is less robust among the CMIP5 models compared to the weakening of convection.

The weakening effect of the mean SST warming also dominates the pattern of convective mass flux change in the aqua_mean simulation. The strongest weakening happens over regions of large climatological convection, consistent with the AMIP_mean simulation. It is interesting that convection is strengthened at the Equator (where convection is the strongest) in the aqua_mean simulation, although this is not a robust projection. The anomalous equatorial convection in the aqua_mean simulation could be driven dynamically by a positive moisture-convection feedback (Chou and Neelin 2004;

Chou et al. 2009) or the anomalous equator-ward surface wind associated with the weakening of convection off Equator; it could also be a result of internal variability due to the short length (5 years) of the aqua planet simulations.

The pattern of convection change in the AMIP_pattern simulation (Fig. 5.4e) generally follows the pattern of SST change (Fig. 5.1e), with increased convection over the warmest SST change and decreased convection over the less warm SST change. This "warmer-get-wetter" response reflects the changes in convective stability determined by the pattern of surface warming, as upper tropospheric warming is nearly uniform due to fast wave actions (Xie et al. 2010). Interestingly, the pattern of convection change caused by the pattern of SST warming generally opposes the climatological pattern of convection over the Pacific Ocean. Although this has little impact on the tropical mean convection, it weakens the pattern of convection by reducing its spatial variation.

This weakening effect of the pattern of SST warming can also be seen from the 500hPa vertical velocity (Omega500, Fig. 5.6e) – the anomalous convection weakens the descending motion at the equatorial and southeast Pacific, whereas the anomalous subsidence weakens the ascending motion at the Pacific ITCZ. It has been shown that the slowdown of equatorial surface wind causes an increase of ocean heat transport that warms the equatorial Pacific (DiNezio et al. 2009; Xie et al. 2010); here it is shown that the equatorial Pacific warming in turn enhances the weakening of the pattern of convection. Therefore, a positive feedback may very likely exist between the circulation weakening and the pattern of SST change, although the mechanism behind this feedback needs further verification. On the other hand, the pattern of SST change has little impact

on the convection over land, which is due to the insensitivity of Rossby wave generation associated with the pattern of SST change (Chapter 3).

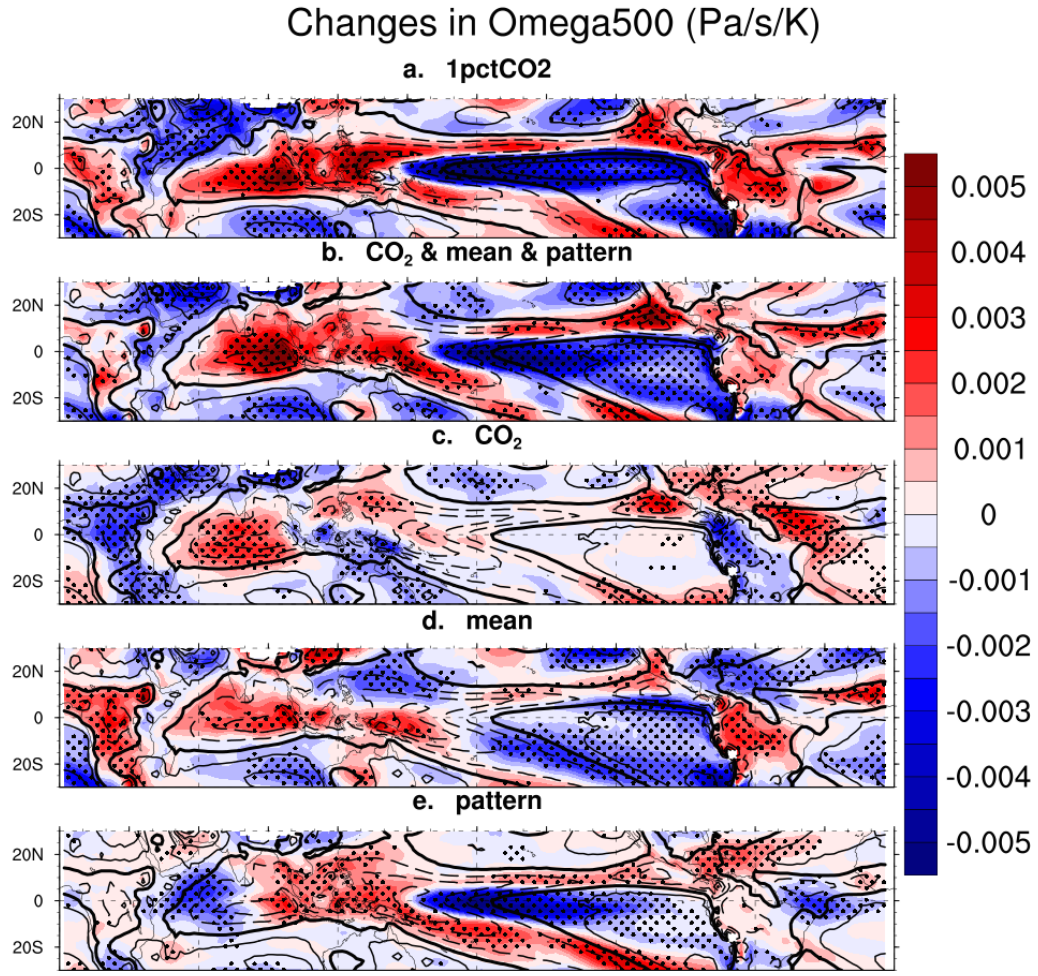

Figure 5.6 Same as Figure 5.4, except for Omega500. Contour interval is 0.02Pa/s. Zero contours are thickened.

The direct CO_2 forcing, the mean SST warming and the pattern of SST warming all act to weaken the tropical circulation spatially, as indicated by the negative spatial correlation between the changes in Omega500 and the climatological Omega500 in all three AMIP simulations (Figure 5.7). Over land, the weakening is dominated by the mean SST warming (Fig. 5.7c). This is expected because most of the land warming happens in the AMIP_mean simulation (Fig. 5.1d) as a result of the ocean's remote influence on the

water vapor and radiative feedback over land (Compo and Sardeshmukh 2009). On the other hand, land circulation strengthens in the AMIP_CO2 simulation due to the land-sea warming contrast.

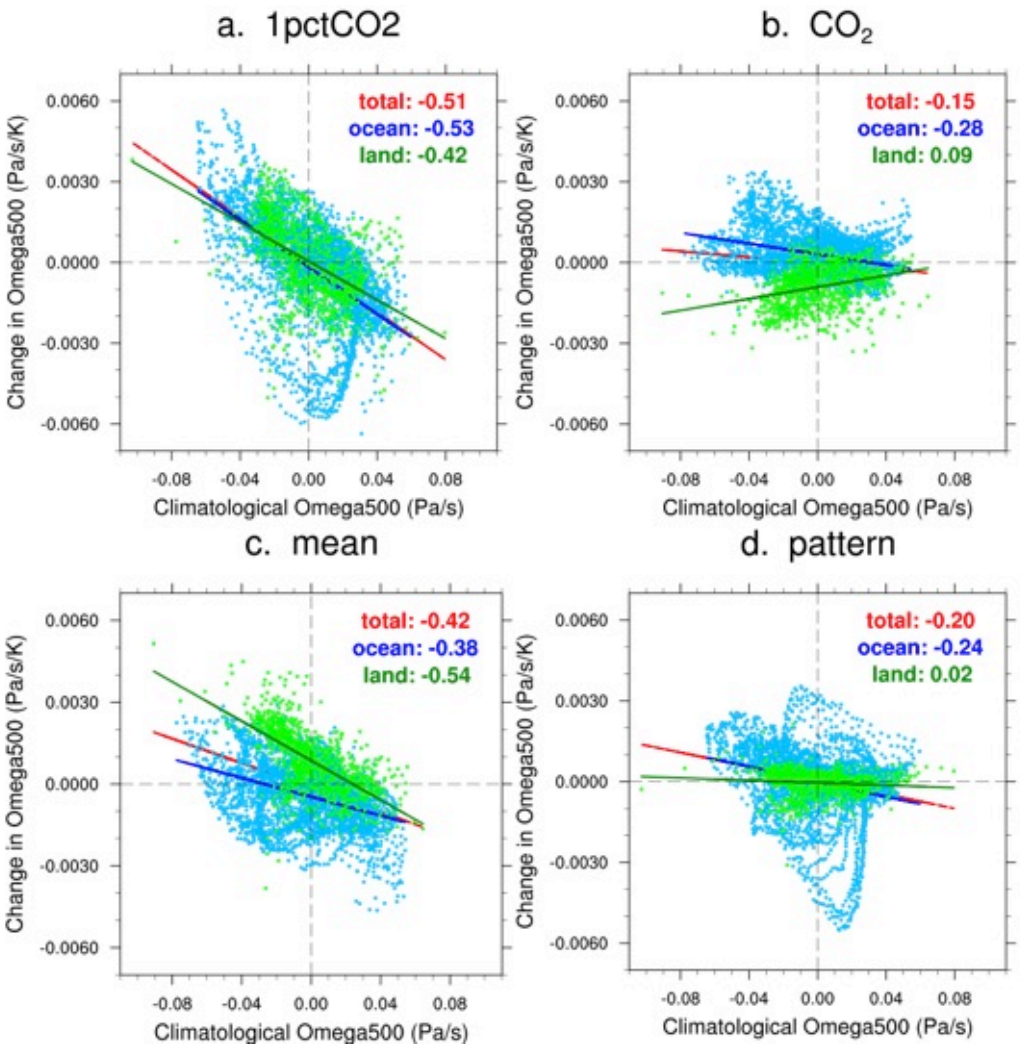

Figure 5.7 Scatterplot of ensemble mean changes in Omega500 VS the climatological Omega500 from the 1pctCO2 and the AMIP simulations. Values are taken from a $2^{o} \times 2^{o}$ grid. Ocean and land grid points are separated by color blue and green. The solid lines are the least square fit to the data. Red lines represent all tropical grid points. The numbers on the top right corner are the multi-model mean of the spatial correlation between changes in Omega500 and the climatological Omega500. The climatology in panel d is taken as the climatology in 1pctCO2 (same as panel a), as the pattern of SST change is calculated based on the 1pctCO2 simulation.

Over ocean, all three forcing agents weaken the circulation, with the change in Omega500 generally opposing the climatological Omega500 (Fig. 5.7b-d). On the other

hand, no single forcing agent is able to reproduce the total rate of weakening in Figure 5.7a by itself. As shown in the maps of Omega500 (Fig. 5.6), much of the pattern of weakening over the tropical Pacific is reflected in the AMIP_pattern simulation, with anomalous ascent over the equatorial and southeast Pacific, and anomalous descent over the Pacific ITCZ. The weakening by the direct CO_2 forcing is most evident in convective zones over oceans, including the tropical Indian Ocean, the equatorial Atlantic and northeast Pacific. The mean SST warming weakens circulation over both ocean and land, with notable exceptions over the west Pacific ITCZ.

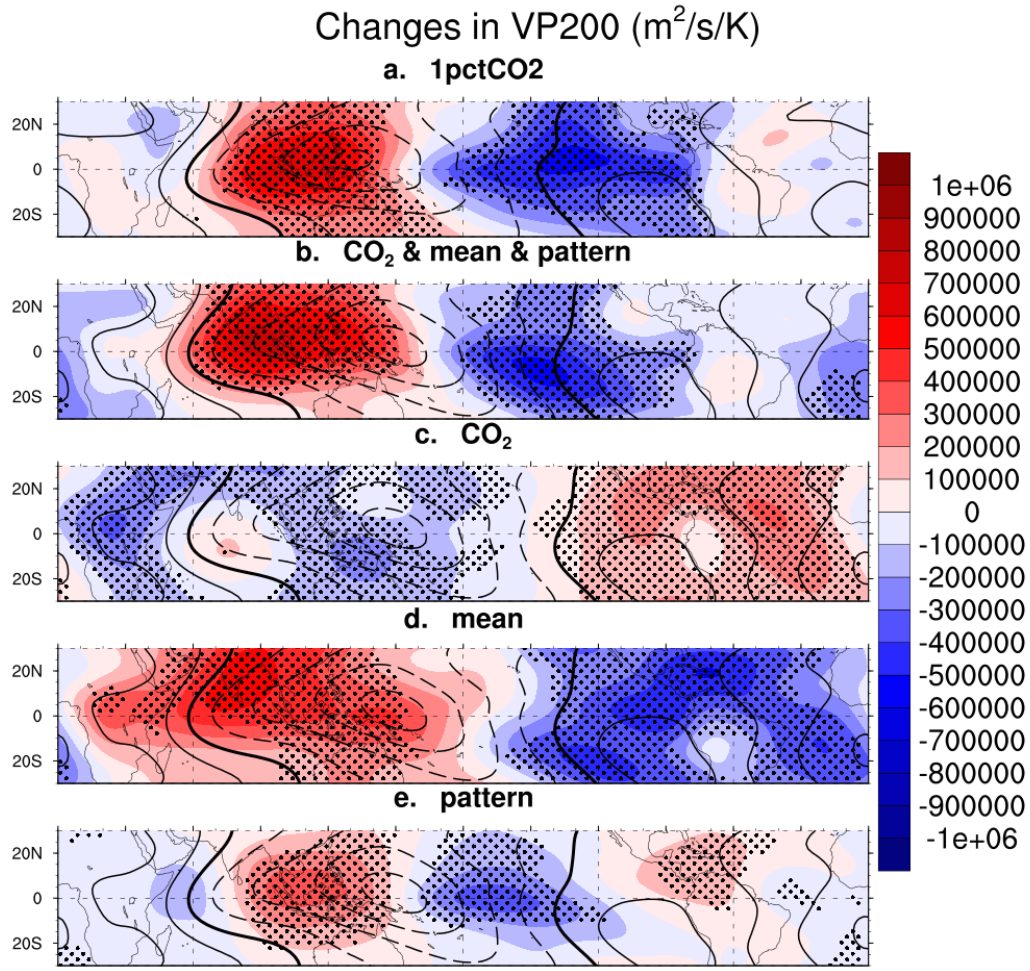

Figure 5.8 The same as Figure 5.4, except for 200hPa velocity potential. Contour interval is $3*10^6$ m/s.

5.3.3 Weakening of the Walker circulation

It has been shown that the large-scale weakening of the tropical overturning circulation occurs primarily through the zonally asymmetric component of the circulation (Held and Soden 2006; Vecchi and Soden 2007), a key element of which is the Walker circulation. An anthropogenic weakening of the Walker circulation has been detected from both the upper-level velocity potential (e.g., TANAKA et al. 2004) and the large-scale zonal gradient of sea level pressure (SLP, e.g., Vecchi et al. 2006). Figure 5.8 shows a weakening and an eastward shift in the 200hPa velocity potential from both the 1pctCO2 simulation and the sum of AMIP_CO2, AMIP_mean and AMIP_pattern, consistent with the findings of Vecchi and Soden (2007). The weakening is caused primarily by the mean SST warming (Fig. 5.8d), through the MASC mechanism and the feedback between convection and latent heat release Ma et al. (2012). The eastward shift is mostly caused by the pattern of SST warming (Fig. 5.8e) through the enhanced SST warming at the central equatorial Pacific. It is interesting that the upper-level velocity potential does not weaken under an "El Niño-like" warming pattern (e.g., Liu et al. 2005; Xie et al. 2010; Ma and Xie 2013). This can be understood from the spatial structure of SLP response to the pattern of SST warming (Fig. 5.9e). The zonal SLP gradient is indeed reduced at the Equator by the enhanced equatorial warming, but it drastically reverses its sign at about 10^{o}S due to the minimum SST warming off Equator (Xie et al. 2010). Therefore, due to the narrow meridional structure of the warming pattern, the overall change in the zonal SLP gradient over the tropical Pacific is not enough to weakening the upper-level velocity potential, which represents the large-scale integral of

circulation. This minor difference in the structure of SST responses to anthropogenic forcing and El Niño leads to very different responses in the Walker circulation, as well as other aspects of the atmospheric circulation (e.g., Lu et al. 2008; Chapter 3).

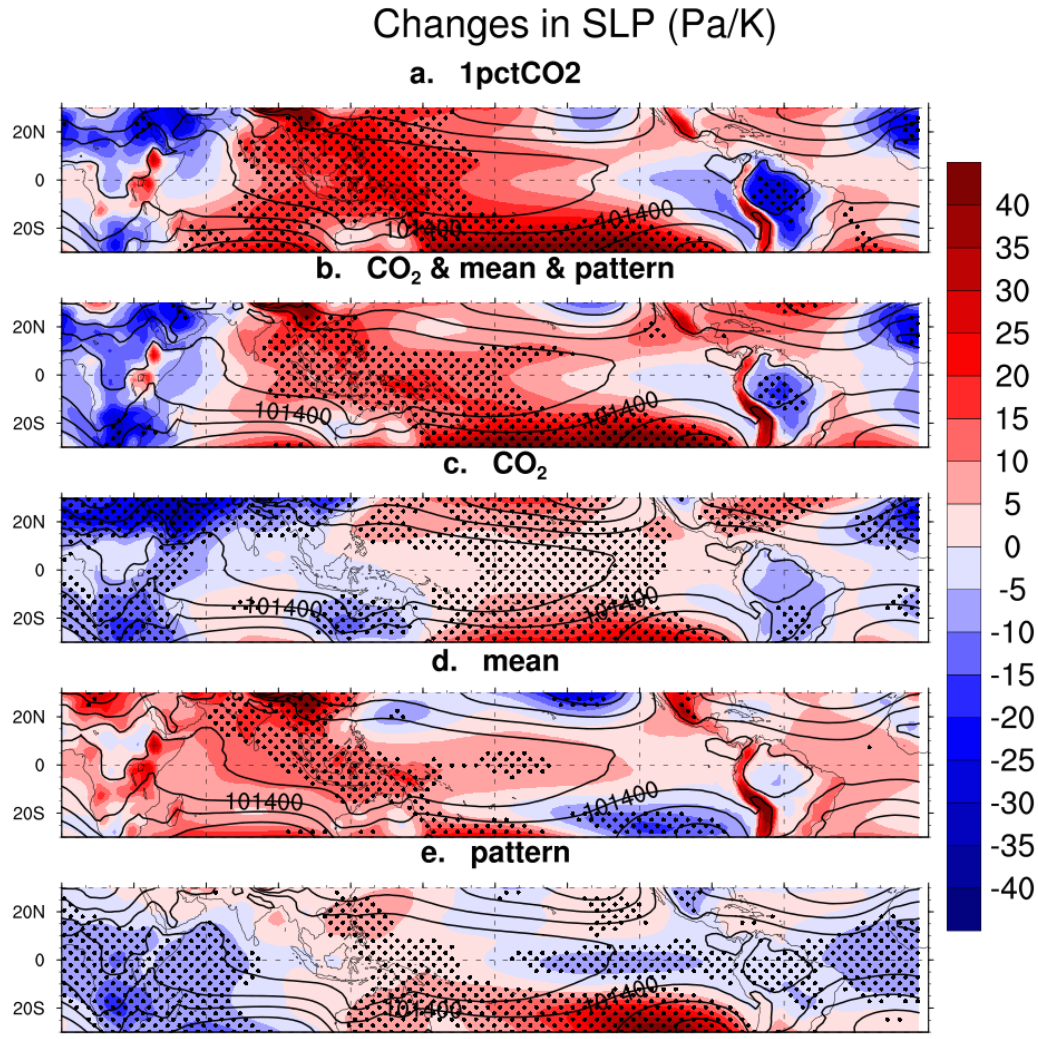

Figure 5.9 Same as Figure 5.4, except for SLP. Contour interval is 300Pa.

In the AMIP_CO2 simulation, the 200hPa velocity potential strengthens (Fig. 5.8c), consistent with the result from the GFDL model by Ma et al. (2012). Considering the fact that the direct CO_2 forcing weakens the circulation, the strengthening of the Walker circulation is most likely caused by the land-sea warming contrast as an indirect effect of CO_2 (Fig. 5.1c). As shown in Figure 5.9c, the warming of land relative to the

ocean reduces SLP throughout the land while increasing SLP over most of the ocean (e.g., Bayr and Dommenget 2013). As a result, the zonal SLP gradient is increased between the eastern tropical Pacific and the western Pacific-Indonesian region, consistent with a strengthening of the Walker circulation. This shows the importance of land-sea warming contrast in regulating the Walker circulation. With this experimental design, it is impossible to separate the effect of land-sea warming contrast and direct CO_2 forcing on the weakening of the Walker circulation. However, the results show that the weakening effect of direct CO_2 forcing could be overpowered by the strengthening effect of the fast land warming (as an indirect effect of CO_2 forcing) regarding changes in the Walker circulation.

5.3.4 Changes in the Hadley circulation

Despite the weakening in the zonally asymmetric component of tropical circulation, current CGCMs do not simulate a robust weakening in the meridional overturning circulation (e.g., Held and Soden 2006; Vecchi and Soden 2007; Ma and Xie 2013). This section examines changes in the Hadley circulation by analyzing the zonal mean stream function (Fig. 5.10). In the 1pctCO2 simulation, the northern Hadley cell weakens, whereas the southern Hadley cell shows no consistent weakening or strengthening, which is in agreement with the results from the CMIP3 ensemble (Ma and Xie 2013). However, in the sum of AMIP simulations both the northern and the southern cell weaken. The discrepancy between the 1pctCO2 and the sum of AMIP simulations could be due to either the differences in SST or nonlinearity of the responses to the forcing agents.

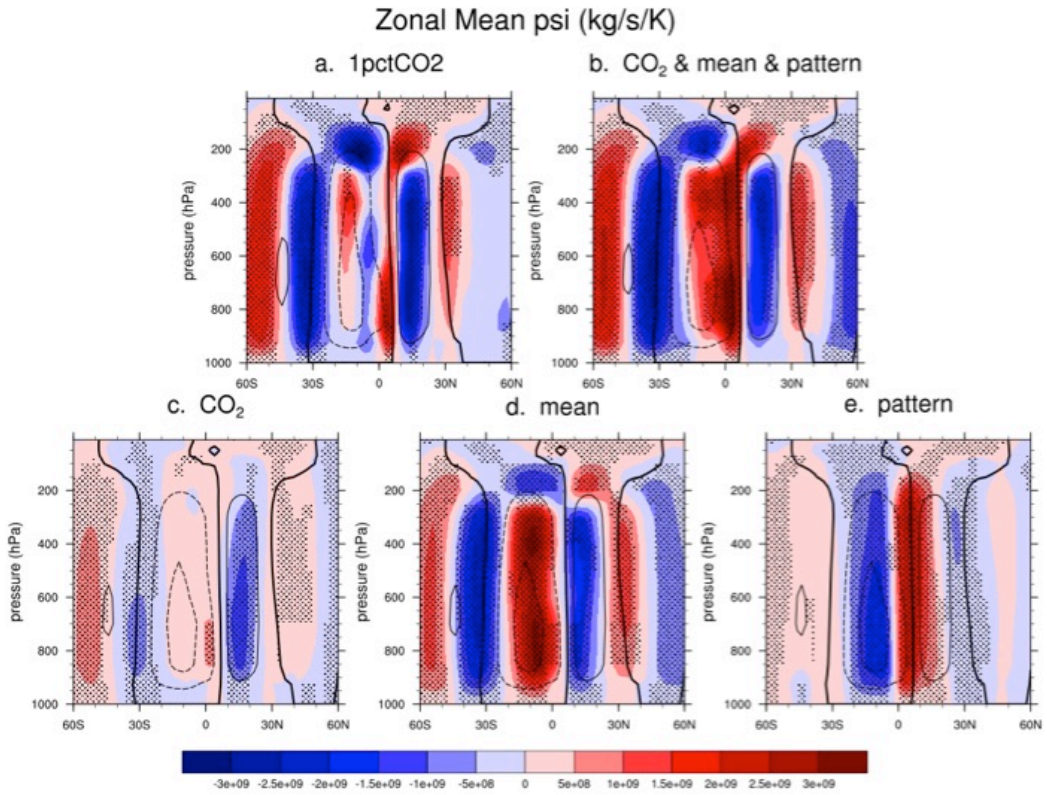

Figure 5.10 Ensemble mean changes in zonal mean stream function (shading) superimposed on the climatology (contour) from the 1pctCO2 (a) and the AMIP simulations (b through e). Areas where at least 8 (out of 9) models agree on the sign of change are stippled. Contour interval is $4*10^{10}$kg/s. Dashed contours indicate negative values. Zero contours are thickened.

As shown in Figure 5.10d, most of the weakening of the Hadley circulation is caused by the mean SST warming. In addition, the mean SST warming is responsible for the poleward shift of the boundary between the Hadley and Ferrel cells, which has been detected in model simulations (e.g., Lu et al. 2007; Frierson et al. 2007). The direct CO_2 weakens the Hadley cell in both Hemispheres, although the weakening in the Southern Hemisphere is insubstantial. The pattern of SST change generally strengthens the Hadley circulation and shifts the center of the Hadley cell southward to the Equator. This is mostly associated with the Equatorial warming and the subtropical cooling in the Pacific (Ma and Xie 2013). Overall, the weakening effect from the mean SST warming overpowers the strengthening effect of the pattern of SST change, as indicated by the

general weakening in the sum of AMIP simulations. Above 200mb, the Hadley circulation strengthens, reflecting an increase in tropopause (e.g., Holzer and Boer 2001; Santer et al. 2003). This is mostly caused by the mean SST warming.

5.4 Conclusions

This chapter has investigated the relative impacts of direct CO_2 forcing, mean SST warming and pattern of SST warming on the anthropogenic weakening of the tropical circulation using a 9-model ensemble of AMIP simulations, in which the three forcing agents were specified individually. Overall, the sum of the AMIP simulations successfully reproduces the fully coupled simulation in terms of both the tropical mean weakening and the spatial pattern of weakening, giving justification to my approach.

For the weakening of the tropical mean circulation, the mean SST warming is the largest contributor through its dominance over changes in tropical mean precipitation and atmospheric moisture. The direct CO_2 forcing contributes moderately to the mean weakening through the radiative warming of the atmosphere. The pattern of SST warming has virtually no impact on the tropical mean hydrological cycle. The relative importance of the three forcing agents in the weakening of the tropical mean circulation can be dynamically explained through changes in the tropospheric stratification. The vertical profile of tropical mean temperature change showed that most of the increased tropospheric stratification is a result of the mean SST warming through its influence on the tropical mean moisture and latent heat release. In contrast, the direct CO_2 forcing only increases stratification moderately in the lower troposphere, whereas the pattern of SST warming has overall little impact.

In terms of the spatial pattern of circulation weakening, the direct CO_2 forcing, mean SST warming and pattern of SST warming all contribute, especially over the ocean. The AMIP_CO2 simulation produces a weakening of convection over most of the tropical oceans with the largest weakening over convective zones. This weakening effect is a result of both the direct CO_2 forcing and the land-sea warming contrast, as the weakening is also simulated in the aqua planet experiment but with a somewhat smaller magnitude. On the other hand, the increasing CO_2 strengthens convection over land by warming the land relative to the ocean. The mean SST warming induces strong weakening of convection over both ocean and land. The weakening happens mostly at the center and the edge of convective zones. On the other hand, the mean SST warming also strengthens convection over certain convective regions in both the AMIP_mean and aqua_mean simulations, which is most likely driven by the positive moisture-convection feedback (Chou and Neelin 2004; Chou et al. 2009). The pattern of SST warming also contributes to the pattern of circulation weakening. This contribution is trivial over land but is very important over the tropical Pacific. It has been shown that the enhanced equatorial Pacific warming is closely linked to the weakening of surface wind (DiNezio et al. 2009; Xie et al. 2010). This study indicates that the pattern of SST change could in turn influence circulation weakening. Such feedback may help better understand the anthropogenic changes in tropical circulation and SST.

This chapter also shows that the weakening of the Walker circulation is primarily caused by the mean SST warming. This is consistent with the study by Ma et al. (2012) using the GFDL model. Studies have shown that the pattern of SST change causes equatorial changes in precipitation and convection that resemble the characteristics of an

El Niño event (e.g., Xie et al. 2010). However, changes in the upper-level velocity potential indicate that the pattern of SST warming has little impact on the weakening of the Walker circulation despite having an "El Niño-like" spatial structure. The narrow meridional width of the equatorial warming limits its impact on the large-scale zonal SLP gradient. The use of the AMIP_CO2 simulation maybe inadequate to evaluate the direct CO_2 impact on the Walker circulation, but the previous conclusion that the direct CO_2 forcing weakens circulation may shed some light on this issue. Nevertheless, it was shown that the increasing CO_2 could strengthen the Walker circulation indirectly by warming the land faster than the ocean, which could outweigh the weakening effect of the direct CO_2 forcing.

It has been shown that the pattern of SST change is the largest source of inter-model uncertainty in changes in the Hadley circulation (Ma and Xie 2013). But in terms of the ensemble mean response, this chapter showed that weakening effect of the mean SST warming generally overpowers the strengthening effect of the pattern of SST change. This results in a weakening of the Hadley cell in the sum of AMIP simulations. However, the coupled models do not simulate the weakening of the southern cell, which indicates that the response of the Hadley circulation could be nonlinear. In addition, the mean SST warming is also the main cause of the Hadley cell expansion and the lift of the tropopause.

Chapter 6: Physical Mechanisms of the Precipitation Changes in the Subtropics and Extratropics

6.1 Background

Precipitation is one of the most important elements of climate, affecting almost every aspect of society ranging from agriculture to daily human activities. As the greenhouse gas concentrations continue to rise, the distribution of precipitation is almost certain to change (e.g., Seager et al. 2007; Solomon 2007), posing serious socioeconomic challenges. To understand the precipitation responses to global warming, large collections of model projections have been analyzed (Meehl et al. 2007; Taylor et al. 2012). These projections show substantial uncertainty in the tropics (e.g., Knutti and Sedlacek 2013; Ma and Xie 2013; Kent et al. 2015); nevertheless, a decrease in the subtropical precipitation and an increase in the extratropical precipitation emerge ubiquitously from current climate models (e.g., Held and Soden 2006; Knutti and Sedlacek 2013; Scheff and Frierson 2012).

The subtropical precipitation decrease and extratropical precipitation increase have been commonly related to the intensification of the global hydrological cycle. According to Held and Soden (2006), the global pattern of precipitation minus evaporation (P – E) strengthens as a simple response to the Clausius-Clapeyron increase of moisture in a warmer climate. Under the assumption of a fixed atmospheric circulation, an increase in moisture intensifies the moisture transport, leading to a more negative P – E in the subtropics and a more positive P – E in the extratropics (Fig 1a). Because the changes in precipitation have considerably more spatial structure than the

changes in evaporation, one may expect the changes in precipitation to follow a very similar pattern as the changes in P – E.

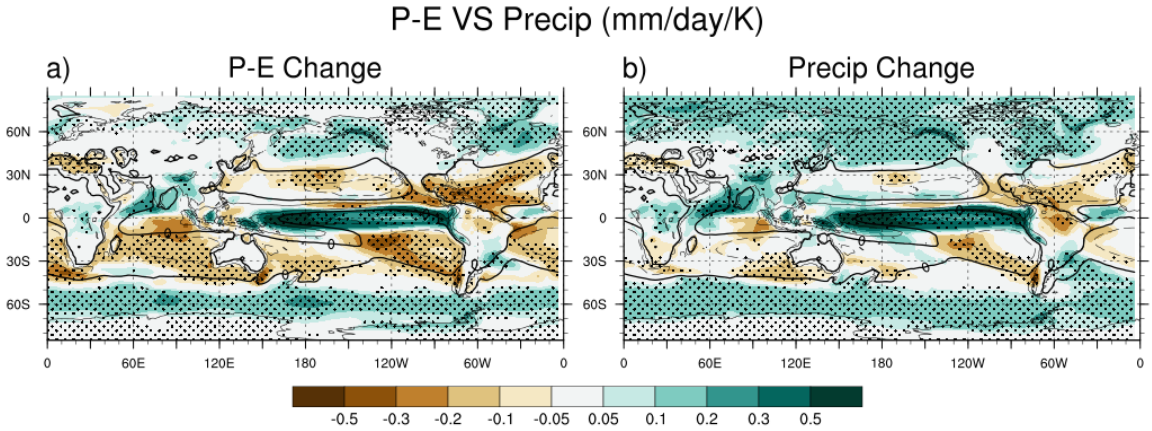

Figure 6.1 Annual mean changes (shading) in a) P – E and b) precipitation from the 1pctCO2 simulation, superimposed on the climatological P – E (contour). Contour interval is 3 mm/day. Dashed lines represent negative values. Zero contours are thickened. Robust regions where the ensemble mean change exceeds one inter-model standard deviation are stippled.

However, the actual pattern of precipitation change differs substantially from the pattern of changes in P – E (compare Fig. 6.1a and Fig. 6.1b). In the subtropics, the precipitation reductions are mostly located poleward of the climatological P – E minima, suggesting that their main cause is a dynamic shift of the subtropical dry zones instead of the thermodynamic response to increasing moisture (Scheff and Frierson 2012a,b). In the extratropics, the increase in precipitation is larger and more robust than the increase in P – E. Lorenz and DeWeaver (2007) showed that the extratropical precipitation increase does not exactly follow the Clausius-Clapeyron rate and is explained substantially better when changes in the zonal wind are taken into account.

The above studies demonstrated the complexity of the mechanisms of subtropical and extratropical precipitation changes and suggested that these changes should involve more than thermodynamic processes. If regional precipitation changes were simply a thermodynamic process, they would be largely determined by the present-day

precipitation pattern and would be primarily driven by the global mean surface warming. However, it has been shown that a substantial portion of precipitation change is independent of global mean surface warming.

Recent studies of the tropics found that changes in precipitation could be driven by both the atmospheric radiative forcing, which is mostly associated with the rising CO_2 concentration, and the increasing sea surface temperature (SST), which includes the mean SST warming and the pattern of SST warming. For example, the mean SST warming dominates changes in the tropical mean hydrological cycle (Thorpe and Andrews 2014), whereas the direct CO_2 forcing (Bony et al. 2013) and the pattern of SST change (e.g., Xie et al. 2010; Ma and Xie 2013; Huang et al. 2013) contribute substantially to the spatial distribution of tropical precipitation change. However, few studies have examined the relative importance of these driving forces for precipitation changes in the subtropics and extratropics.

This study aims to identify the physical drivers of the subtropical and extratropical precipitation changes by analyzing an ensemble of AMIP-type simulations, in which direct CO_2 forcing, mean SST warming and pattern of SST change are specified individually. This study also aims to disentangle the fast and slow precipitation responses by examining the timescales of which the different types of forcing occur. For example, studies have shown that a substantial portion of tropical precipitation change is independent of the slow SST warming but rather a fast response to the direct CO_2 forcing (e.g., Mitchell 1983; Cao et al. 2012; Bony et al. 2013) and the pattern of SST change (Chadwick et al. 2014). However, the timescales of precipitation change outside the tropics are yet to be determined. By identifying the physical drivers of subtropical and

extratropical precipitation changes, this study also explains the timescales of these changes.

6.2 Data and Methods

6.2.1 Model simulations

I analyze the monthly output of coupled and atmosphere-only simulations from the Coupled Model Intercomparison Project, phase 5 (CMIP5) archive. To show the total effect of direct CO_2 forcing and SST change, I use the 1pctCO2 simulation, in which the mean climate is defined as the average of years 1 to 20 and the perturbed climate as the average of years 121 to 140. To study the individual effect of the forcing agents, I examine the atmosphere-only simulations: 1) the CO_2 only simulations (AMIP_CO2), in which the atmospheric CO_2 concentration is quadrupled, 2) the mean SST increase simulations (AMIP_mean), in which a uniform +4K SST anomaly is prescribed, 3) the structured SST increase simulations (AMIP_future), in which the SST anomalies are prescribed as the composite of the SST responses taken from the coupled model CMIP3 experiments at the time of CO_2 quadrupling. The effect of the pattern of SST change is estimated by subtracting the climate changes in AMIP_mean from AMIP_future; and I refer to the residual as AMIP_pattern. All AMIP simulations are run for 30 years, using the observed SST from 1979 to 2008 as the base climate. Nine CGCMs and their AGCM counterparts are used for the 1pctCO2 and AMIP simulations: bcc-csm1-1, CanESM2/CanAM4, CNRM-CM5, HadGEM2-ES/HadGEM2-A, IPSL-CM5B-LR, MIROC5, MPI-ESM-LR, MPI-ESM-MR and MRI-CGCM3.

The forcing in the AMIP_CO2 simulation includes both the atmospheric radiative forcing and the land-sea warming contrast (Chadwick et al. 2014). For simplicity, I refer to the total forcing in the AMIP_CO2 simulation (forcing independent of changes in SST) as the direct CO_2 forcing, but I will add necessary clarifications to the context. To estimate the impact of land-sea warming contrast, I also analyze an ensemble of idealized aqua planet simulations forced with quadruple CO_2 (aqua_CO2) and 4K uniform warming (aqua_mean). The aqua planet simulations are run for 5 years with prescribed SST. Six models are used for the aqua planet simulations, namely CCSM4, CNRM-CM5, IPSL-CM5A-LR, MPI-ESM-LR, MPI-ESM-MR and MRI-CGCM3.

To equalize the magnitude of CO_2 and SST forcing in the 1pctCO2 and uncoupled simulations, climate changes in the AMIP and aqua simulations are first scaled linearly to match the CO_2 and tropical SST forcing in the 1pctCO2 simulations. Specifically, the changes from the quadrupled AMIP_CO2 simulation are multiplied by a factor of 3.3/4.0 to account for the smaller increase in CO_2 (which increases by only a factor of 3.3 between years 1 and 120) in the 1pctCO2 simulation; i.e., I assume that the climate responds linearly to increasing CO_2. Finally, climate change is normalized by each model's global mean surface temperature change in the 1pctCO2 simulation and then averaged across models to yield a multi-model ensemble mean, in order to avoid dominance by models with large climate sensitivity.

To study the fast and slow responses of precipitation change, I examine the abrupt4xCO2 simulation, in which the atmospheric CO_2 concentration is instantaneously quadrupled from the pre-industrial level. Following previous studies (e.g., Bony et al. 2013; Chadwick et al. 2014), the fast response is defined as the ensemble mean climate

change one year after the CO_2 quadrupling. The base climate for the abrupt4xCO2 simulation is calculated from the last 100 years of the pre-industrial control simulation. Ten models are used for the abrupt4xCO2 simulation: bcc-csm1-1, CanESM2, CCSM4, CNRM-CM5, GFDL-CM3, GFDL-ESM2M, IPSL-CM5A-LR, IPSL-CM5B-LR, MIROC5, MPI-ESM-LR, MPI-ESM-MR, MRI-CGCM3 and NorESM1-M. For all simulations, one realization from each model is taken.

6.2.2 Regions of robust precipitation change

I define robust precipitation change as the ensemble mean precipitation change that exceeds one inter-model standard deviation, which is a common definition of robustness in climate modeling studies. It is validated by defining robustness as 90% (or more) model agreement on the sign of precipitation change, which yields similar results (figures not shown). Following this definition, most of the subtropical and extratropical precipitation changes shown in Figure 6.1b are robust. I categorize the robust precipitation decrease regions between 10^o and 60^o latitude as the subtropical drying zones and the robust precipitation increase regions poleward of 40^o as the extratropical moistening zones.

Overall, both the magnitude and the structure of subtropical and extratropical precipitation changes in the 1pctCO2 simulation are well reproduced by the sum of the AMIP_CO2, AMIP_mean and AMIP_pattern simulations (compare Fig. 6.1b and Fig. 6.2a). This means that the responses of subtropical and extratropical precipitation to the forcing agents are linearly additive. The location of the subtropical drying zones and extratropical moistening zones are very similar in the 1pctCO2 simulation and the sum of

AMIP simulations, except the tropical northeast Pacific and the North Atlantic where precipitation change is only robust in the AMIP simulations. For consistency, I use the robust regions in Figure 6.2a for the analyses of all AMIP simulations, but the inclusion of the tropical northeast Pacific and the North Atlantic regions does not impact my main conclusions. For brevity, I mainly analyze the annual mean precipitation change instead of the seasonal mean. My main conclusions do not depend on seasons.

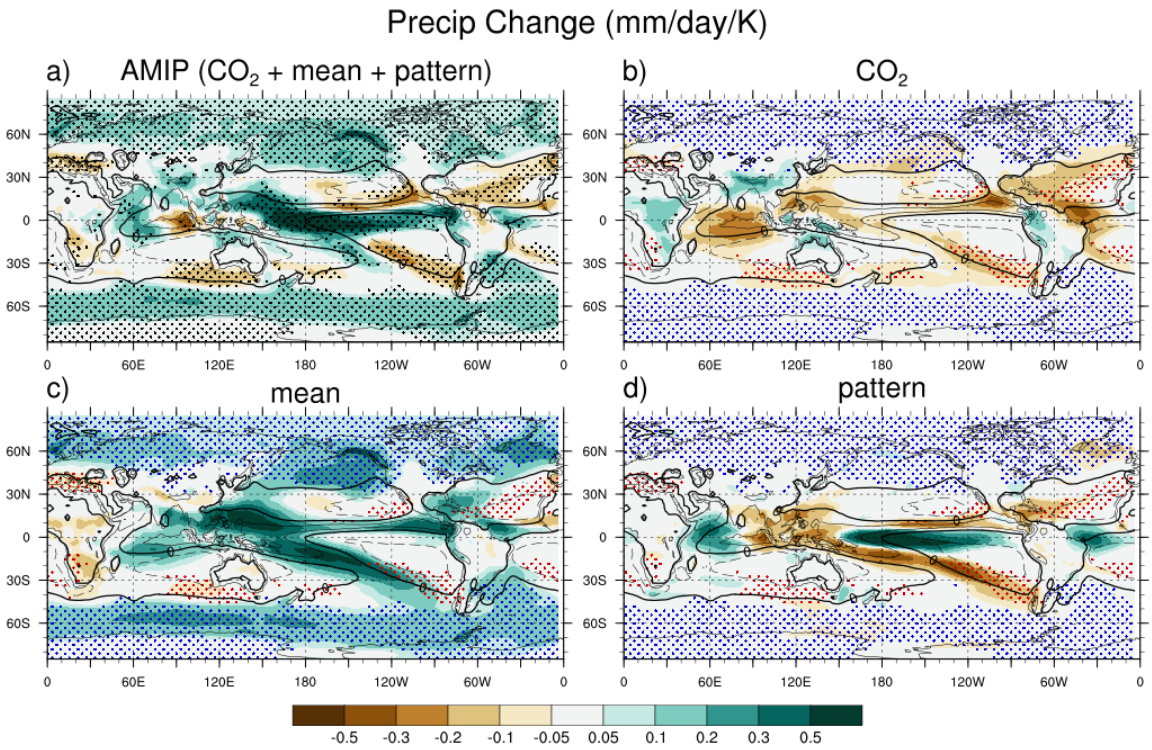

Figure 6.2 Annual mean precipitation changes (shading) from a) the sum of AMIP_CO2, AMIP_mean and AMIP_pattern, b) AMIP_CO2, c) AMIP_mean and d) AMIP_pattern, superimposed on the climatological P – E (contour). Contour interval is 3 mm/day. Dashed lines represent negative values. Zero contours are thickened. In a), robust regions where the ensemble mean precipitation change exceeds one inter-model standard deviation are stippled in black. Red and blue stippling indicates the subtropical drying zones and the extratropical moistening zones as defined in Section 6.2.

6.2.3 Moisture budget decomposition

To understand the mechanisms of precipitation change, I decompose precipitation change based on the column integrated moisture budget (Seager et al. 2010)

$$\partial P = -\langle \Delta(V \cdot \partial q) \rangle - \langle \Delta(\partial V \cdot q) \rangle - \langle \Delta(\partial V \cdot \partial q) \rangle + \partial E + R, \qquad (6.1)$$

where P, V, q and E are the monthly mean precipitation, horizontal velocity, specific humidity and evaporation, respectively. ∂ denotes the perturbation from the base climate. $\langle * \rangle$ represents column mass integration from surface to 50 hPa, where I assume the pressure velocity to be zero. The first term on the right hand side represents the precipitation change due to moisture change and is referred to as the thermodynamic change, whereas the second term represents the precipitation change due to the mean circulation change and is referred to as the dynamic change. The dynamic term consists of changes due to convergence change and advection change and is dominated by the convergence change in the tropics (Seager et al. 2010). The third term on the right hand side is much smaller than the other terms and will be neglected for discussion. R is the residual and consists mostly of changes in transient eddy transport. Discrepancies between R and the actual changes in transient eddy transport exist mainly in regions of topography and are very small outside the tropics (Seager et al. 2010).

6.3 Results

6.3.1 P – E changes VS precipitation changes

I start my analyses by examining the changes in P – E. As shown in Figure 6.1a and 3a, changes in P – E closely follows a "wet-get-wetter and dry-get-dryer" pattern, which is simply a response to the increase in moisture (Held and Soden 2006). Because

the increase in moisture is dominated by the mean SST warming (Compo and Sardeshmukh 2009), the changes in P – E are well reproduced in the AMIP_mean simulation (Fig. 6.3c). Discrepancies between Fig. 6.3a and Fig. 6.3c exist primarily in the deep tropics (Fig. 6.3d), where the pattern of SST change induces large changes in the hydrological cycle through changes in circulation (e.g., Xie et al. 2010).

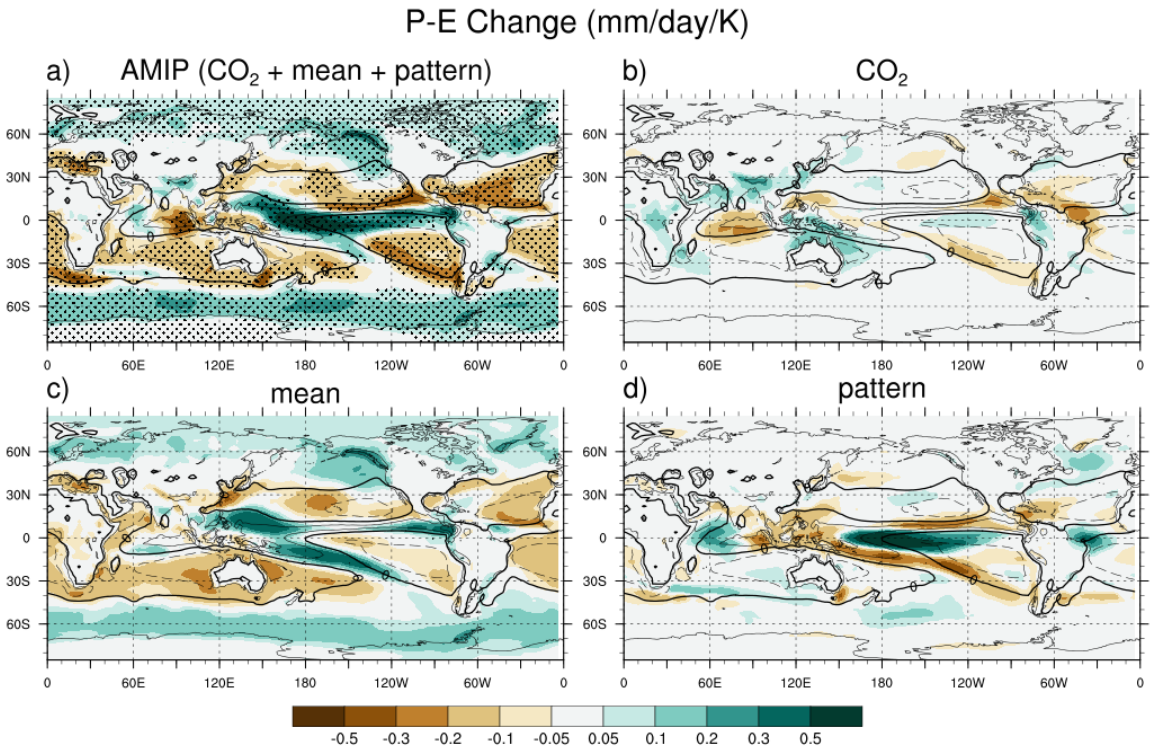

Figure 6.3 Annual mean P – E changes (shading) from a) the sum of AMIP_CO2, AMIP_mean and AMIP_pattern, b) AMIP_CO2, c) AMIP_mean and d) AMIP_pattern, superimposed on the climatological P – E (contour). Contour interval is 3 mm/day. Dashed lines represent negative values. Zero contours are thickened. In a), robust regions where the ensemble mean P – E change exceeds one inter-model standard deviation are stippled.

Compared to the changes in P – E, changes in precipitation have a very different structure (compare Fig. 6.1a and 1b or Fig. 6.3a and 2a). This difference is particularly apparent in the subtropics, where the majority of precipitation declines is only found poleward of the subtropical precipitation minima. This is consistent with the seasonal analysis by Scheff and Frierson (2012a,b). They suggested that the cause of the

subtropical declines should be dynamical shifts of the mid-latitude dry zones instead of the thermodynamic "dry-get-dryer" mechanism since the thermodynamic mechanism would require precipitation to decrease both poleward and equatorward of the subtropical precipitation minima. These dynamic shifts may be related to changes in atmospheric circulation that have already been identified, including the expansion of the Hadley cell (Lu et al. 2007; Frierson et al. 2007), the shift of the storm tracks (McCabe et al. 2001; Fyfe 2003) and the weakening of convection (e.g., Vecchi and Soden 2007; Ma et al. 2012; Chadwick et al. 2013).

Furthermore, the AMIP_mean simulation fails to capture the majority of subtropical precipitation declines (Fig. 6.2c), which further suggested that changes in the subtropical precipitation are most likely driven by factors other than the increase in moisture. This is in contrast to the mechanisms of changes in P – E (Fig. 6.3c). I devote the remaining sections of this study to investigating the mechanisms of changes in precipitation, a variable of more direct applications and socioeconomic importance than P – E.

6.3.2 Precipitation changes in the AMIP simulations

Figures 6.2b-d show changes in precipitation due to the direct CO_2 forcing, mean SST warming and the pattern of SST change. The direct CO_2 forcing reduces precipitation over most of tropical and subtropical oceans and increases precipitation over most of the tropical land regions. This pattern of precipitation change is mainly associated with the stabilization of the troposphere and the land-sea warming contrast (Bony et al. 2013; Chadwick et al. 2014). The precipitation decline affects most of the

subtropical drying zones (red stippling) with a magnitude comparable to the total subtropical drying (Fig. 6.2a). In the extratropical moistening zones (blue stippling), however, the direct CO_2 forcing has little impact except for decreasing precipitation in the northeast Pacific.

The mean SST warming induces substantial precipitation increase over convective zones, especially over tropical oceans. This "wet-get-wetter" response is consistent with the thermodynamic theory by Held and Soden (2006). In comparison, however, the "dry-get-dryer" response is almost indiscernible, indicating that other processes may exist in the subtropics to counter the thermodynamic effect. In the subtropical drying zones, the mean SST warming induces little drying except the Mediterranean Sea and the southeast Indian Ocean; it even increases precipitation over the northwest Atlantic and the southeast Pacific. On the other hand, the mean SST warming contributes substantially to the extratropical moistening, with a magnitude similar to the total moistening (Fig. 6.2a).

The pattern of SST change plays an important role in setting the spatial distribution of precipitation change over tropical oceans, where warmer (colder) SST increases (decreases) local precipitation (e.g., Xie et al. 2010; Ma and Xie 2013). Nevertheless, it has little impact over the extratropics and land (Chapter 3). In the subtropical drying zones, the pattern of SST change appears only effective over the southeast Pacific and the northeast Atlantic, but the magnitude of the precipitation declines it causes is considerable. In the extratropical moistening zones, precipitation is overall insensitive to the pattern of SST change except the North Atlantic Ocean and certain parts of the Southern Ocean, where precipitation declines due to the cold SST.

Note that the North Atlantic Ocean is not a robust zone in the 1pctCO2 simulation (Fig. 6.1b).

6.3.3 Moisture budget analysis

To understand the mechanism of the subtropical and extratropical precipitation changes, I decompose the total precipitation change into thermodynamic change, dynamic change, evaporation change and eddy transport change (Eq. 6.1). As shown in Figure 6.4, the thermodynamic and dynamic terms mainly affect the tropics and to some degree oppose each other (with an ensemble mean spatial correlation of -0.42). The opposing patterns of the thermodynamic term and the dynamic term reflect the competing effect of moisture increase and circulation weakening (Chadwick et al. 2013). The thermodynamic term reduces precipitation substantially at regions of subtropical precipitation minima but has much less impact in the subtropical drying zones, which are generally located poleward of the precipitation minima (Fig. 6.1b; Scheff and Frierson 2012a,b). In comparison, the dynamic term has more impact in the subtropical drying zones. This confirms the implication by Scheff and Frierson (2012a,b) that the subtropical drying is mainly caused by dynamic processes instead of the thermodynamic "dry-get-dryer" mechanism. The evaporation term contributes positively to precipitation change with considerably less spatial structure than the thermodynamic term and the dynamic term. It reduces drying in the subtropics and increases moistening in the extratropics, especially over ocean. The eddy moisture transport decreases at the poleward flank of the subtropics and increases at higher latitudes, consistent with an intensification of eddy moisture transport (e.g., Yin 2005; Seager et al. 2010; Wu et al.

2011). It does not appear to have a consistent impact on the subtropical drying zones but contributes substantially to the precipitation increase in the extratropics.

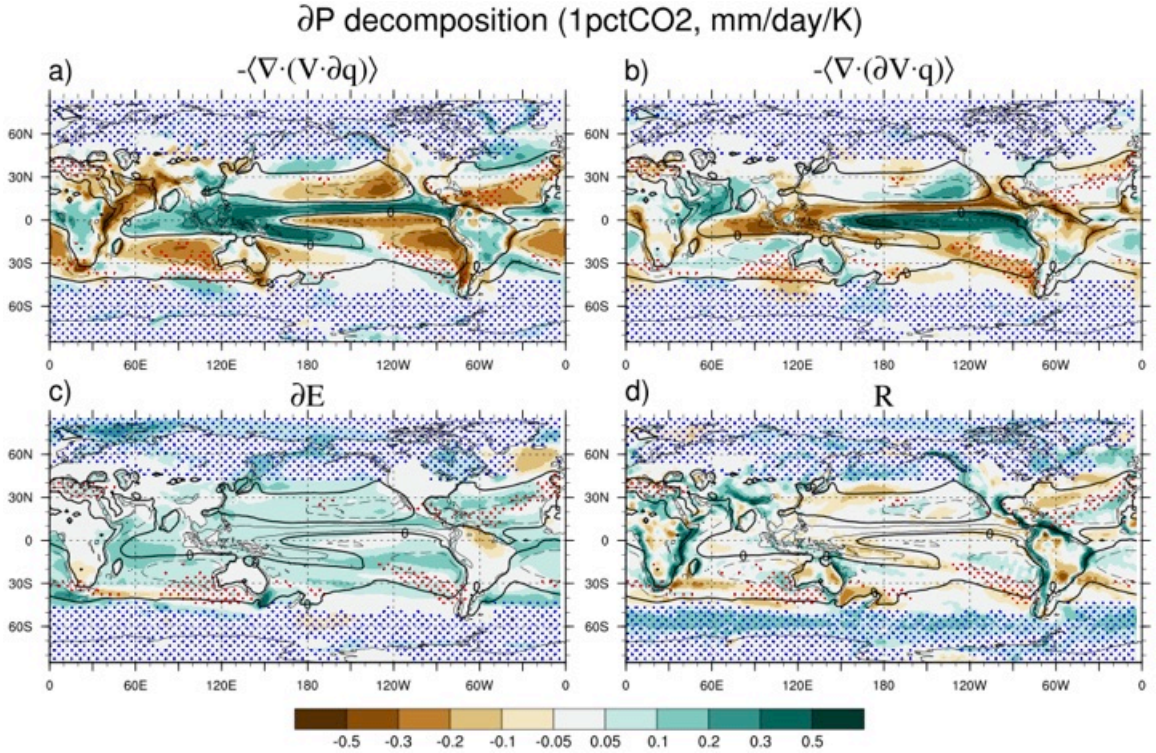

Figure 6.4 Maps of the decomposition terms of the annual mean precipitation change from the 1pctCO2 simulation as defined in Eq. 6.1 (shading), superimposed on the climatological P – E (contour). Contour interval is 3 mm/day. Dashed lines represent negative values. Zero contours are thickened. Red and blue stippling indicates the subtropical drying zones and the extratropical moistening zones as defined in Section 6.2.

Figures 6.5 to 6.7 show the decomposition of precipitation change in the AMIP_CO2, AMIP_mean and AMIP_pattern simulations. In the AMIP_CO2 simulation (Fig. 6.5), the largest terms in Eq. 6.1 are the dynamic term and the evaporation term, both of which contribute negatively to precipitation change over tropical and subtropical oceans. On the other hand, the dynamic term also increases precipitation over land with a magnitude similar to that of the dynamic precipitation decrease over ocean. This indicates that the dynamic drying in AMIP_CO2 is mostly due to the land-sea warming contrast (Chadwick et al. 2014) instead of the stabilizing effect of CO_2 (e.g., Cao et al. 2012;

Bony et al. 2013). I will further demonstrate this point with the aqua planet simulations in Section 3d. Nevertheless, because the subtropical drying zones are generally located over ocean, the dynamic term leads to an overall drying in these regions.

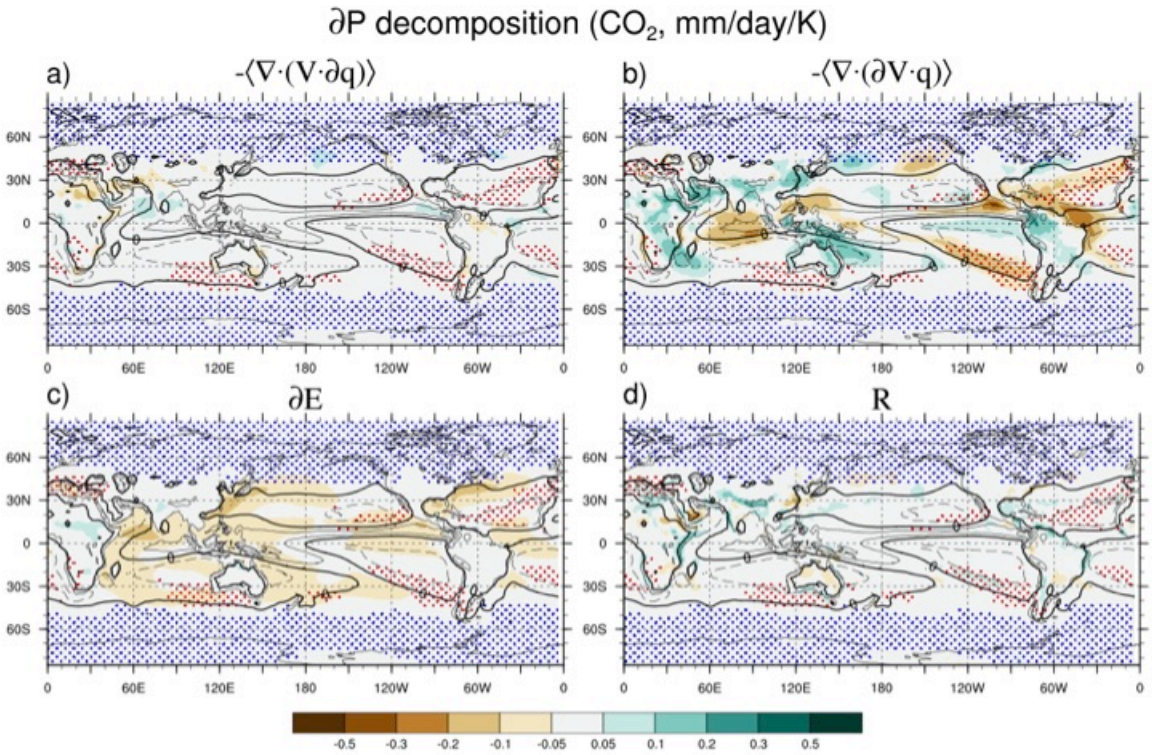

Figure 6.5 Same as Fig. 6.4 except for the AMIP_CO2 simulation.

As shown in Figure 6.6, the mean SST warming is the largest contributor to the thermodynamic change in precipitation due to its dominance over moisture (e.g., Compo and Sardeshmukh 2009). The increase in moisture amplifies precipitation considerably in the northwest Atlantic and the northeast Pacific (the latter is not a robust zone in the 1pctCO2 simulation) but is relatively less impactful in the other subtropical drying zones, which are located poleward of the precipitation minima. The dynamic term is generally smaller than the thermodynamic term and does not appear to have a consistent impact on the subtropical drying zones except the Mediterranean Sea and the southeast Indian Ocean. Evaporation increases consistently over ocean, reducing the precipitation decline

in the subtropics while amplifying the precipitation increase in the extratropics. The mean SST warming is also the largest contributor to changes in the eddy transport (compare Fig. 6.4d and Fig. 6.6d), which has a large impact on the extratropical precipitation increase.

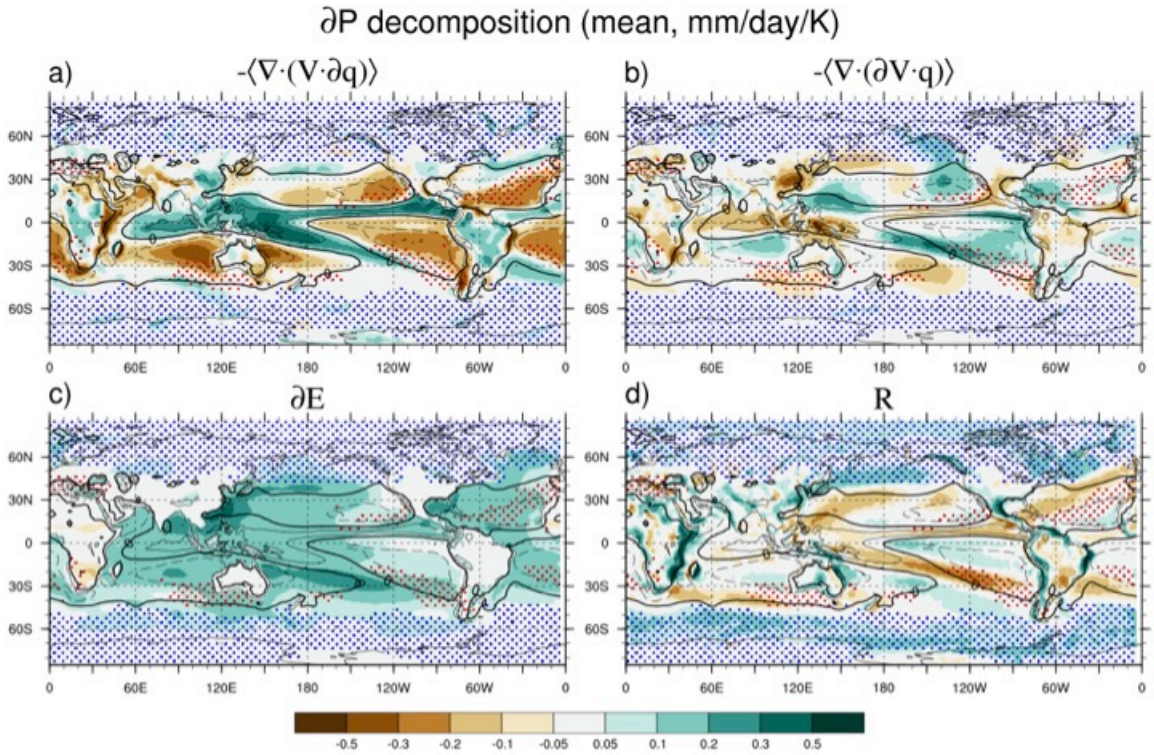

Figure 6.6 Same as Fig. 6.4 except for the AMIP_mean simulation.

The pattern of SST change impacts the pattern of precipitation change primarily through its influence on the mean circulation (Fig. 6.7). The reduced SST warming in the subtropical southeast Pacific and northwest Atlantic causes anomalous moisture divergence, which contributes considerably to the precipitation decline. The southeast Pacific also features a weak reduction in evaporation and a north-south dipole pattern of eddy transport change. The latter generally opposes the intensification of eddy moisture transport that can be seen in the 1pctCO2 and AMIP_mean simulations (Fig. 6.4d and Fig. 6.6d). In the extratropical North Atlantic (not a robust zone in 1pctCO2) and certain

parts of the Southern Ocean, the cold SST also reduces precipitation by suppressing evaporation.

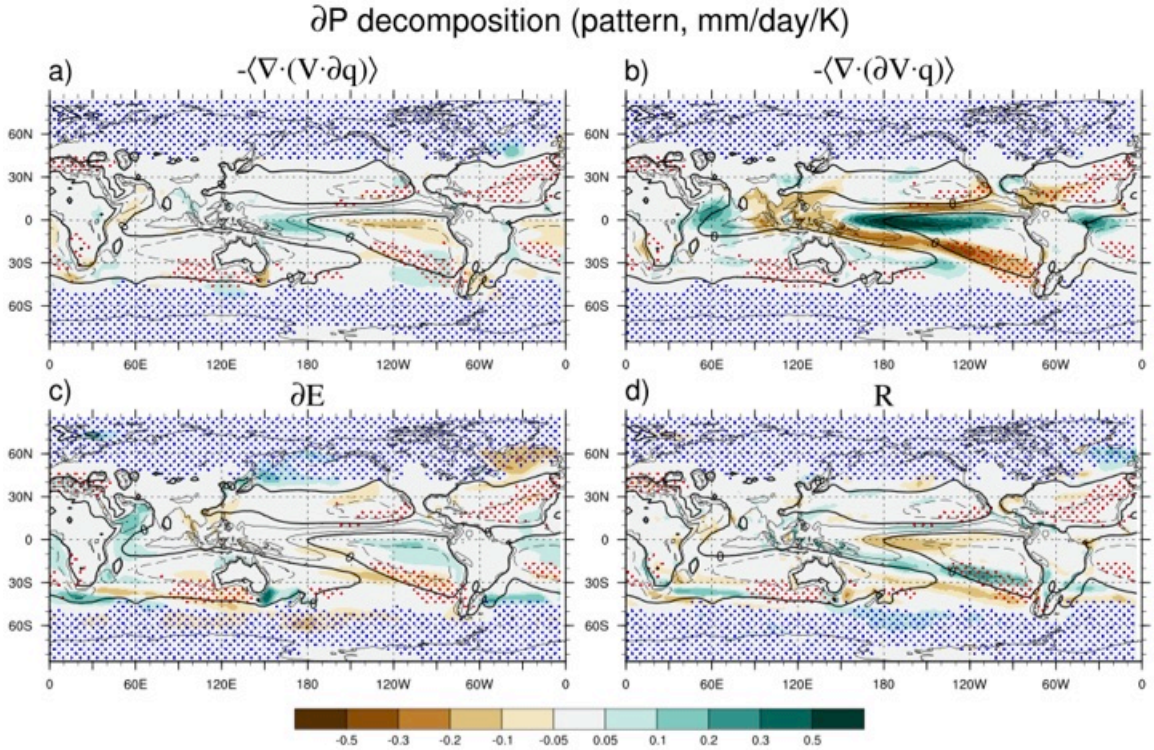

Figure 6.7 Same as Fig. 6.4 except for the AMIP_pattern simulation.

Figures 6.8 and 6.9 summarize the individual impacts of the forcing agents on subtropical drying and extratropical moistening. As shown in Figure 6.8, the subtropical precipitation decline is primarily driven by the direct CO_2 forcing and the pattern of SST change, both of which reduce precipitation through dynamic changes and evaporation declines. The mean SST warming has virtually no impact on the total precipitation decline in the subtropics. It slightly increases the annual mean precipitation and slightly reduces precipitation in DJF and JJA (supplementary material). The "dry-get-dryer" mechanism is approximately counterbalanced by the increase in evaporation. On the other hand, the mean SST warming dominates the extratropical precipitation increase (Fig. 6.9). The increased evaporation and eddy transport provide most of the extra

moisture for extratropical precipitation, whereas changes in the mean moisture transport are less important.

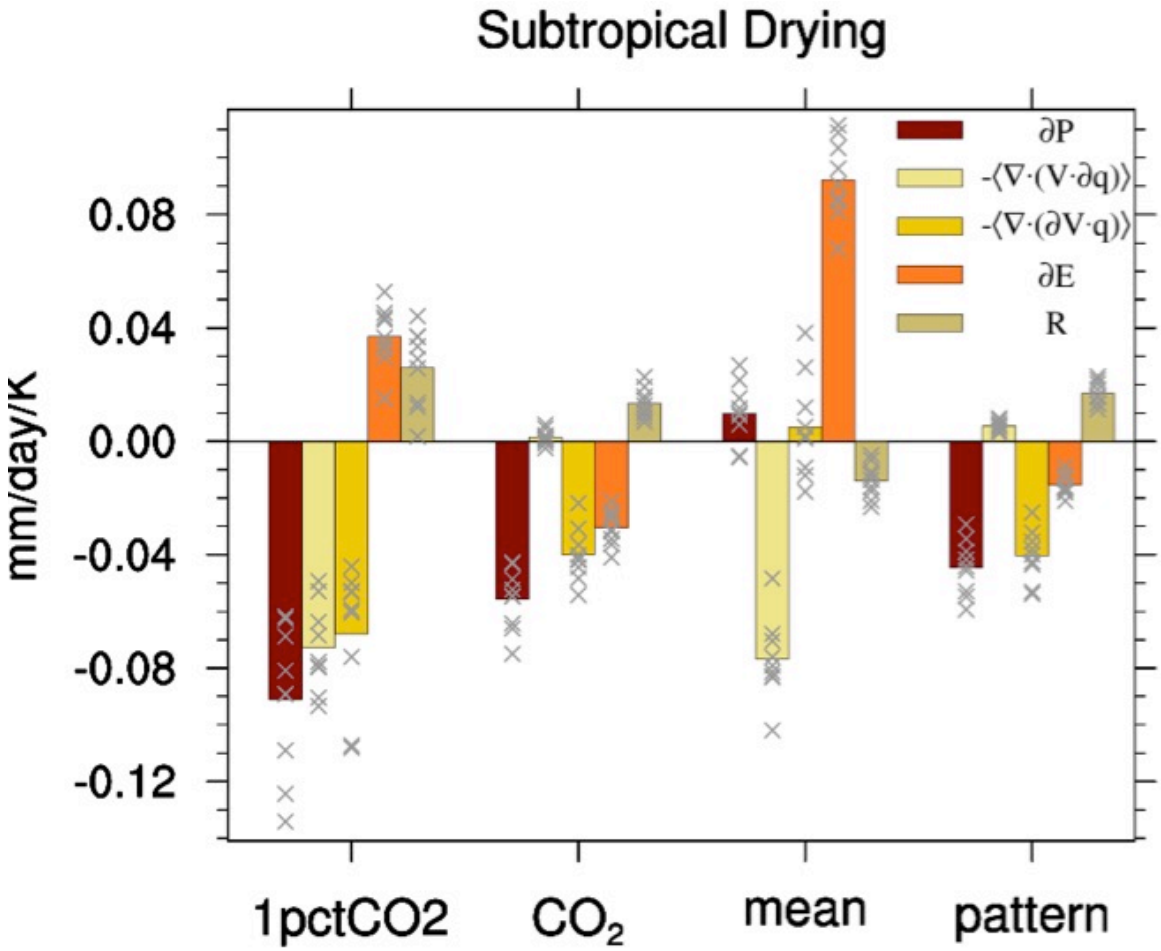

Figure 6.8 Annual mean values of the terms in Eq. 6.1 averaged over the subtropical drying zones from the 1pctCO2 simulation and the AMIP simulations. Bars represent the ensemble mean value, whereas crosses represent each individual model.

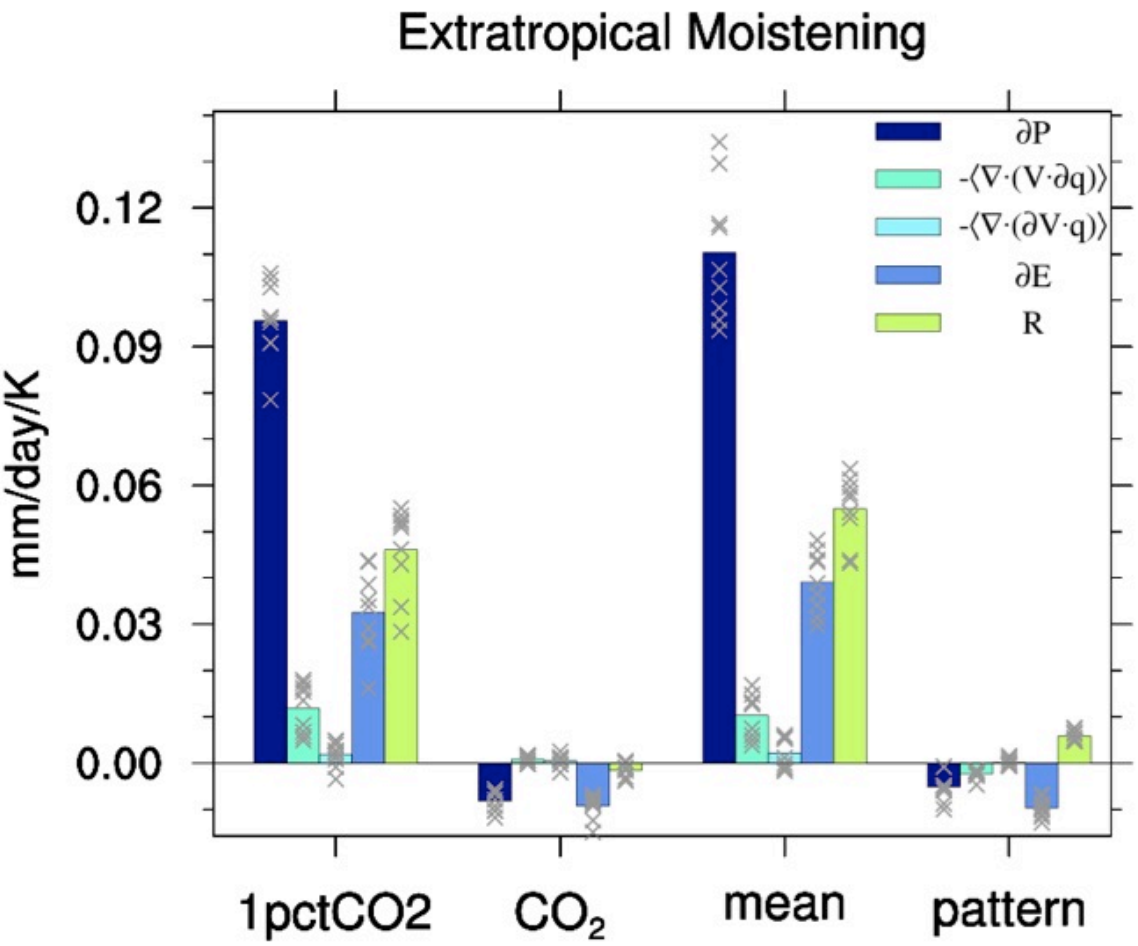

Figure 6.9 Same as Fig. 6.8 except for the extratropical moistening zones.

6.3.4 Idealized aqua planet simulations

To further understand the roles of direct CO_2 forcing and mean SST warming, I analyze the precipitation responses in the idealized aqua planet simulations. As shown in Figure 6.10, the latitudinal positions of the subtropical drying zones and extratropical moistening zones are reasonably reproduced in the sum of aqua_CO2 and aqua_mean. Similar to the AMIP simulations, the extratropical precipitation increase in the aqua planet simulations is also driven by the mean SST warming, with evaporation and transient eddy transport being the major components of moisture contribution. Changes in

the eddy transport are the largest at the equatorward flank of the extratropics (Wu et al. 2011), which is also seen in the realistic simulations (Fig. 6.4d and Fig. 6.6d). In comparison, changes in evaporation are more meridionally uniform.

The magnitude of subtropical precipitation decline caused by the direct CO_2 forcing is much smaller in the aqua planet simulation (Fig. 6.10a) than that in the AMIP simulation (Fig. 6.2b). In the aqua_CO2 simulation, the subtropical precipitation decline is mainly due to the reduced evaporation instead of changes in the circulation. Therefore, the dynamic reduction in the subtropical precipitation in the AMIP_CO2 simulation is most likely caused by the land-sea warming contrast instead of the increased static stability. Previous studies showed that the direct CO_2 forcing only stabilizes the atmosphere near the surface (Cao et al. 2012). It is likely that the stabilization of the lower troposphere only suppresses evaporation at the surface but has a relatively small impact on the overturning circulation above the boundary layer.

The mean SST warming also reduces precipitation in the subtropics, with a magnitude similar to the drying of the Mediterranean Sea and the southeast Indian Ocean in the AMIP_mean simulation (Fig. 6.2c). The thermodynamic term, the dynamic term and the eddy transport term all contribute to the precipitation reduction, while the increased evaporation partially offsets it. The role of mean SST warming in the idealized aqua planet simulation is somewhat different than that in the realistic simulation (Fig. 6.8), which is expected as the two simulations have very different patterns of circulation and circulation change.

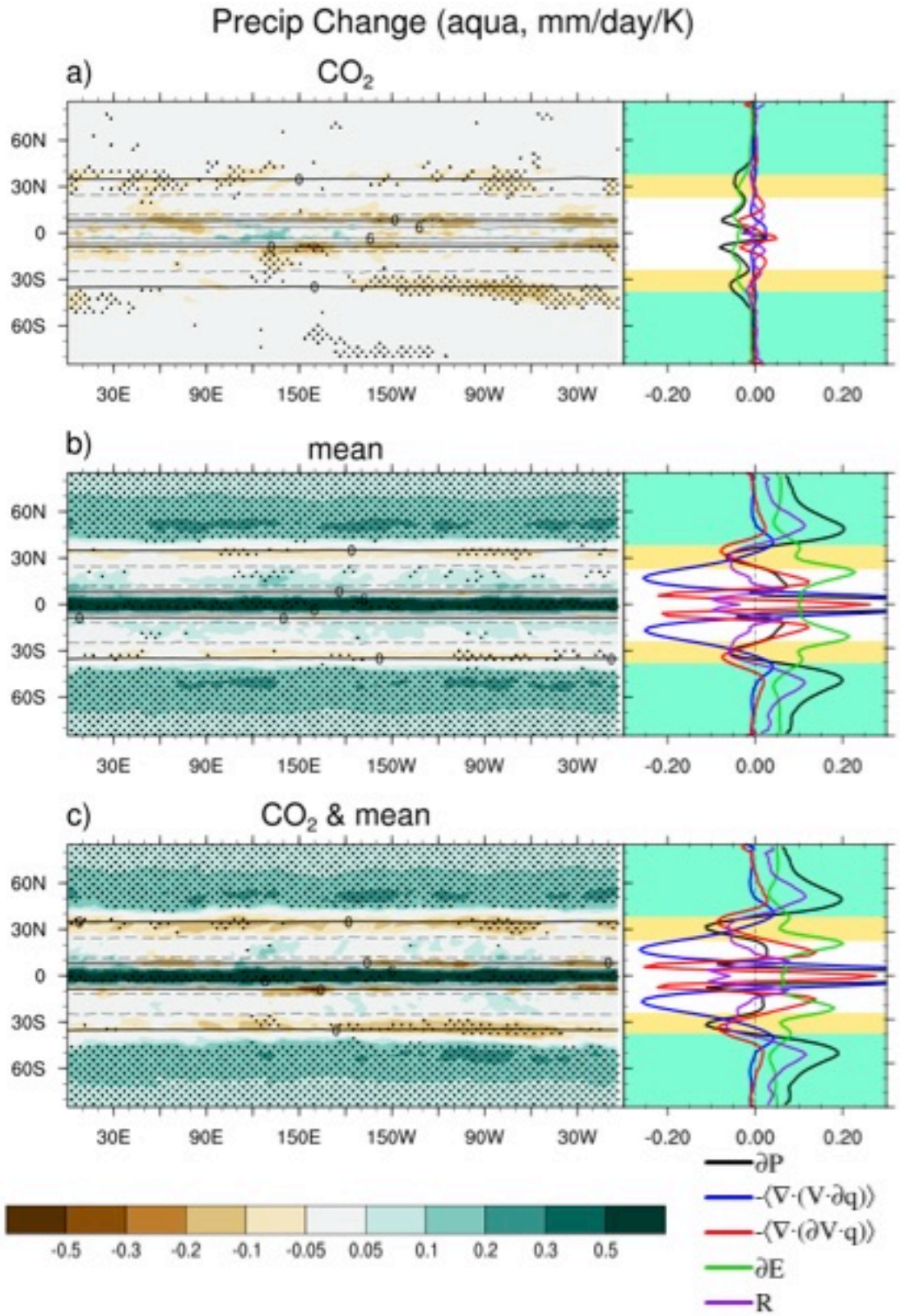

Figure 6.10 Maps (left) of precipitation changes (shading) from a) the aqua_CO2 simulation, b) the aqua_mean simulation and c) the sum of the aqua_CO2 and aqua_mean simulations, superimposed on the climatological P – E (contour). Contour interval is 3 mm/day. Dashed lines

represent negative values. Zero contours are thickened. Regions where the ensemble mean precipitation change exceeds one inter-model standard deviation are stippled. The line plots on the right shows the zonal mean values of the terms in Eq. 6.1. The yellow shading indicates the subtropical drying belts where the zonal mean precipitation change is negative in the sum of the aqua_CO2 and aqua_mean simulations. Likewise, the green shading shows the extratropical moistening belts with positive zonal mean precipitation change.

6.3.5 Timescales of precipitation change

Results from the AMIP simulations have shown that the subtropical precipitation decline is primarily driven by the direct CO_2 forcing and the pattern of SST change, whereas the extratropical precipitation increase is mainly due to the mean SST warming. The difference in the physical drivers indicates that the subtropical precipitation decline and extratropical precipitation increase may form at different timescales. In a climate of rising CO_2, changes in precipitation can be conceptualized as a combination of a fast and a slow component (e.g., Bala et al. 2010, p. 20; Cao et al. 2012; Bony et al. 2013). The fast component is induced through the direct impact of CO_2 on radiation and the rapid adjustments in land surface and SST pattern (e.g., Cao et al. 2012; Bony et al. 2013; Chadwick et al. 2014), whereas the slow component is driven by the mean SST warming, which is delayed due to the large ocean heat capacity. To understand the timescales of subtropical and extratropical precipitation change, I analyze the abrupt4xCO2 simulation, in which the fast precipitation can be detected immediately after the abrupt CO_2 quadrupling.

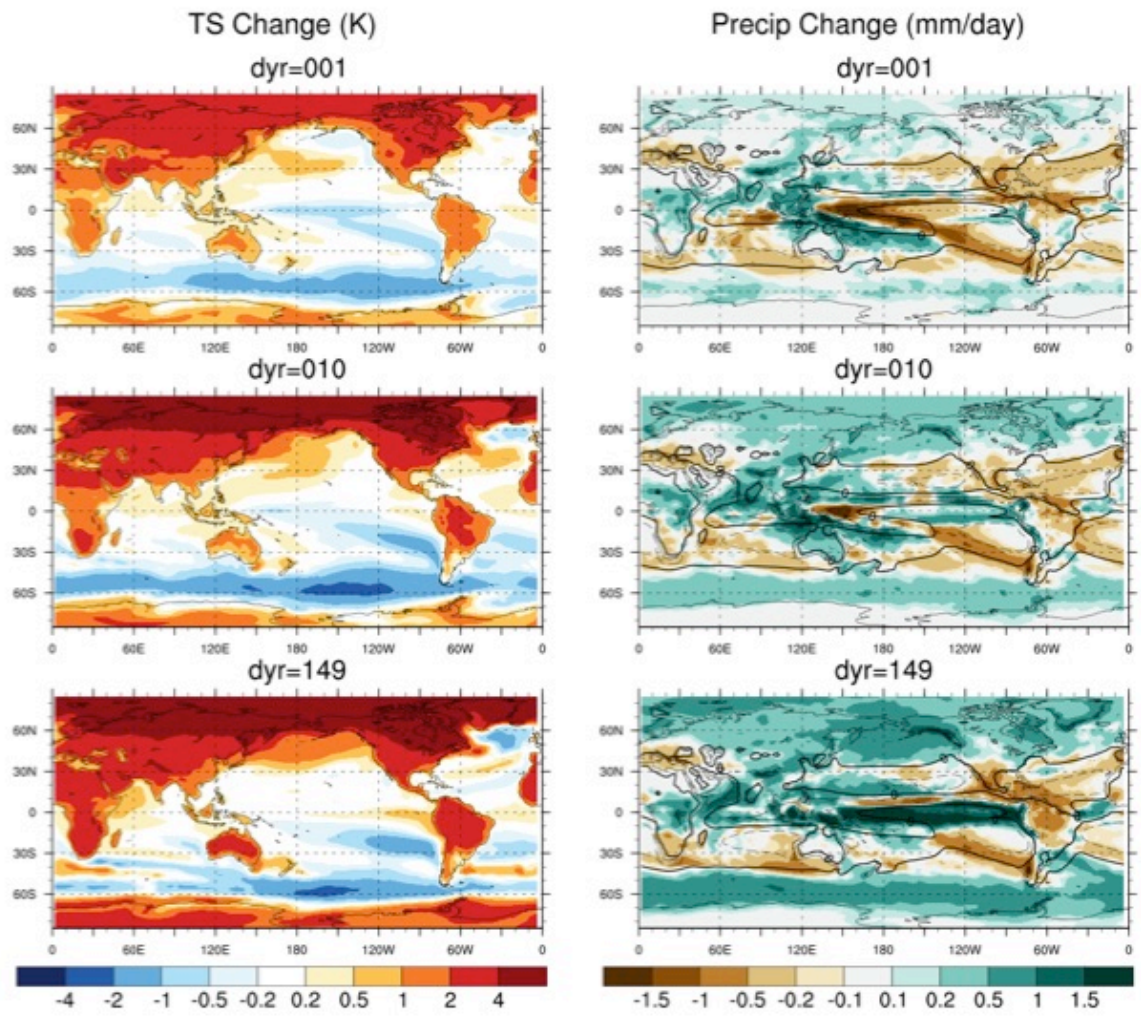

Figure 6.11 Annual mean changes in surface temperature with tropical mean SST change subtracted (left) and annual mean changes in precipitation (right) from the abrupt4xCO2 simulation one year (top), 10 years (middle) and 149 years (bottom) after the simulation starts. Contours in the precipitation maps represent the climatological P – E calculated from the pre-industrial control simulation. Contour interval is 3 mm/day. Dashed lines represent negative values. Zero contours are thickened.

As shown in Figure 6.11 (left), both the land-sea warming contrast and the pattern of SST change form immediately after the CO_2 quadrupling. Although certain SST structures evolve slowly including the equatorial Pacific warming (Andrews et al. 2015) and the North Atlantic cooling (Long et al. 2014), the subtropical SST cooling, which drives the subtropical precipitation decline, forms rapidly (Chadwick et al. 2014; Long et al. 2014). The fast and slow responses of precipitation are shown in Fig. 6.11 (right).

Because the direct radiative forcing, the land-sea warming contrast and the subtropical SST cooling all form at short timescales, the subtropical precipitation decline is primarily a fast response and does not depend on sea surface warming. In contrast, the extratropical precipitation increase is a slow response due to its dependence on the mean SST warming.

Figure 6.12 shows the time evolution of the zonal mean precipitation change and the tropical mean SST change. The subtropical precipitation decline happens immediately after the start of the simulation when the mean SST has barely warmed. The zonal mean precipitation reduction weakens slightly as time passes mainly due to the moistening in the subtropical western Pacific (Fig. 6.11, right), which is likely associated with the slow increase in moisture (Fig. 6.6a; Fig. 6.2 in Bony et al. 2013). In contrary to the fast subtropical precipitation decline, the extratropical precipitation does not increase instantly but rather slowly as the mean SST warms. In addition to the extratropics, precipitation response at the Equator also shows variation over time, which is likely associated with the transition of equatorial Pacific SST response (Andrews et al. 2015).

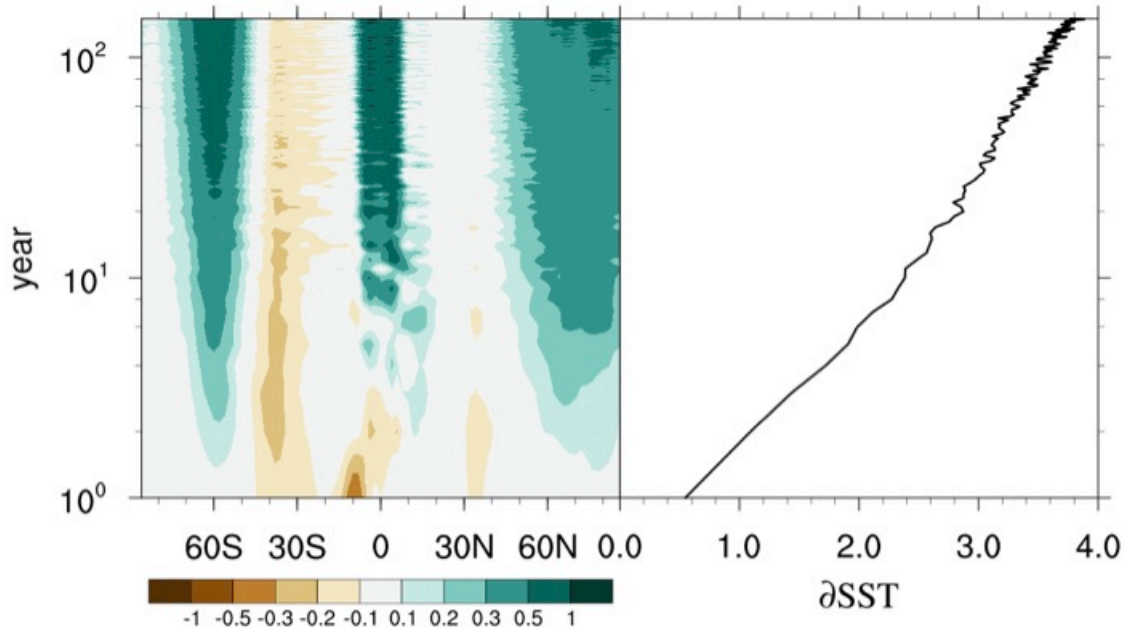

Figure 6.12 Time evolution of the annual mean changes in the zonal mean precipitation (left) and the tropical mean SST (right) in the abrupt4xCO2 simulation. The time (y) axis is logarithmically spaced. Units for the precipitation change and SST change are mm/day and K, respectively.

6.4 Summary

This chapter investigated the relative roles of the direct CO_2 forcing, mean SST warming, and pattern of SST change on the subtropical and extratropical precipitation changes by using an ensemble of AMIP simulations in which the forcing agents are specified individually. Overall, the sum of the AMIP simulations successfully reproduced the subtropical and extratropical precipitation change in the coupled 1pctCO2 simulation, giving credence to my approach.

Results from the AMIP simulations showed that the subtropical precipitation decline is primarily driven by the direct CO_2 forcing and the pattern of SST change, whereas the extratropical precipitation increase is mainly driven by the mean SST warming. In the AMIP_CO2 simulation, the atmospheric radiative forcing and land-sea warming contrast cause reduce precipitation over most of the tropical and subtropical

oceans. The moisture budget analysis showed that this reduction in precipitation is mainly associated with a dynamic weakening of convection and a reduction in evaporation.

The mean SST warming increases precipitation over convective zones but has overall little contribution to the subtropical precipitation decline. This is because the subtropical drying zones are generally located poleward of the subtropical precipitation minima, where the intensified moisture export due to the moisture increase is relatively small and is compensated by the increased evaporation. On the other hand, the mean SST warming is the main driver of the extratropical precipitation increase through its dominance over evaporation and eddy moisture transport.

The pattern of SST change reduces precipitation over the subtropical southeast Pacific and northwest Atlantic, where the SST is relatively cold. This reduction in precipitation is mostly dynamically driven through changes in circulation, although the reduced evaporation also contributes. The pattern of SST change also reduces precipitation over the North Atlantic Ocean and certain parts of the Southern Ocean but is overall ineffective in the extratropics.

This chapter also examined the precipitation responses to direct CO_2 forcing and mean SST warming in the idealized aqua planet simulations. Although the aqua planet simulations have very different patterns of climatology and climate change than those in the realistic simulations, they help to simplify the fundamental processes involved in the subtropical and extratropical precipitation change. The aqua planet simulations showed that the subtropical precipitation decline is mainly associated with the reduced evaporation instead of changes in circulation, which was found in the AMIP_CO2

simulation. This indicates that the dynamic reduction in precipitation in the AMIP_CO2 simulation is predominantly driven by the land-sea warming contrast instead of the tropospheric stratification, which was only found near the surface (Cao et al. 2012).

The physical mechanisms of the subtropical changes in precipitation are very different from those of the changes in P – E. The latter is primarily driven by the mean SST warming through its dominance over moisture increase. These results confirmed previous implications by Scheff and Frierson (2012a,b) that the subtropical precipitation decline is caused dynamically instead of thermodynamically through the "dry-get-dryer" mechanism. These dynamic processes are primarily driven by the radiative impact of CO_2 and the adjustments in land surface and SST patterns, which generally have much shorter timescales than the mean SST warming. On the other hand, the extratropical precipitation increase depends on the slow warming of SST. The difference in the timescales of subtropical and extratropical precipitation changes is evident in the abrupt4xCO2 simulation, in which the subtropical precipitation declines immediately after the CO_2 quadrupling whereas the extratropical precipitation increases rather slowly.

Chapter 7: Conclusions

Climate change has substantially impacted and will continue to impact our society and environment. As a result, there is great demand for accurate predictions of anthropogenic climate change. To achieve better numerical projections, we need to not only improve and innovate our prediction procedures but also understand the mechanisms of climate changes that have already been simulated with the current climate models.

This work addresses some of the challenges in anthropogenic climate change simulations and investigates the mechanisms of anthropogenic changes in precipitation and atmospheric circulation from a collection of state-of-the-art climate models. While climate models will continue to have errors, this work demonstrates that we may be able to achieve better projections of regional climate change by emphasizing the important elements in our simulations, such as an accurate SST climatology. Although uncertainties inevitably exist, many of the simulated characteristics of anthropogenic climate changes are robust. This work shows that some of these robust characteristics can be physically explained and attributed to the changes in the atmospheric radiation and the warming of the earth's surface.

Chapter 2 assessed the importance of two-way air-sea coupling and the validity of AGCMs for the simulation of anthropogenic climate change. AGCMs are often considered inadequate for studying natural climate variability due to their lack of coupling with an underlying ocean. This lack of two-way air-sea coupling results in an inconsistency in surface energetics. However, a comparison between coupled and AGCM simulations showed that anthropogenic climate change can be well reproduced by an AGCM and that errors due to the lack of two-way coupling are primarily limited to

internal variability. Simulations using a stochastic linear model are shown to further support this conclusion. These results suggest a greater utility for AGCMs as computationally efficient tools for understanding and downscaling coupled model simulations of anthropogenic climate change.

Chapter 3 studied the impact of anthropogenic SST change on the atmospheric circulation by comparing AGCM simulations forced with a spatially uniform SST increase and a structured SST increase. The structured SST increase is calculated from the response of an ensemble of coupled ocean-atmosphere models to increased CO_2. *Most of the impact of SST pattern change is confined to equatorial Indo-Pacific.* However, the circulation change under the two types of SST forcing is *almost identical over land and in the extratropics*, indicating that the pattern of future SST change has *overall little* impact on the response of the atmospheric circulation and, in turn, on the resulting changes in precipitation. The similarity between the uniform and structured simulations likely results from the insensitivity of Rossby Wave generation to the changes in near-equatorial upper-level divergence.

Chapter 4 examined the impact of SST biases and compared the utility of CGCMs and AGCMs for simulating regional climate change. CGCMs are traditionally chosen over AGCMs for projections of anthropogenic climate change, despite AGCMs' superior computational efficiency. This choice assumes that the incorporation of the ocean model improves the simulation by allowing for air-sea coupling and the dynamic prediction of SSTs. However, coupling to an ocean model often results in large systematic biases in SSTs, which also impacts the projected changes in climate. This chapter assessed the advantages and disadvantages of both modeling frameworks and show that an accurate

SST climatology is more critical than air-sea coupling or the spatial pattern of SST change for the simulation of anthropogenic climate change over land. These results advocate for a greater application of AGCM simulations or flux-adjusted CGCMs to improve regional projections of anthropogenic climate change.

Chapter 5 investigated the relative roles of direct CO_2 forcing, mean SST warming and the pattern of SST change on the weakening of the tropical circulation using an ensemble of AMIP and aqua planet simulations. In terms of the mean weakening of the tropical circulation, the SST warming dominates over the direct CO_2 forcing through its control over the tropical mean hydrological cycle and tropospheric stratification. In terms of the spatial pattern of circulation weakening, however, the three forcing agents are all important contributors, especially over the ocean. The increasing CO_2 weakens convection over ocean directly by stabilizing the lower troposphere and indirectly via the land-sea warming contrast. The mean SST warming drives strong weakening over the center and edges of convective zones. The pattern of SST warming plays a crucial role on the spatial pattern of circulation weakening over the tropical Pacific. The anthropogenic weakening of the Walker circulation is mostly driven by the mean SST warming. Increasing CO_2 strengthens the Walker circulation through its indirect effect on land-sea warming contrast. Changes in the upper-level velocity potential indicate that the pattern of SST warming does not weaken the Walker circulation despite being “El Niño-like”. A weakening caused by the mean SST warming also dominates changes in the Hadley circulation in the AMIP simulations. However, this weakening is not simulated in the Southern Hemisphere in coupled simulations.

Chapter 6 focused on the mechanisms of the robust changes in the subtropical and extratropical precipitation. The subtropical precipitation decline and extratropical precipitation increase are robust anthropogenic responses from current climate models. These precipitation changes have considerably different spatial structures than the changes in P – E. Contrary to the changes in P – E, the subtropical precipitation decline is not directly associated with the increase in moisture. This is supported by the fact that the subtropical precipitation decline is independent of the global mean SST warming, which dominates the increase in moisture. Instead, the subtropical precipitation decline is primarily driven by the atmospheric radiative forcing, land-sea warming contrast and the pattern of SST change. The increasing CO_2 suppresses evaporative moisture supply directly by stabilizing the lower troposphere and reduces convection over subtropical oceans indirectly through land-sea warming contrast. The pattern of SST change also plays an important role in the subtropical precipitation decline due to the reduced warming in the subtropics. One the other hand, the extratropical precipitation increase is primarily driven by the mean SST warming. Because the radiative forcing of CO_2 and the adjustments in land surface and SST patterns generally have much shorter timescales than the mean SST warming, the subtropical precipitation decline is a much faster response than the extratropical precipitation increase. In the abrupt CO_2 quadrupling simulation, the subtropical precipitation decreases immediately upon CO_2 quadrupling whereas the extratropical precipitation increases slowly following the warming of the SST.

Chapter 8: Future Work

The results presented in the previous chapters are important for understanding the current simulations of anthropogenic climate change. They also suggest practical ways to improve climate projections. In addition to the anthropogenic climate change, internal climate variability is also an important component of near-future climate change. Analyses similar to those applied in the previous chapters might help understand the impacts and mechanisms of low-frequency internal variability. This chapter discusses these research questions as future work. Specifically, I will focus on the following two topics.

- Can we improve the projection of anthropogenic climate change by applying flux adjustments to correct biases in SST? How should the flux adjustment procedure be designed in order to fit in a global warming scenario?
- How are our current projections affected by internal climate variability? Is it possible to predict low-frequency precipitation variability based on the projected changes in SST?

8.1 Flux-adjusted simulations of anthropogenic climate change

As shown in Chapter 4, the climatological biases in the current climate models could result in unrealistic projections of anthropogenic climate change. These biases can be effectively reduced with AGCMs by incorporating observed SSTs. However, AGCMs are unable to directly simulate changes in SST due to the lack of coupling with an underlying ocean. Although the changes in SST might not be impactful for regional

climate change over land, they are important for understanding changes in the climate system as a whole (e.g., Xie et al. 2010). For this purpose, I plan to explore an alternative model framework - the flux-adjusted simulation.

In a typical flux-adjusted experiment, both the heat fluxes and momentum fluxes at the ocean surface are corrected in order to achieve minimum biases in SST climatology. The idea of flux-adjusted simulations is very similar to that of AGCMs with observed SST. The advantage of flux adjustments is that they not only provide more accurate boundary conditions for the sub-systems of the climate (e.g., atmosphere and ocean) but also maintain the dynamic interactions between these sub-systems (Sausen et al. 1988). Therefore, the flux-adjusted experiments may also provide better projections of the pattern of SST change, which have substantial impacts over tropical oceans.

Recent studies have demonstrated that the incorporation of flux adjustments improves seasonal climate predictions (e.g., Magnusson et al. 2013; Vecchi et al. 2014; Jia et al. 2015). Although flux adjustments are a common procedure in the early studies of anthropogenic climate change (Manabe et al. 1991; Murphy 1995), they are rarely applied in the current climate change simulations. Traditionally, the flux-adjustments are applied as a constant correction term regardless of changes in the model's mean climatic state. However, a study by Tziperman (2000) suggested that theses adjustment terms should vary according to the model state. For example, if the flux adjustments are applied to correct the errors in ocean heat transport by the Atlantic meridional overturning circulation (AMOC), they should weaken as the AMOC weakens in a warmer climate. Therefore, the interactive flux adjustment procedure should theoretically be more accurate than the constant flux adjustment procedure, but has yet to be tested. In my

future work, I plan to fully develop the interactive procedure and compare it with the constant procedure. Such work should not only facilitate the improvement of climate simulations but also help understand the interaction between climate changes and the present-day climate.

8.2 Impact of ocean on multi-decadal precipitation variability

Internal climate variability plays an important role in climate change. Deser et al. (2012) showed that regional climate changes at multi-decadal timescales are dominated by internal variability. However, due to the lack of long-term observation, internal variability beyond the decadal timescale is poorly understood. In my future work, I plan to use model simulations to study the mechanisms of multi-decadal climate variability with a focus on precipitation – a highly variable quantity of significant socioeconomic impact.

The internal variability of precipitation can be considered, to first order, as a superposition of a part due to the intrinsic atmospheric dynamics and a part through the atmospheric interaction with other components of the climate system, particularly the ocean. Precipitation variability internal to the atmosphere is characteristic of a white noise and spans a wide range of timescales. Due to the atmosphere's short memory, this part of precipitation variability is inherently unpredictable. On the other hand, the atmospheric white noise can interact with the much slower processes in the ocean mixed layer to yield precipitation fluctuations characteristic of a red noise. This part of precipitation variability can be predictable if it is associated with a predictable SST

variability. Therefore, understanding how much SST controls multi-decadal precipitation variability is the first step toward predicting such precipitation variability.

Previous studies have demonstrated that precipitation variability that is a result of ENSO can be predictable at seasonal timescales (e.g., Shukla 1998). The predictability is found both locally in the tropical Indo-Pacific and remotely in the extratropics and over land. However, the notion of precipitation prediction at longer timescales (including the multi-decadal timescale) is yet to be fully tested. One way to understand how multi-decadal precipitation variability is influenced by SST variability is by comparing long-term simulations from fully coupled models (CGCMs) and atmospheric-only models forced with climatological SST (climSST). Such comparison was recently made possible thanks to the CESM large ensembles conducted at NCAR (Kay et al. 2014).

Due to the slowness of the ocean, it is reasonable to assume a larger impact of SST at longer timescales, hence a larger portion of precipitation variability associated with the SST variability. However, preliminary results from the CESM large ensembles show that the total variance of precipitation at the multi-decadal timescale is similar in the CGCM and climSST simulations over the extratropics and land (Fig. 8.1). This indicates a minimal contribution of ocean to the total precipitation variance. Nevertheless, it is likely that the ocean still impacts the characteristics of precipitation variability.

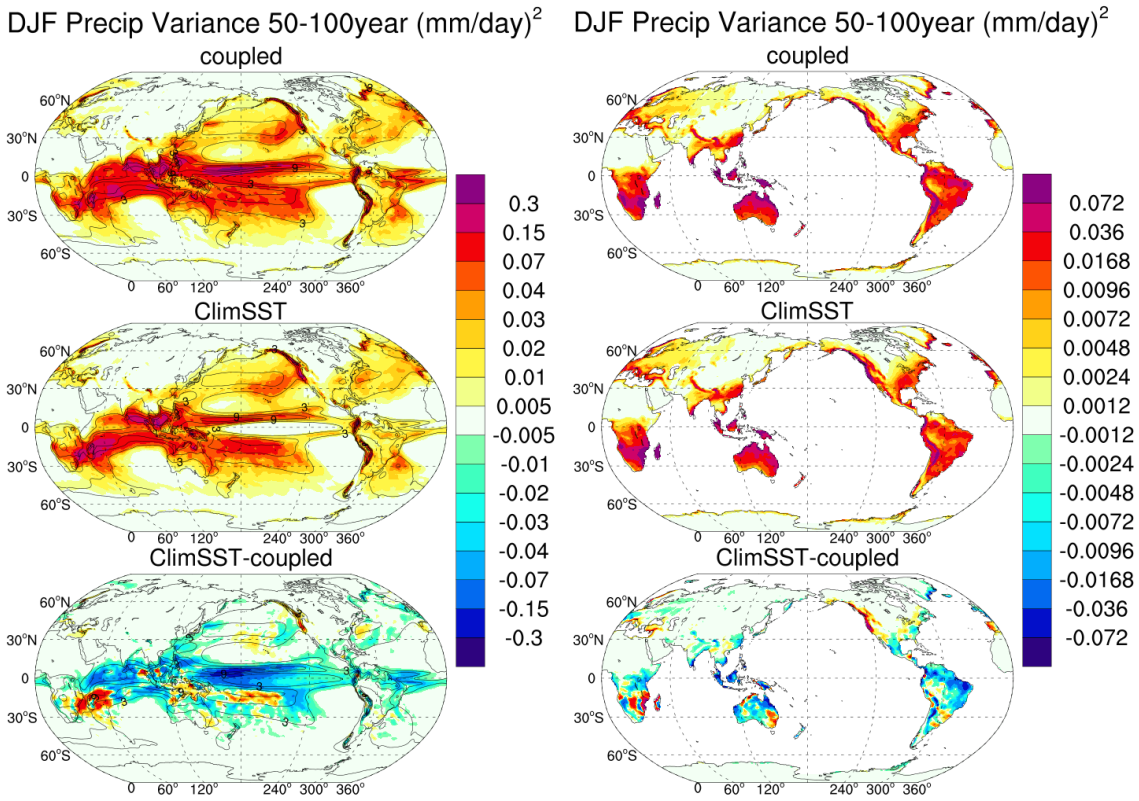

Figure 8.1 Sum of DJF precipitation power spectra between the 50-year and 100-year periods (shading) superimposed on the DJF precipitation climatology (contour). Left panels are for land only. Contour interval is 3 mm/day.

Along the equator, precipitation variance is smaller in the climSST simulation, indicating positive contribution from the local SST variability. In the subtropics, however, precipitation variance is larger in the climSST simulation, indicating negative contribution from SST. Wu et al. (2006) studied the local feedbacks between precipitation and SST and found that such feedbacks can both amplify and damp local precipitation variability at monthly timescale. Similar analyses can be applied on multi-decadal timescale to understand the impact of SST variation on precipitation variability.

Bibliography

Allan, R. P., and B. J. Soden, 2008: Atmospheric warming and the amplification of precipitation extremes. *Science*, **321**, 1481–1484, doi:10.1126/science.1160787.

Allen, M. R., and W. J. Ingram, 2002: Constraints on future changes in climate and the hydrologic cycle. *Nature*, **419**, 224–232, doi:10.1038/nature01092.

Andrews, T., P. M. Forster, and J. M. Gregory, 2009: A surface energy perspective on climate change. *J. Clim.*, **22**, 2557–2570, doi:10.1175/2008JCLI2759.1.

——, J. M. Gregory, and M. J. Webb, 2015: The dependence of radiative forcing and feedback on evolving patterns of surface temperature change in climate models. *J. Clim.*, **28**, 1630–1648, doi:10.1175/JCLI-D-14-00545.1.

Bala, G., K. Caldeira, and R. Nemani, 2010: Fast versus slow response in climate change: implications for the global hydrological cycle. *Clim. Dyn.*, **35**, 423–434, doi:10.1007/s00382-009-0583-y.

Barsugli, J. J., and D. S. Battisti, 1998: The basic effects of atmosphere–ocean thermal coupling on midlatitude variability. *J. Atmospheric Sci.*, **55**, 477–493, doi:10.1175/1520-0469(1998)055<0477:TBEOAO>2.0.CO;2.

Bayr, T., and D. Dommenget, 2013: The tropospheric land–sea warming contrast as the driver of tropical sea level pressure changes. *J. Clim.*, **26**, 1387–1402, doi:10.1175/JCLI-D-11-00731.1.

Boer, G., 1993: Climate change and the regulation of the surface moisture and energy budgets. *Clim. Dyn.*, **8**, 225–239, doi:10.1007/BF00198617.

Bony, S., G. Bellon, D. Klocke, S. Sherwood, S. Fermepin, and S. Denvil, 2013: Robust direct effect of carbon dioxide on tropical circulation and regional precipitation. *Nat. Geosci*, **6**, 447–451.

Bracco, A., F. Kucharski, R. Kallummal, and F. Molteni, 2004: Internal variability, external forcing and climate trends in multi-decadal AGCM ensembles. *Clim. Dyn.*, **23**, 659–678, doi:10.1007/s00382-004-0465-2.

Bretherton, C. S., and D. S. Battisti, 2000: An interpretation of the results from atmospheric general circulation models forced by the time history of the observed sea surface temperature distribution. *Geophys. Res. Lett.*, **27**, 767–770, doi:10.1029/1999GL010910.

Cao, L., G. Bala, and K. Caldeira, 2012: Climate response to changes in atmospheric carbon dioxide and solar irradiance on the time scale of days to weeks. *Environ. Res. Lett.*, **7**, 034015.

Cash, B., E. Schneider, and L. Bengtsson, 2005: Origin of regional climate differences: role of boundary conditions and model formulation in two GCMs. *Clim. Dyn.*, **25**, 709–723, doi:10.1007/s00382-005-0069-5.

Cayan, D. R., 1992: Latent and sensible heat flux anomalies over the northern oceans: driving the sea surface temperature. *J. Phys. Oceanogr.*, **22**, 859–881, doi:10.1175/1520-0485(1992)022<0859:LASHFA>2.0.CO;2.

Chadwick, R., I. Boutle, and G. Martin, 2013a: Spatial patterns of precipitation change in CMIP5: why the rich do not get richer in the tropics. *J. Clim.*, **26**, 3803–3822, doi:10.1175/JCLI-D-12-00543.1.

——, P. Wu, P. Good, and T. Andrews, 2013b: Asymmetries in tropical rainfall and circulation patterns in idealised CO2 removal experiments. *Clim. Dyn.*, **40**, 295–316, doi:10.1007/s00382-012-1287-2.

——, P. Good, T. Andrews, and G. Martin, 2014: Surface warming patterns drive tropical rainfall pattern responses to CO2 forcing on all timescales. *Geophys. Res. Lett.*, **41**, 610–615, doi:10.1002/2013GL058504.

Chen, H., E. K. Schneider, B. P. Kirtman, and I. Colfescu, 2013: Evaluation of weather noise and its role in climate model simulations. *J. Clim.*, **26**, 3766–3784, doi:10.1175/JCLI-D-12-00292.1.

Chou, C., and J. D. Neelin, 2004: Mechanisms of global warming impacts on regional tropical precipitation. *J. Clim.*, **17**, 2688–2701, doi:10.1175/1520-0442(2004)017<2688:MOGWIO>2.0.CO;2.

——, ——, C.-A. Chen, and J.-Y. Tu, 2009: Evaluating the "rich-get-richer" mechanism in tropical precipitation change under global warming. *J. Clim.*, **22**, 1982–2005, doi:10.1175/2008JCLI2471.1.

Collins, M., 2005: El Niño- or La Niña-like climate change? *Clim. Dyn.*, **24**, 89–104, doi:10.1007/s00382-004-0478-x.

Collins, M., and Coauthors, 2010: The impact of global warming on the tropical Pacific Ocean and El Nino. *Nat. Geosci*, **3**, 391–397, doi:10.1038/ngeo868.

Compo, G., and P. Sardeshmukh, 2009: Oceanic influences on recent continental warming. *Clim. Dyn.*, **32**, 333–342, doi:10.1007/s00382-008-0448-9.

Coppola, E., and F. Giorgi, 2005: Climate change in tropical regions from high-resolution time-slice AGCM experiments. *Q. J. R. Meteorol. Soc.*, **131**, 3123–3145, doi:10.1256/qj.04.166.

Deser, C., and M. S. Timlin, 1997: Atmosphere–ocean interaction on weekly timescales in the North Atlantic and Pacific. *J. Clim.*, **10**, 393–408, doi:10.1175/1520-0442(1997)010<0393:AOIOWT>2.0.CO;2.

——, and A. S. Phillips, 2009: Atmospheric circulation trends, 1950–2000: the relative roles of sea surface temperature forcing and direct atmospheric radiative forcing. *J. Clim.*, **22**, 396–413, doi:10.1175/2008JCLI2453.1.

——, A. Phillips, V. Bourdette, and H. Teng, 2012: Uncertainty in climate change projections: the role of internal variability. *Clim. Dyn.*, **38**, 527–546, doi:10.1007/s00382-010-0977-x.

DiNezio, P. N., A. C. Clement, G. A. Vecchi, B. J. Soden, B. P. Kirtman, and S.-K. Lee, 2009: Climate response of the equatorial pacific to global warming. *J. Clim.*, **22**, 4873–4892, doi:10.1175/2009JCLI2982.1.

Emori, S., and S. J. Brown, 2005: Dynamic and thermodynamic changes in mean and extreme precipitation under changed climate. *Geophys. Res. Lett.*, **32**, L17706, doi:10.1029/2005GL023272.

Frierson, D. M. W., J. Lu, and G. Chen, 2007: Width of the Hadley cell in simple and comprehensive general circulation models. *Geophys. Res. Lett.*, **34**, L18804, doi:10.1029/2007GL031115.

Fyfe, J. C., 2003: Extratropical southern hemisphere cyclones: harbingers of climate change? *J. Clim.*, **16**, 2802–2805, doi:10.1175/1520-0442(2003)016<2802:ESHCHO>2.0.CO;2.

Held, I. M., and B. J. Soden, 2006: Robust responses of the hydrological cycle to global warming. *J. Clim.*, **19**, 5686–5699, doi:10.1175/JCLI3990.1.

Hertwig, E., J.-S. von Storch, D. Handorf, K. Dethloff, I. Fast, and T. Krismer, 2015: Effect of horizontal resolution on ECHAM6-AMIP performance. *Clim. Dyn.*, **45**, 185–211, doi:10.1007/s00382-014-2396-x.

Holzer, M., and G. J. Boer, 2001: Simulated changes in atmospheric transport climate. *J. Clim.*, **14**, 4398–4420, doi:10.1175/1520-0442(2001)014<4398:SCIATC>2.0.CO;2.

Huang, P., S.-P. Xie, K. Hu, G. Huang, and R. Huang, 2013: Patterns of the seasonal response of tropical rainfall to global warming. *Nat. Geosci*, **6**, 357–361.

Hurrell, J. W., J. J. Hack, D. Shea, J. M. Caron, and J. Rosinski, 2008: A new sea surface temperature and sea Ice boundary dataset for the community atmosphere model. *J. Clim.*, **21**, 5145–5153, doi:10.1175/2008JCLI2292.1.

——, and Coauthors, 2013: The community earth system model: a framework for collaborative research. *Bull. Am. Meteorol. Soc.*, **94**, 1339–1360, doi:10.1175/BAMS-D-12-00121.1.

Jia, L., and Coauthors, 2015: Improved seasonal prediction of temperature and precipitation over land in a high-resolution GFDL climate model. *J. Clim.*, **28**, 2044–2062, doi:10.1175/JCLI-D-14-00112.1.

Jin, F., and B. J. Hoskins, 1995: The direct response to tropical heating in a baroclinic atmosphere. *J. Atmospheric Sci.*, **52**, 307–319, doi:10.1175/1520-0469(1995)052<0307:TDRTTH>2.0.CO;2.

Joshi, M., J. Gregory, M. Webb, D. H. Sexton, and T. Johns, 2008: Mechanisms for the land/sea warming contrast exhibited by simulations of climate change. *Clim. Dyn.*, **30**, 455–465, doi:10.1007/s00382-007-0306-1.

Kay, J. E., and Coauthors, 2014: The Community Earth System Model (CESM) large ensemble project: a community resource for studying climate change in the presence of internal climate variability. *Bull. Am. Meteorol. Soc.*, doi:10.1175/BAMS-D-13-00255.1. http://dx.doi.org/10.1175/BAMS-D-13-00255.1 (Accessed July 12, 2015).

Kent, C., R. Chadwick, and D. P. Rowell, 2015: Understanding uncertainties in future projections of seasonal tropical precipitation. *J. Clim.*, **28**, 4390–4413, doi:10.1175/JCLI-D-14-00613.1.

Kharin, V. V., F. W. Zwiers, and X. Zhang, 2005: Intercomparison of near-surface temperature and precipitation extremes in AMIP-2 simulations, reanalyses, and observations. *J. Clim.*, **18**, 5201–5223, doi:10.1175/JCLI3597.1.

Kirtman, B. P., D. A. Paolino, J. L. Kinter, and D. M. Straus, 2001: Impact of tropical subseasonal SST variability on seasonal mean climate simulations. *Mon. Weather Rev.*, **129**, 853–868, doi:10.1175/1520-0493(2001)129<0853:IOTSSV>2.0.CO;2.

Knutson, T. R., and S. Manabe, 1995: Time-mean response over the tropical Pacific to increased C02 in a coupled ocean-atmosphere model. *J. Clim.*, **8**, 2181–2199, doi:10.1175/1520-0442(1995)008<2181:TMROTT>2.0.CO;2.

Knutti, R., and J. Sedlacek, 2013: Robustness and uncertainties in the new CMIP5 climate model projections. *Nat. Clim Change*, **3**, 369–373, doi:10.1038/nclimate1716.

Kociuba, G., and S. B. Power, 2015: Inability of CMIP5 models to simulate recent strengthening of the walker circulation: implications for projections. *J. Clim.*, **28**, 20–35, doi:10.1175/JCLI-D-13-00752.1.

Kopparla, P., E. M. Fischer, C. Hannay, and R. Knutti, 2013: Improved simulation of extreme precipitation in a high-resolution atmosphere model. *Geophys. Res. Lett.*, **40**, 5803–5808, doi:10.1002/2013GL057866.

Krishna Kumar, K., M. Hoerling, and B. Rajagopalan, 2005: Advancing dynamical prediction of Indian monsoon rainfall. *Geophys. Res. Lett.*, **32**, L08704, doi:10.1029/2004GL021979.

Kumar, A., Q. Zhang, J.-K. E. Schemm, M. L'Heureux, and K.-H. Seo, 2008: An assessment of errors in the simulation of atmospheric interannual variability in uncoupled AGCM simulations. *J. Clim.*, **21**, 2204–2217, doi:10.1175/2007JCLI1743.1.

Liu, Z., S. Vavrus, F. He, N. Wen, and Y. Zhong, 2005: Rethinking tropical ocean response to global warming: the enhanced equatorial warming. *J. Clim.*, **18**, 4684–4700, doi:10.1175/JCLI3579.1.

Long, S.-M., S.-P. Xie, X.-T. Zheng, and Q. Liu, 2014: Fast and slow responses to global warming: sea surface temperature and precipitation patterns. *J. Clim.*, **27**, 285–299, doi:10.1175/JCLI-D-13-00297.1.

Lorenz, D. J., and E. T. DeWeaver, 2007: The response of the extratropical hydrological cycle to global warming. *J. Clim.*, **20**, 3470–3484, doi:10.1175/JCLI4192.1.

Lu, J., G. A. Vecchi, and T. Reichler, 2007: Expansion of the Hadley cell under global warming. *Geophys. Res. Lett.*, **34**, L06805, doi:10.1029/2006GL028443.

——, G. Chen, and D. M. W. Frierson, 2008: Response of the zonal mean atmospheric circulation to El Niño versus global warming. *J. Clim.*, **21**, 5835–5851, doi:10.1175/2008JCLI2200.1.

Magnusson, L., M. Alonso-Balmaseda, S. Corti, F. Molteni, and T. Stockdale, 2013: Evaluation of forecast strategies for seasonal and decadal forecasts in presence of systematic model errors. *Clim. Dyn.*, **41**, 2393–2409, doi:10.1007/s00382-012-1599-2.

Ma, J., and S.-P. Xie, 2013: Regional patterns of sea surface temperature change: a source of uncertainty in future projections of precipitation and atmospheric circulation. *J. Clim.*, **26**, 2482–2501, doi:10.1175/JCLI-D-12-00283.1.

——, ——, and Y. Kosaka, 2012: Mechanisms for tropical tropospheric circulation change in response to global warming. *J. Clim.*, **25**, 2979–2994, doi:10.1175/JCLI-D-11-00048.1.

Manabe, S., R. J. Stouffer, M. J. Spelman, and K. Bryan, 1991: Transient responses of a coupled ocean–atmosphere model to gradual changes of atmospheric CO2. Part I. annual mean response. *J. Clim.*, **4**, 785–818, doi:10.1175/1520-0442(1991)004<0785:TROACO>2.0.CO;2.

May, W., 2008: Potential future changes in the characteristics of daily precipitation in Europe simulated by the HIRHAM regional climate model. *Clim. Dyn.*, **30**, 581–603, doi:10.1007/s00382-007-0309-y.

McCabe, G. J., M. P. Clark, and M. C. Serreze, 2001: Trends in northern hemisphere surface cyclone frequency and intensity. *J. Clim.*, **14**, 2763–2768, doi:10.1175/1520-0442(2001)014<2763:TINHSC>2.0.CO;2.

Meehl, G. A., C. Covey, K. E. Taylor, T. Delworth, R. J. Stouffer, M. Latif, B. McAvaney, and J. F. B. Mitchell, 2007: The WCRP CMIP3 multimodel dataset: a new era in climate change research. *Bull. Am. Meteorol. Soc.*, **88**, 1383–1394, doi:10.1175/BAMS-88-9-1383.

Meng, Q., M. Latif, W. Park, N. Keenlyside, V. Semenov, and T. Martin, 2012: Twentieth century Walker Circulation change: data analysis and model experiments. *Clim. Dyn.*, **38**, 1757–1773, doi:10.1007/s00382-011-1047-8.

Mitchell, J. F. B., 1983: The seasonal response of a general circulation model to changes in CO2 and sea temperatures. *Q. J. R. Meteorol. Soc.*, **109**, 113–152, doi:10.1002/qj.49710945906.

Murphy, J. M., 1995: Transient response of the hadley centre coupled ocean-atmosphere model to increasing carbon dioxide. Part 1: control climate and flux adjustment. *J. Clim.*, **8**, 36–56, doi:10.1175/1520-0442(1995)008<0036:TROTHC>2.0.CO;2.

Neelin, J. D., C. Chou, and H. Su, 2003: Tropical drought regions in global warming and El Niño teleconnections. *Geophys. Res. Lett.*, **30**, 2275, doi:10.1029/2003GL018625.

O'Gorman, P. A., and M. S. Singh, 2013: Vertical structure of warming consistent with an upward shift in the middle and upper troposphere. *Geophys. Res. Lett.*, **40**, 1838–1842, doi:10.1002/grl.50328.

Pielke, R. A., and R. L. Wilby, 2012: Regional climate downscaling: What's the point? *Eos Trans. Am. Geophys. Union*, **93**, 52–53, doi:10.1029/2012EO050008.

Power, S. B., and I. N. Smith, 2007: Weakening of the Walker Circulation and apparent dominance of El Niño both reach record levels, but has ENSO really changed? *Geophys. Res. Lett.*, **34**, L18702, doi:10.1029/2007GL030854.

——, and G. Kociuba, 2011: What caused the observed twentieth-century weakening of the Walker circulation? *J. Clim.*, **24**, 6501–6514, doi:10.1175/2011JCLI4101.1.

Santer, B. D., and Coauthors, 2003: Contributions of anthropogenic and natural forcing to recent tropopause height changes. *Science*, **301**, 479–483, doi:10.1126/science.1084123.

Sardeshmukh, P. D., and B. J. Hoskins, 1988: The generation of global rotational flow by steady idealized tropical divergence. *J. Atmospheric Sci.*, **45**, 1228–1251, doi:10.1175/1520-0469(1988)045<1228:TGOGRF>2.0.CO;2.

Sausen, R., K. Barthel, and K. Hasselmann, 1988: Coupled ocean-atmosphere models with flux correction. *Clim. Dyn.*, **2**, 145–163, doi:10.1007/BF01053472.

Scheff, J., and D. Frierson, 2012a: Twenty-first-century multimodel subtropical precipitation declines are mostly midlatitude shifts. *J. Clim.*, **25**, 4330–4347, doi:10.1175/JCLI-D-11-00393.1.

——, and D. M. W. Frierson, 2012b: Robust future precipitation declines in CMIP5 largely reflect the poleward expansion of model subtropical dry zones. *Geophys. Res. Lett.*, **39**, L18704, doi:10.1029/2012GL052910.

Schneider, E. K., L. Bengtsson, and Z.-Z. Hu, 2003: Forcing of northern hemisphere climate trends. *J. Atmospheric Sci.*, **60**, 1504–1521, doi:10.1175/1520-0469(2003)060<1504:FONHCT>2.0.CO;2.

Schubert, S. D., M. J. Suarez, P. J. Pegion, R. D. Koster, and J. T. Bacmeister, 2004: Causes of long-term drought in the U.S. great plains. *J. Clim.*, **17**, 485–503, doi:10.1175/1520-0442(2004)017<0485:COLDIT>2.0.CO;2.

Seager, R., and Coauthors, 2007: Model projections of an imminent transition to a more arid climate in southwestern North America. *Science*, **316**, 1181–1184, doi:10.1126/science.1139601.

——, N. Naik, and G. A. Vecchi, 2010: Thermodynamic and dynamic mechanisms for large-scale changes in the hydrological cycle in response to global warming. *J. Clim.*, **23**, 4651–4668, doi:10.1175/2010JCLI3655.1.

Shin, S.-I., and P. Sardeshmukh, 2011: Critical influence of the pattern of Tropical Ocean warming on remote climate trends. *Clim. Dyn.*, **36**, 1577–1591, doi:10.1007/s00382-009-0732-3.

Shukla, J., 1998: Predictability in the midst of chaos: a scientific basis for climate forecasting. *Science*, **282**, 728–731, doi:10.1126/science.282.5389.728.

Soden, B. J., 2000: The sensitivity of the tropical hydrological cycle to ENSO. *J. Clim.*, **13**, 538–549, doi:10.1175/1520-0442(2000)013<0538:TSOTTH>2.0.CO;2.

Solomon, S., 2007: *Climate change 2007-the physical science basis: Working group I contribution to the fourth assessment report of the IPCC*. Cambridge University Press,.

Stephens, G. L., and T. D. Ellis, 2008: Controls of global-mean precipitation increases in global warming GCM experiments. *J. Clim.*, **21**, 6141–6155, doi:10.1175/2008JCLI2144.1.

Talandier, C., and Coauthors, 2014: Improvements of simulated Western North Atlantic current system and impacts on the AMOC. *Ocean Model.*, **76**, 1–19.

TANAKA, H. L., N. ISHIZAKI, and A. KITOH, 2004: Trend and interannual variability of Walker, monsoon and Hadley circulations defined by velocity potential in the upper troposphere. *Tellus A*, **56**, 250–269, doi:10.1111/j.1600-0870.2004.00049.x.

Taylor, K. E., R. J. Stouffer, and G. A. Meehl, 2012: An overview of CMIP5 and the experiment design. *Bull. Am. Meteorol. Soc.*, **93**, 485–498, doi:10.1175/BAMS-D-11-00094.1.

Thorpe, L., and T. Andrews, 2014: The physical drivers of historical and 21st century global precipitation changes. *Environ. Res. Lett.*, **9**, 064024.

Ting, M., and P. D. Sardeshmukh, 1993: Factors determining the extratropical response to equatorial diabatic heating anomalies. *J. Atmospheric Sci.*, **50**, 907–918, doi:10.1175/1520-0469(1993)050<0907:FDTERT>2.0.CO;2.

Tokinaga, H., S.-P. Xie, C. Deser, Y. Kosaka, and Y. M. Okumura, 2012: Slowdown of the Walker circulation driven by tropical Indo-Pacific warming. *Nature*, **491**, 439–443, doi:10.1038/nature11576.

Tziperman, E., 2000: Uncertainties in thermohaline circulation response to greenhouse warming. *Geophys. Res. Lett.*, **27**, 3077–3080, doi:10.1029/2000GL006108.

Vecchi, G. A., and B. J. Soden, 2007: Global warming and the weakening of the tropical circulation. *J. Clim.*, **20**, 4316–4340, doi:10.1175/JCLI4258.1.

——, ——, A. T. Wittenberg, I. M. Held, A. Leetmaa, and M. J. Harrison, 2006: Weakening of tropical Pacific atmospheric circulation due to anthropogenic forcing. *Nature*, **441**, 73–76, doi:10.1038/nature04744.

Vecchi, G. A., and Coauthors, 2014: On the seasonal forecasting of regional tropical cyclone activity. *J. Clim.*, **27**, 7994–8016, doi:10.1175/JCLI-D-14-00158.1.

Wang, B., Q. Ding, X. Fu, I.-S. Kang, K. Jin, J. Shukla, and F. Doblas-Reyes, 2005: Fundamental challenge in simulation and prediction of summer monsoon rainfall. *Geophys. Res. Lett.*, **32**, L15711, doi:10.1029/2005GL022734.

Wu, R., and B. P. Kirtman, 2004: Impacts of the indian ocean on the indian summer monsoon–ENSO relationship. *J. Clim.*, **17**, 3037–3054, doi:10.1175/1520-0442(2004)017<3037:IOTIOO>2.0.CO;2.

——, ——, and K. Pegion, 2006: Local air–sea relationship in observations and model simulations. *J. Clim.*, **19**, 4914–4932, doi:10.1175/JCLI3904.1.

Wu, Y., M. Ting, R. Seager, H.-P. Huang, and M. Cane, 2011: Changes in storm tracks and energy transports in a warmer climate simulated by the GFDL CM2.1 model. *Clim. Dyn.*, **37**, 53–72, doi:10.1007/s00382-010-0776-4.

Xie, S.-P., C. Deser, G. A. Vecchi, J. Ma, H. Teng, and A. T. Wittenberg, 2010: Global warming pattern formation: sea surface temperature and rainfall. *J. Clim.*, **23**, 966–986, doi:10.1175/2009JCLI3329.1.

Yin, J. H., 2005: A consistent poleward shift of the storm tracks in simulations of 21st century climate. *Geophys. Res. Lett.*, **32**, L18701, doi:10.1029/2005GL023684.

——, and D. S. Battisti, 2001: The importance of tropical sea surface temperature patterns in simulations of last glacial maximum climate. *J. Clim.*, **14**, 565–581, doi:10.1175/1520-0442(2001)014<0565:TIOTSS>2.0.CO;2.

Yu, B., and G. Boer, 2002: The roles of radiation and dynamical processes in the El Niño-like response to global warming. *Clim. Dyn.*, **19**, 539–554, doi:10.1007/s00382-002-0244-x.

Zarzycki, C. M., C. Jablonowski, D. R. Thatcher, and M. A. Taylor, 2015: Effects of localized grid refinement on the general circulation and climatology in the Community Atmosphere Model. *J. Clim.*, **28**, 2777–2803, doi:10.1175/JCLI-D-14-00599.1.

Zheng, L., and R. H. Weisberg, 2012: Modeling the west Florida coastal ocean by downscaling from the deep ocean, across the continental shelf and into the estuaries. *Ocean Model.*, **48**, 10–29.

Zheng, X.-T., S.-P. Xie, Y. Du, L. Liu, G. Huang, and Q. Liu, 2013: Indian Ocean dipole response to global warming in the CMIP5 multimodel ensemble. *J. Clim.*, **26**, 6067–6080, doi:10.1175/JCLI-D-12-00638.1.